DESIGN AND EVALUATION OF THE SENSING CHARACTERISTICS OF A POLYANILINE-BIOTINYLATED ANTIBODY *PSEUDOMONAS AERUGINOSA* BIOSENSOR

By

Hanzooma Hatwiko

512802221

A dissertation submitted in partial fulfilment

of the requirements for the degree of

Master of Science in Chemistry

The University of Zambia

June, 2015

Declaration

I hereby declare that this Master's dissertation is my own work, and it does not contain other people's work without being stated and that the references contains all the literature that I have used in writing the dissertation, and that all references refer to this bibliography. I also declare that this dissertation has not previously been submitted for a degree to this or any other university.

APPROVAL

This dissertation titled "DESIGN AND EVALUATION OF THE SENSING CHARACTERISTICS OF A POLYANILINE- BIOTINYLATED ANTIBODY *PSEUDOMONAS AERUGINOSA* BIOSENSOR" of **HANZOOMA HATWIKO** is approved as partial fulfilment of the requirements for the award of the degree of Master of Science in Chemistry by the University of Zambia.

Supervisors name	Signature	Date
M.O. MUNYATI		10/06/2016

Examiner's name	Signature	Date
S. PRAKASH		10/06/2016

Examiner I

BACKSION TEMBO		10/6/2016

Examiner II

J. NYIRENDA		13/06/2016

Examiner III

Chairperson of Board of Examiners

Abstract

Although there are many diagnostic and detection platforms for detection of various bacteria, these often require large elaborate procedures and well trained experts to execute. The turnaround time for results can sometimes be long. The development of portable and low power devices integrated biosensors is making available devices that can be used at the point-of-care. Such devices often can give immediate results. Rapid detection of bacterial pathogens is critical in the diagnosis of infectious disease. *Pseudomonas aeruginosa* is a nuisance bacteria that is also found in hospital environment that can cause fatality if there is a delay in detection. A biosensor based on polyaniline thin films and biotinylated anti-*Pseudomonas aeruginosa* polyclonal antibodies has been developed that enables the detection of *P. aeruginosa* bacteria. Thin films comprising polyaniline nano fibres were developed via in-situ polymerization on glass slides. Fourier Transform Infrared (FTIR) spectroscopy and UV/Vis spectroscopy were used for functional group analysis and determination of optical properties. The effect of polymerization time and thermal treatment on morphology and electrical properties was investigated. The morphological characteristics were determined using Atomic Force Microscopy (AFM) whilst electrical properties were determined using a four-point probe coupled to a source meter. Anti-*P. aeruginosa* biotinylated polyclonal antibodies were immobilized on avidin treated polyaniline thin films. Sensing characteristics of polyaniline films were evaluated in biosensor detection set-up. The set-up consisted of a helium-neon laser interfaced with a cadmium sulphide LDR detector connected to a circuit incorporating a multimeter. The changes in light intensity were observed to be directly proportional to the amount of bacteria bound by the antibodies that reflected an increase in the resistance of the films. The resistance was found to increase linearly with increasing bacteria concentration. Bacteria concentrations in unknown samples were determined rapidly in under 5 minutes. The lower detection limit of the sensor was found to be 9.0×10^5 CFU/ml. Selectivity was demonstrated with the *E.coli* cross-reactivity test, which showed no biosensor response in comparison to the response seen with the *P. aeruginosa* tests. We have successfully developed and tested a biochip that can be used in sensor devices for rapid determination of *P. aeruginosa* bacteria.

Dedication

To Eunice, Brenda, Lushomo and Lubuto

Acknowledgments

To The Most High, I am eternally indebted to you for your lifelong guidance, protection and continued inspiration.

I would like to thank my research supervisor, Dr M.O. Munyati for his advice, guidance and support that made light the heavy task of carrying out this project.

Many thanks also go to my co-supervisor, Dr. K.S. Nalubamba whose support and inspiration enabled me to go on with this research with much fervour and vigour.

Special thanks also go to The University of Zambia, Departments of Chemistry and Physics (School of Natural Sciences), Department of Clinical studies and Disease Control (School of Veterinary Medicine) and Department of Microbiology (School of Medicine, UTH) for providing me with invaluable access to materials and facilities required to ensure that this project was a success.

Thanks to Mr. C. Siabbamba and Mr. C. Mubita and their teams for their valued assistance.

To my friends in the Material Science Research Group, Jimmy, Abigail, Simon and Ken you made the burden and work lighter.

To my sponsors, The International Science Program (ISP), I offer my deep appreciation for awarding me a fully funded research scholarship that ultimately made this research project possible.

Finally, thanks to my wife and children for their enduring support during the long periods of research work.

Table of Contents

List of Figures

List of Tables

List of Abbreviations

AC	Alternating Current
AFM	Atomic Force Microscope
ATR-FTIR	Attenuated Total Reflectance- Fourier Transform Infrared
BA	Bulk Acoustic
BAEE	*N*-benzoyl-L-arginine ethyl ester
BSA	Bovine Serum Albumin
BVDV	Bovine Viral Diarrhoea Virus
CCD	Charge-Coupled Device
CCID	Cell Culture Infective Dose
CFU	Colony Forming Units
CP	Conducting Polymer
DC	Direct Current
DDE	Dichlorodiphenyldichloroethylene
DDT	Dichlorodiphenyltrichloroethane
DMSO	Dimethyl Sulfoxide
DNA	Deoxyribonucleic Acid
EMI	Electromagnetic Interference
FTIR	Fourier Transform Infrared
HCH	Hexachlorocyclohexane
IgA	Immunoglobulin A
IgD	Immunoglobulin D
IgE	Immunoglobulin E
IgG	Immunoglobulin G
IgM	Immunoglobulin M
InlB	Internalin B
IR	Infrared
IUPAC	International Union of Pure and Applied Chemistry
LDH	Lactate Dehydrogenase
LDR	Light Dependent Resistor
LED	Light Emitting Diode
LOD	Lactate Oxidase
LPS	Long Chained Lipopolysaccharide
LUMO	Lowest Unoccupied Molecular Orbital
LB	Lysogeny Broth
MAMPs	Microbe-Associated Molecular Patterns

MEP	Mucoid Exopolysaccharide
MV	Membrane Vesicle
NAD+	Nicotinamide Adenine Dinucleotide (oxidized form)
NADH	Nicotinamide Adenine Dinucleotide (reduced form)
NADPH	Nicotinamide Adenine Dinucleotide phosphate
NLRs	Nucleotide-binding Oligomerization Domain (NOD)-Like Receptors
O-Antigen	The heterogeneous portion of lipopolysaccharide
OM	Outer Membrane
OMP	Outer Membrane Proteins
OPH	Organophosphate Hydrolase
PANI	Polyaniline
PANI-Pec	Polyaniline-Pectin
PBS	Phosphate Buffered Saline
PCR	Polymerase Chain Reaction
PET	Polyethylene Terephthalate
PQC	Piezoelectric Quartz Crystal
PRRs	Pattern Recognition Receptors
QCM	Quartz Crystal Microbalance
RNA	Ribonucleic Acid
SAT	Serum Agglutination Test
SAW	Surface Acoustic Wave
SPR	Surface Plasmon Resonance
TIR	Total Internal Reflection
TLRs	Toll-Like Receptors
UNZA	University of Zambia
UTH	University Teaching Hospital
UV	Ultra Violet
UV/Vis	Ultraviolet-Visible

List of Symbols

M^{-1}	Per Molar
Hz	Hertz
ΔF	Change in Frequency
^{o}C	Degrees Celsius
M	Mu
pg/ml	Pico Gram Per Millilitre
P	Rho
m	Mass
ng/ml	Nano Gram Per Millilitre
ng/µl	Nano Gram Per Microlitre
KJ mol^{-1}	Kilo Joule Per Mole
M	Molar
kDA	Kilo Dalton
Δm	Change in Mass
cm^{-1}	Per Centimetre
S/cm	Siemens Per Centimetre
Б	Shima
Eg	Band Gap Energy
T	Temperature
α	Alpha
Y	Upsilon
mV	Millivolt
mA	Milliamp
mmol/L	Millimole Per Litre
Ml	Millilitre
%T	Percent Transmittance

CHAPTER 1: INTRODUCTION

1.1 Background to the Study

1.1.1 Biosensors and Their Applications

The International Union of Pure and Applied Chemistry (IUPAC) defines a biosensor as "a self-contained integrated device, which is capable of providing specific quantitative or semi-quantitative analytical information using a biological recognition element (biochemical receptor) which is retained in direct spatial contact with an electrochemical transduction element."(Thévenot, Toth, Durst and Wilson, 2001). The first biosensor was an enzyme-based device developed by Leland C. Clark in 1962. Since then, tremendous advances have been made in the field of biosensor research. These advances have mainly been due to the integration and use of knowledge from Physics, Chemistry and Material Science to develop devices that are not only highly complex but also more reliable in their bio-sensing applications (Darsanaki et al., 2013). Biosensors are composed of two important components, that is, the bio-molecular recognition element and the transducer. Bio-molecular recognition elements used for biosensor applications include nucleic acids, cell receptors, antibodies, whole cells, enzymes and cellular organelles. The transducer is the biosensor component that converts the analyte detection into a signal that can be measured.

The application for which a biosensor is used is dependent on the specificity of the bio-molecular recognition element incorporated in the sensor. Biosensors have wide-ranging applications and have been used in the detection of pathogens such as *Escherichia coli*, antibodies, toxins, tumour markers, pollutants, other toxic chemicals (Moina and Ybarra, 2012). The detection of glucose in blood is the major application for which biosensors have found the most commercial success.

1.1.2 Advantages of Biosensors

Biosensors have several advantages that make their use desirable over conventional methods such as their ability to detect low concentrations of analyte in samples. Biosensors for detection of pathogenic bacteria can be developed using label-free techniques. Label-free techniques offer low cost and simplicity in their applications(Justin Gooding, 2006). In medical applications, the low cost of biosensors allows for increased accessibility to diagnostic services. Biosensors are also advantageous because they offer real-time detection which reduces the time required to obtain results from sample analysis. The quick response times provided by biosensors are essential especially in biomedical applications where treatment is dependent on fast and accurate identification of pathogens.

1.1.3 Conventional Methods of Bacterial Detection and Their Challenges

In order to establish the bacterial cause of a particular infection, the offending bacteria must first be identified. Conventional methods of detecting and identifying bacteria in samples involve culture, plate colony counting and isolation of bacterial colonies which are then subjected to further morphological, biochemical and physiological tests to confirm their identity. Furthermore, the genotypic and phenotypic characteristics of the isolated bacteria also need to be studied for accurate identification of the bacteria (Tang et al., 1998b; Houpikian and Raoult, 2002b; a; Emerson, Agulto, Liu and Liu, 2008; Pan et al., 2014; Otto, Persing and Tang, 2014). Identification of bacteria using conventional methods requires more than 48 hours to yield results after a single colony has been isolated from a culture plate while in cases of slow growing bacteria this may take up to 14 days. Identification however is not guaranteed even after 14 days of testing (Tang et al., 1998a). This is undesirable because rapid and accurate identification of bacteria is critical to the enhancement of diagnosis and treatment of infections. Detection and identification of *Pseudomonas aeruginosa* using conventional methods involves the use of culture techniques, microscopy and biochemical tests which typically take 2-5 days (Hall, 2013).

1.1.4 Application of Biosensors to *Pseudomonas aeruginosa* Detection

Pseudomonas aeruginosa causes infections in both humans and animals. In humans, it may cause serious life threatening infections especially in people who have prolonged hospital admissions or have weakened immune systems due to disease. Research however, shows that healthy individuals are also prone to developing *P. aeruginosa* infections when they are exposed to contaminated water sources. Children have been known to also develop ear infections and extensive skin rashes when they are exposed to water that is insufficiently chlorinated, while eye infections can develop in people who wear contact lenses for long periods of time (Bodey, Bolivar, Fainstein and Jadeja, 1983; Mena and Gerba, 2009). The rapid detection of *P. aeruginosa* is therefore, of interest to improve treatment outcomes. Langer and co-workers (2009) report a polyaniline-based nanobiodetector for the detection of *Klebsiella pneumonia, Escherichia coli, Pseudomonas aeruginosa* and *Enterococcus faecalis* (Langer et al., 2009). This sensor was not specific to the detection of *P. aeruginosa* and was able to detect the other three strains of bacteria with equal intensity. The report by Langer was the only literature source that reported the use of polyaniline for application to the detection of *Pseudomonas aeruginosa* albeit in a non-selective manner.

1.1.5 This work

In recent times there has been a drive to make the detection of dangerous microbial pathogens more efficient and less time consuming through the use of biosensors (Singh, Poshtiban and Evoy, 2013). Conducting polymers have become important in this regard because of their suitable properties for use in biosensor devices. Polyaniline for instance is inexpensive, thermally stable and possesses excellent electrochemical stability making it suitable for a wide range of sensor applications (Arshak et al., 2009). This polymer is very responsive when applied as a thin film and is quite suitable for the immobilization of

biomolecules making it useful for construction of biosensors (Geise, Adams, Barone and Yacynych, 1991).

The research work presented in this dissertation relates to the design, development and testing of a biosensor based on a conducting polyaniline transducer with anti-*P. aeruginosa* antibodies as the sensing layer and the use of a coherent monochromatic light source for potential application in the optical detection of bio-molecular interactions. The polyclonal anti-*P .aeruginosa* antibodies were immobilized on polyaniline thin films via chemical adsorption with the aid of biotin and avidin.

1.2 Aim

The aim of this study was to develop a biosensor based on conductive polyaniline and biotinylated antibodies and evaluate its sensing characteristics.

1.3 Statement of the Problem

Pseudomonas aeruginosa is a Gram-negative bacterium that is generally able to colonize the digestive tract of patients that are hospitalized for prolonged periods. *Pseudomonas aeruginosa* can only be isolated from incubated agar (at 32 ± 2^{o}C) after 48 hours. This time period required for positive confirmation of the presence of the bacteria in a sample is sufficient to cause mortality in most critically ill patients. Therefore, reduction of this time is of paramount importance. This study aimed to evaluate a biosensor that would provide real-time detection of *Pseudomonas aeruginosa*.

1.4 Research Objectives

The research objectives of this study are outlined below;

(1) To synthesise and characterise polyaniline thin films.
(2) To generate antibodies for biotinylation of the biosensor and prepare thin films of biotinylated polyaniline.

(3) To evaluate the sensing characteristics of the biosensor.

1.5 Research Questions

This study aimed to answer the research questions highlighted below;

(i) What is the most conducive film thickness of conductive polyaniline for use in an antibody based biosensor?

(ii) What is the optimum configuration and material properties of a biosensor based on polyaniline and biotinylated antibodies?

(iii) Can a biotinylated antibody/polyaniline thin film detect the presence of *Pseudomonas aeruginosa*?

1.6 Significance of the Study

Biosensors based on polyclonal or monoclonal antibodies and electro-active polyaniline provide an opportunity for the development of low cost and sensitive point of care devices for the fast diagnosis of infectious diseases. Definitive diagnosis of infections may take up to 7 days in most cases leaving clinicians to rely on differential diagnoses and empirical treatment in order to treat a patient. Biosensors would drastically reduce the time and cost required to offer evidence based treatment in disease management.

CHAPTER 2: BIOSENSOR FUNDAMENTALS

2.1 Introduction

Biosensors are compact analytical devices that are able to convert biological activity into measurable signals (Sethi, 1994). When the bio-molecular reactions occur on a suitable transducer, they may bring about changes in the physical properties that are measurable such as optical or electrical signals. Thus, the transducer plays a critical role in converting signals that are typically not measurable into those that are. A transducer is an element, such as a conducting polymer, that is able to convert one form of energy into another. Transducers in biosensors convert the physicochemical changes that occur when a target analyte is bound by the bio-recognition layer into electronic, optical or mass changes (Bhavana Gupta, 2010; Sungkanak et al., 2010). In order for the two important parts of a biosensor to function optimally, they need to be brought together and integrated into one functional unit. Biosensor integration usually involves immobilization of the biological recognition element onto the transducer surface using strategies that ensure that they still maintain their innate biological activities (Tan, Lue, Chen and Yao, 2004). Proper integration of the biomolecule by using site-specific immobilization techniques such as chemical adsorption improves the sensitivity and performance of the biosensor (Putzbach and Ronkainen, 2013). A characteristic biosensor setup is shown in Figure 2.1.

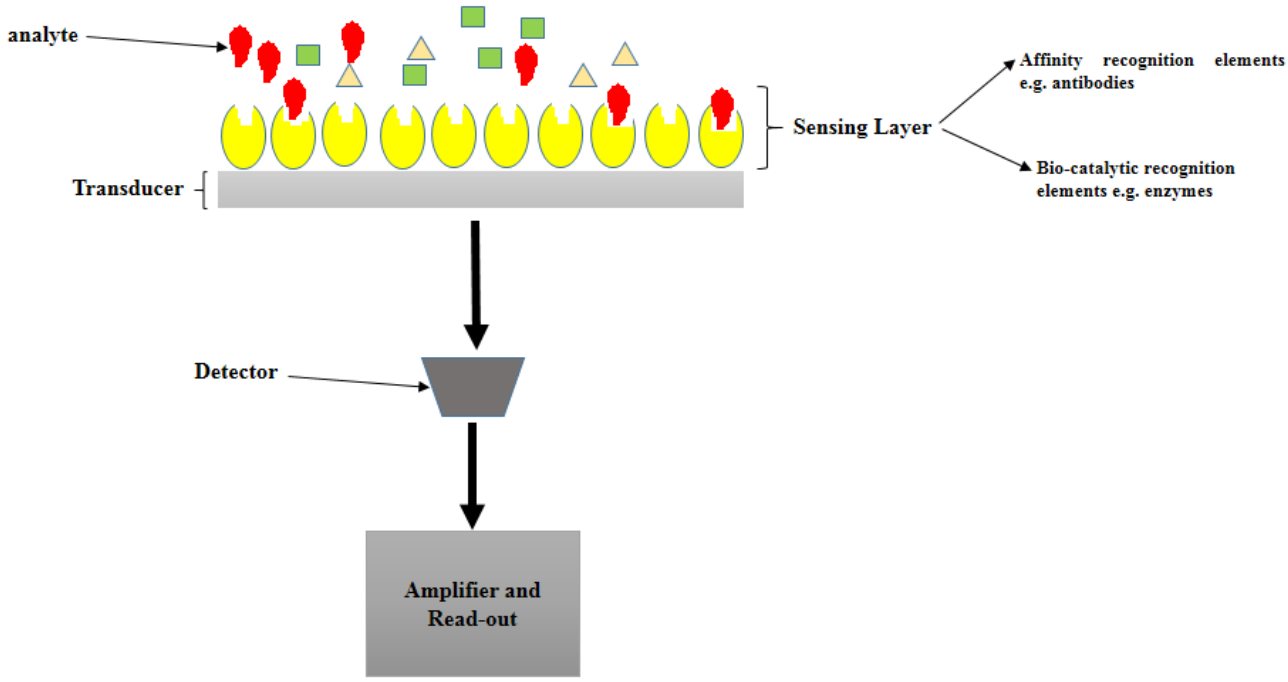

Figure 2.1: Graphic of a characteristic biosensor set-up

The first biosensor was described by Leland C. Clark in 1962 who is widely credited as being the father of biosensors (Koyun, Ahlatcıoğlu and İpek, 2012). Clark first published his work on an oxygen electrode that formed the basis of a variety of sensors that were later designed by other researchers. These sensors used immobilized oxidase enzymes as the sensing layers and were commercially viable (Setford and Newman, 2005). The design of Clark's electrode is presented in Figure 2.2. The oxygen electrode shown in Figure 2.2 consisted of an enzyme (glucose oxidase), which was encased in a dialysis membrane. When the electrode was exposed to a sample of blood, it was noted that the reduction in the amount of measured oxygen corresponded directly to the glucose concentration present in the sample. Clark later referred to his electrode as an enzyme electrode (Clark and Lyons, 1962). Using Clark's original concept, a glucose biosensor using amperometric detection of hydrogen peroxide was brought to market in 1975 (Yoo and Lee, 2010).

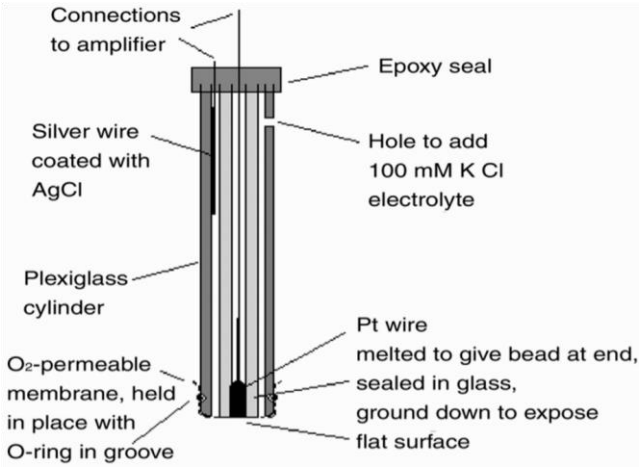

Figure 2.2: A graphic of Clark's oxygen electrode (Setford and Newman, 2005)

Biosensor design strategies should enable development of devices that are easy to use, low cost, highly sensitive, analyte specific and able to provide real-time results (Kissinger, 2005). The past 39 years of biosensor use has seen their applications evolve into a variety of uses.

Biosensor technologies have been applied to a wide range of fields including the following (Singh, 2011):

- Health monitoring
- Disease screening
- Clinical diagnostics
- Veterinary and agriculture
- Processing industry
- Pollution monitoring

2.2 Types of Biosensors

Biosensors are categorised based on their biological recognition element or the transducer that they use. The most widely used biological recognition elements in biosensors include

antibodies, bio-tissue, cellular organelles, enzymes and whole cells. Transducers and biological recognition elements in biosensors while acting together convert biochemical event that occurs during binding to analyte into chromic changes or electrical signals. The types of biosensors classified based on transduction method together with a description of how they function is presented in the sections that follow;

2.2.1 Resonant Biosensors

This type of biosensor uses acoustic wave transducers that are paired with antibodies. The antibodies on the acoustic wave transducer bind to specific antigens in samples under analysis leading to mass loading on the sensor interface. The increased mass loaded on the sensor surface due to antigen-antibody interactions is detected as a change in the resonant frequency of the transducer. The measured frequency change corresponds to how much antigen is present in the sample (Darsanaki et al., 2013).

2.2.2 Optical Biosensors

In optical biosensors, light is the signal measured. The light measured emanates from either scattering, reflection, absorption with intensity changes or from chemiluminescence occurring at the sensor surface after a binding event. In biosensors where light is inputted, it experiences a change in amplitude, polarization, phase or frequency as a result of physical or chemical changes induced by the binding event. Optical biosensors consist of a light source, a transmission medium, a sensing layer with immobilized bio-molecular recognition elements and an optical detector (Patel, Mishra and Mandloi, 2010).

2.2.3 Electrochemical Biosensors

These biosensors measure changes in electrical signals when an analyte binds to a biological recognition element. The three main types of electrochemical biosensors are amperometric, potentiometric and conductimetric. Amperometric biosensors are the most

common electrochemical biosensors. They measure the current that occurs when a potential is applied across two electrodes, one being a reference electrode (usually silver/silver chloride) while the other is an enzyme electrode. The application of a potential across the electrodes causes a redox reaction to occur at the enzyme electrode where oxygen is reduced while the analyte is oxidized. The amount of oxygen reduced is directly proportional to the current produced while the current is proportional to the analyte in the sample. The electrodes are suspended in saturated solutions of potassium chloride separated from mass solution by a membrane through which oxygen can permeate (Chaplin and Bucke, 1990). Potentiometric biosensors measure electrode potential or voltage changes across electrodes while conductimetric biosensors measure conductivity or resistance changes of sample solutions when electrochemical reactions occur.

2.2.4 Bioluminescence Biosensors

Bioluminescence exploits the characteristic property of some enzymes such as luciferase to emit photons of light as they catalyse reactions. The intensity of the emitted photons that occur during the catalysis of the analyte corresponds directly to the concentration of analyte present in a sample. Bioluminescence biosensors have been used to detect bacteria in samples. These bacteria possess a gene known as *lux* which codes for luciferase enzyme. This enzyme catalyses the oxidation of long-chain fatty aldehydes and flavin mononucleotide by oxygen. Bioluminescence is observed during the breakdown of these substrates with the emission of blue-green light (Su, Jia, Hou and Lei, 2011). The amount of bacteria in a sample is directly proportional to the amount of luminescence produced by the enzyme (D'Souza, 2001).

2.2.5 Nucleic Acid-Based Biosensors

This type of biosensor incorporates short nucleotide strands immobilized on a transducer. These nucleotide strands detect complementary strands of DNA or RNA in samples under

analysis (Syam et al., 2012). Standard methods of identification of specific sequences of DNA such as polymerase chain reaction (PCR) rely on isolation of paired strands of DNA and amplification of the DNA sequence after exposure to labelled probes containing DNA. Nucleic acid-based biosensors do not require such sample preparation and amplification but rather exploit reactions that occur when two complimentary single strands of DNA or RNA bind to each other. Such reactions may produce fluorescence when a fluorophore label is used which can then be detected by optical means (Didenko, 2001).

2.3 Biosensor Components

As stated above, biosensors are composed of two critical constituents, that is, the sensing layer which is composed of bio-molecular recognition elements and the transducer. These two components are combined to form one integrated device with the aid of suitable immobilization methods. Two main types of bio-molecular recognition elements are commonly applied to biosensors. These are bio-catalytic recognition elements and affinity recognition elements. Transducers for biosensors are numerous and their selection depends on the type of sensor setup desired (D'Orazio, 2003).

2.3.1 Bio-catalytic Recognition Elements

The most commonly used bio-catalytic recognition elements are enzymes, microbial whole cells, and biological tissues.

2.3.1.1 Enzymes

Enzymes are protein macromolecules that possess good catalytic activity and high selectivity to specific substrates. Biosensors that use enzymes as bio-catalytic recognition elements are able to provide detectable reaction products that result from the enzymatic catalysis. These products may include electrons, protons, heat or light. The enzymes used in biosensors are immobilized on transducer surfaces such as conducting polymers or metal films either by physical adsorption or chemical adsorption (De Corcuera and

Cavalieri, 2003). Oxidases are the most commonly used enzymes in biosensors. They catalyse the conversion of dissolved oxygen to hydrogen peroxide. One of the most widely used biosensor, the glucose biosensor, makes use of glucose oxidase as the bio-catalytic recognition element in detecting the levels of glucose in blood samples via the reaction shown in Figure 2.3 (Chambers et al., 2008);

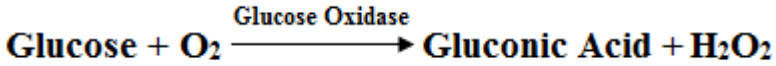

Figure 2.3: Enzyme catalysed reaction of glucose with oxygen (Rechnitz, Kobos, Riechel and Gebauer, 1977)

Glucose oxidase is used in vast majority of glucose biosensors today. It catalyses the reaction between glucose and oxygen to yield gluconic acid and hydrogen peroxide as the products. In certain cases the oxidation of glucose is achieved using the enzyme glucose dehydrogenase whose co-enzyme (prosthetic group) is NAD+, in which case NADH is the product in place of the hydrogen peroxide produced when glucose oxidase is used. The reaction shown in Figure 2.3 predominantly uses electrochemical detection whereby the hydrogen peroxide product is detected electrochemically with the aid of electrochemical mediators such as Prussian blue (an organic based dye) (Chambers et al., 2008). Prussian blue is an electron link between the bio-catalytic recognition element and the transducer for the reaction which aids in the detection of glucose (Castillo et al., 2004). The layout of an enzyme based glucose biosensor is shown in Figure 2.4.

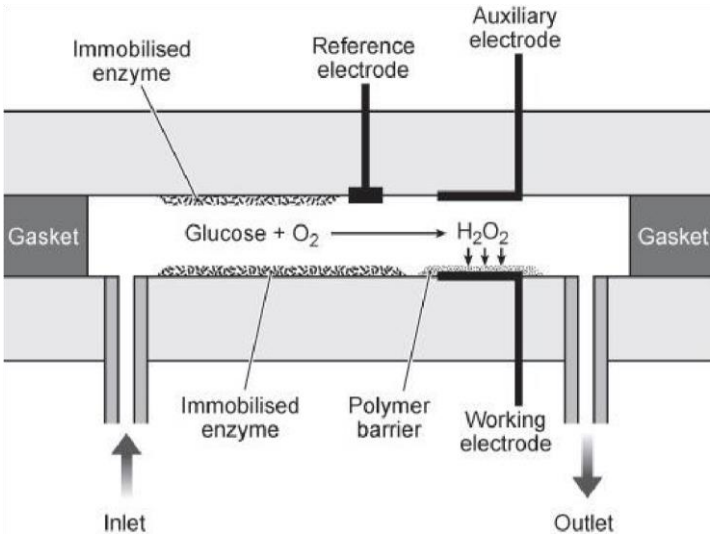

Figure 2.4: General layout of enzyme based glucose biosensors (Chambers et al., 2008)

Glucose sensors, such as the one described in Figure 2.4 above use oxidases as the enzyme whose co-substrate is molecular oxygen, which is converted into hydrogen peroxide after its reaction with the substrate. The redox reaction that occurs in these biosensors produces a substrate-based change in both the oxygen and hydrogen peroxide concentration. Most glucose biosensors are polarized at a specific potential. The current that is recorded is directly proportional to the concentration of the substrate (Castillo et al., 2004).

2.3.1.2 Microbial Whole Cells and Tissues

Sensors that incorporate whole cells as bio-catalytic recognition systems are known as whole cell biosensors. Both prokaryotic and eukaryotic cells have been useful in this regard. Microbial whole cells and tissues are used mostly in amperometric biosensor setups. Such setups permit the surveillance of cellular metabolic activity by retrieval of information pertaining to cellular redox reactions via the use of chemical mediators. The chosen chemical mediator is reduced with the aid of the microbial cell or other tissue used in the biosensor. The reduced mediator thereafter undergoes a re-oxidation reaction at the sensor electrode that has a fixed electrode potential. The overall result of this series of

redox reaction is a flow of current that is directly proportional to the metabolism occurring in the cells (Bentley, Atkinson, Jezek and Rawson, 2001). Microbial cells and tissues are useful in the transduction of the up-take of organic compounds and changes in cellular metabolism among others.

2.3.2 Affinity Based Recognition Elements

Affinity based recognition elements are more specific for their target analyte when compared to bio-catalytic based recognition systems. Such systems have been shown to not only possess specific binding nature but also high binding constants ranging from 10^{9}-10^{12} M^{-1} (Bhadoria and Chaudhary, 2011). Affinity recognition systems do not possess any catalytic activity whatsoever. The implications of the high binding constants and lack of catalytic activity exhibited by affinity based recognition systems is that they are best suited for use for real-time detection of target analyte as opposed to monitoring uses where bio-catalytic systems are better suited. The binding interactions that are present in affinity based systems between the affinity receptors in the sensing layer and the analyte are predominantly irreversible. It is however possible to disrupt the binding complex formed between affinity receptors and analyte by using buffer systems adjusted to a pH of 2 - 2.5. This disruption has have also been reported to occur at pH 3.5 (Katakura et al., 2000; Li et al., 2007; Reverberi and Reverberi, 2007; Bhadoria and Chaudhary, 2011; Devanaboyina et al., 2013). This is the primary consideration that is used to decide whether a sensor device should be single use only or re-usable. The high magnitude of binding constants highlighted above also give affinity based recognition systems the ability to detect analyte that may be present in samples in minute quantities (Lowe et al., 1990). The affinity based recognition elements that are routinely incorporated into affinity based biosensors are antibodies, DNA and RNA as outlined in the sections that follow.

2.3.2.1 Antibodies

Antibodies allow affinity recognition based biosensors the ability to rapidly and sensitively detect a wide variety of both pathogens and toxins. Antibodies, also known as immunoglobulin's (Ig's) are antigen-binding proteins that are found on the cell membranes of B-cells and secreted by plasma cells of the immune system.

The antibody molecule is made up of two identical L (light) chains and two identical H (heavy) chains. The light chains are polypeptides of molecular weight around 25,000 while the heavy chains are larger with molecular weight exceeding 50,000. The light chains are connected to their respective heavy chains via disulphide bonds, hydrophobic bonds and hydrogen bonds. The heavy chains are joined to each other through the same kind of non-covalent interactions (hydrophobic and hydrogen bonds) as well as disulphide bonds. The results of all the bond linkages result in the formation of a four chain structure of dimers are shown in Figure 2.5 (Kindt, Goldsby and Osborne, 2007);

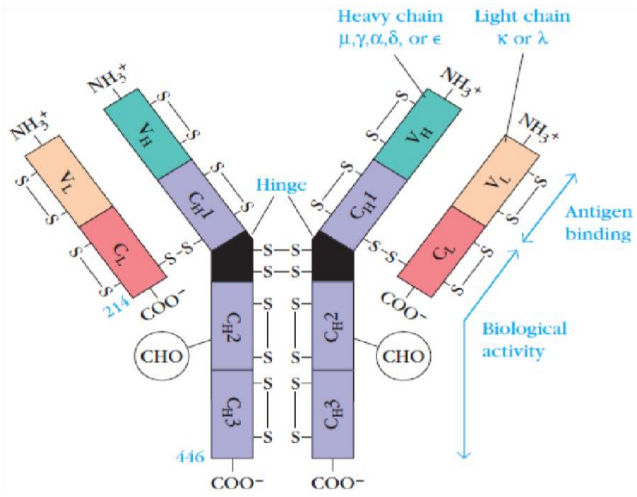

Figure 2.5: A diagram showing the structure of immunoglobulin's showing the heavy and light chains with the variable (V) region highlighted. The constant region (C) is also shown and the possible types of heavy and light chains are shown (Kindt, Goldsby and Osborne, 2007)

The carboxyl-terminal amino acid end of the antibody molecule is found in a region known as the F_c fragment that makes linkage to solid surfaces such as those of transducers possible. This carboxyl-terminal amino acid provides the basis of many antibody immobilization strategies that take advantage of the F_c fragment (Padoa and Crowther, 2006). *In vivo*, the F_c fragment binds to F_c receptors of various immune cells to induce immune mediation and activate the complement system. The F_{ab} fragments, also known as the N-terminal region, are the portions responsible for antigen binding as well as specificity (Schroeder and Cavacini, 2013).

Antibodies when used as affinity based bio-recognition elements in biosensors do not require sample purification before analysis. This lack of need for sample preparation is a big advantage in that analysis can be done with minimal or no prior preparation. This saves time especially in cases where such devices are used for diagnostic purposes (Singh, Poshtiban and Evoy, 2013).

Obtaining antibodies for biosensor applications can be a time consuming endeavour because production of polyclonal and monoclonal antibodies requires new immunizations to be undertaken each time antibodies are needed. This disadvantage has recently been circumvented by the development of recombinant technology which depends on selection of suitable antibodies from antibody gene libraries after which these can be generated in a relatively shorter period of time using bacteria such as *Escherichia coli* (Hock, 1997).

In vivo, molecules with sizes greater than 10 kDa are able to stimulate immune responses while those of smaller size require conjugation to larger macromolecules in order to stimulate a similar response. Because of their superb selectivity, antibodies are being harvested for use in both immunoassays and for biosensor applications. In their application in biosensors, antibodies are immobilized on transducer surfaces by either physical adsorption or by chemical adsorption through their amino, sulfhydryl, aldehyde and carboxylic groups. In order for immobilization to be effective, the transducer surface

should be pre-functionalised with either hydroxyl, carboxylic or amino groups. The most common transducers used for antibody immobilization are optical and acoustic (De Corcuera and Cavalieri, 2003).

2.3.2.2 Nucleic acids (DNA and RNA)

DNA and RNA bind with great affinity as well as specificity to their targets. These targets include small organic compounds, peptides, cells and tissue. DNA and RNA molecules have the ability to form secondary and tertiary structures that impart specificity for their binding to proteins as well as other targets. Nucleic acids are considered chemically equal to antibodies and have the advantage of being small in size with high specificity. Nucleic acids are generally used as short single-strands of oligonucleotides in biosensors. These single-strands of oligonucleotides bind to complementary nucleic acid strands in molecular targets such as proteins, cells and tissues (Ni, Castanares, Mukherjee and Lupold, 2011). Sensors based on nucleic acids are capable of detecting target analyte that may only be in trace amounts in samples and are useful for on-site monitoring of trace amounts of pollutants present in the environment. A graphic representation of a surface Plasmon resonance (SPR) biosensor incorporating a nucleic acid is shown in Figure 2.6. The nucleic acid in the SPR sensor surface bind their target analyte leading to a mass change and changes in the refractive index in the sensing layer. SPR sensors measure changes in the resonant angle that result from changes in refractive index in the sensing layer.

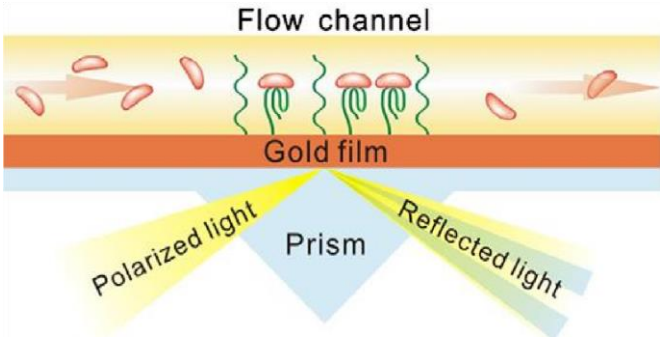

Figure 2.6: Graphic representation of a SPR-based nucleic acid biosensor (Song et al., 2008)

2.3.3 Transduction for Biosensors

Transduction methods for biosensors come in many forms but the most commonly used ones in biosensors are electrochemical, optical and piezoelectric. These are presented in the sections that follow.

2.3.3.1 Electrochemical Transduction

Biosensors that employ electrochemical transducers to determine analyte concentration in samples generally take advantage of reactions that either produce or generate electrons via enzyme catalysis. Such biosensors in most cases incorporate three types of electrodes: (i) a reference electrode (ii) an active electrode (iii) a sink electrode. The change in current that is measured by electrochemical biosensors results from reduction-oxidation reactions that produce current. The current produced is directly proportional to the concentration of the electrically active species in the sample (Gonsalves, Halberstadt, Laurencin and Nair, 2007). Electrochemical techniques that are commonly used in biosensors include impedimetric, potentiometric and amperometric. Electrochemical biosensors that use amperometric transduction are the most common type of electrochemical biosensors available. Three types of amperometric biosensors are shown in Figure 2.7.

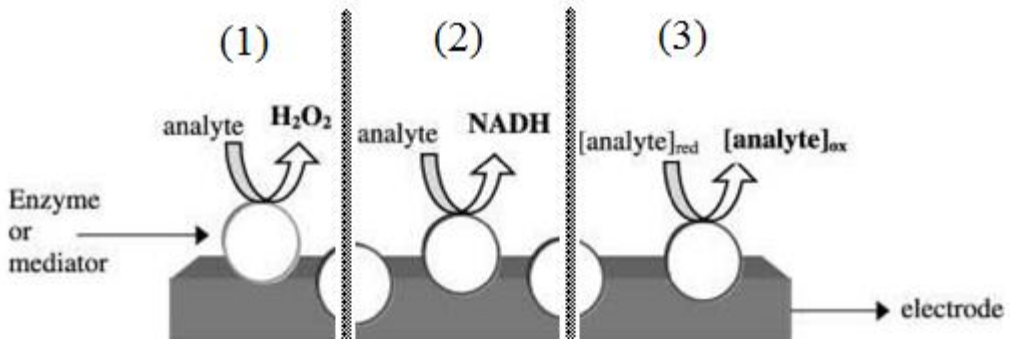

Figure 2.7: Amperometric biosensors based on (1) oxidase enzymes (2) dehydrogenase enzymes and (3) redox reactions (Prodromidis and Karayannis, 2002)

Amperometric biosensors based on oxidases as shown in Figure 2.7 (1) above, generate hydrogen peroxide that is measured at the anode while those based on dehydrogenases shown in Figure 2.7 (2) above catalyse the reduction of NAD+ to NADH whose concentration is directly proportional to the concentration of the analyte. Amperometric biosensors based on redox reactions as shown in Figure 2.7 (3) above generate electrons that are measured at the anode. These biosensors are relatively affordable with high sensitivity as well as offering the potential for production of devices that are small and portable (Patel, 2002).

2.3.3.2 Optical Transduction

A number of optical transduction methods have been used in optical-based biosensors but the most common include surface Plasmon resonance, fluorescence spectroscopy, interferometry and guided mode spectroscopy that uses grating couplers and resonant mirrors (Velasco-Garcia, 2009). Surface plasmon resonance (SPR) is the optical technique most widely used in optical biosensor setups. SPR when used in biosensors gives good implementation of label free sensing. It enables real-time investigation of bio-molecular interactions between the bio-recognition elements in the sensor and the analyte in samples (Hahnefeld, Drewianka and Herberg, 2004). In SPR an analyte in a sample that is in the soluble phase is bound to an affinity based ligand that is immobilized on the biosensor

surface and measured in real-time using optical detection. SPR devices will typically be composed of a light emitting diode (LED) emitting near infrared light, a prism attached to the biosensor surface and a position-sensitive diode array detector as shown in Figure 2.8. The sensor surface has a refractive index that varies with the binding of analyte in the sensing layer. The change in refractive index that occurs in the sensing layer is directly related to the increase in mass of analyte bound. This is the same for all proteins and peptides but minor variations have been seen for glycoproteins and nucleic acids (Stenberg, Persson, Roos and Urbaniczky, 1991). Figure 2.8 shows a Biacore SPR sensor setup.

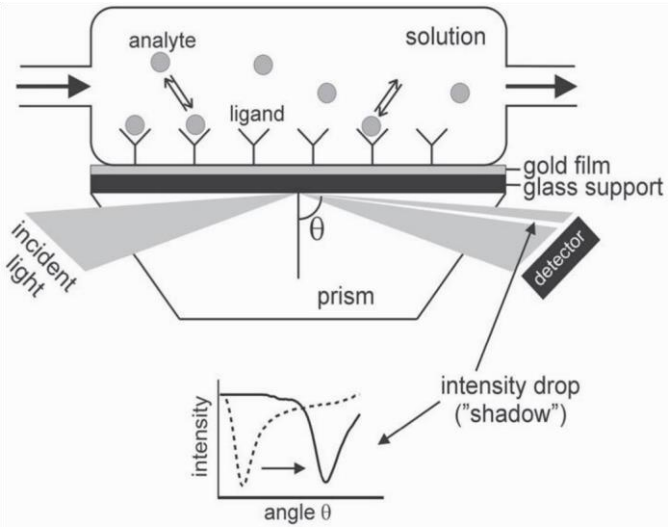

Figure 2.8: An SPR sensor setup as used in Biacore instruments (Hahnefeld, Drewianka and Herberg, 2004)

Figure 2.8 illustrates the generation of surface plasmon resonance phenomenon when light is totally internally reflected from a surface that is coated with a thin metal film at the interface of two media with different refractive indices. The difference in refractive index in this case occurs at the interface of the microfluidic solution (containing the sensing layer) and the glass prism.

2.3.3.3 Piezoelectric Transduction

Biosensors that are piezoelectric-based contain piezoelectric crystals of quartz as transducers. An example of such a sensor is the quartz crystal microbalance (QCM). The QCM was first elaborated by Sauerbrey in 1959. The mass sensitivity of gas phase mass deposition on a piezoelectric quartz crystal (PQC) has been demonstrated (Sauerbrey, 1959), (Bunde, et al., 1998). Sauerbrey's equation is shown in Equation 2.1.

$$\Delta F = -\frac{2\int_0^2 \Delta m}{A\sqrt{\mu_q \rho_q}} = -C\Delta m \qquad \textbf{Equation 2.1}$$

Where ΔF is the measured frequency shift; $\int_0^2$ is the fundamental resonant frequency; Δm is the mass change in grams; A is the piezoelectrically active area of the electrode in $(cm^3)^{-2}$; is the shear modulus of quartz $(2.947 \times 10^{11} gcm)$; is the density of quartz $(2.648\ gcm^{-3})$; C is the mass sensitivity constant $(sg)^{-1}$. The quartz crystals resonate when an alternating electric field is applied and the resultant frequency of the oscillation is a function of the mass of the crystal. In biosensors that use antibodies immobilized on quartz crystals as the bio-recognition element, interactions between the antibodies and antigens in a sample lead to increases in the mass and a resulting change in the frequency of oscillation. Piezoelectric biosensors are available in two device setups;

(i) Bulk Acoustic (BA) devices which involve adsorption of analyte to their specific antibodies that are immobilized onto quartz crystals surfaces. The quartz crystals are connected to an oscillating circuit that detects resonance frequency changes dependent on the mass of the crystals. The crystal mass increase depends on analyte concentration and is inversely proportional to the resonant frequency.

(ii) Surface Acoustic Wave (SAW) devices which have an acoustic wave that travels on the surface of the quartz crystal with immobilized specific

antibodies. Interactions between an analyte and its antibody lead to a change in the frequency of the acoustic wave (Patel, 2002). The most common type of piezoelectric biosensor is a bulk acoustic device known as a quartz crystal microbalance (QCM).

A QCM biosensor system is shown in Figure 2.9.

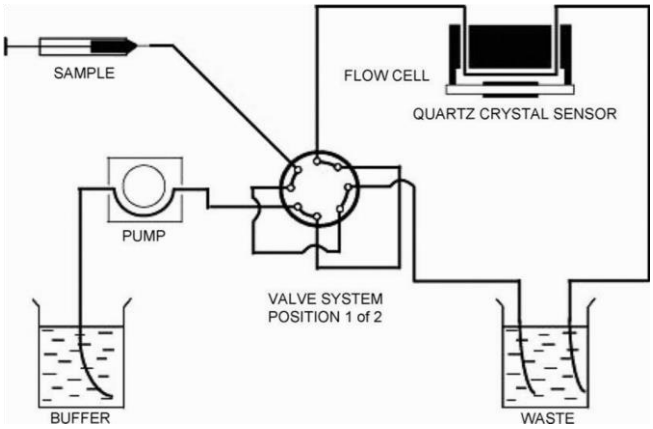

Figure 2.9: A schematic diagram of an Attana 80 QCM biosensor system (Jönsson, Anderson, Lindberg and Aastrup, 2007)

The diagram above shows the following components of a QCM biosensor.

(i) Buffer container: this is the reservoir of the buffer solution that acts as the vehicle for the sample injected into the biosensor

(ii) Pump: pumps the buffer and sample into the quartz crystal sensor and eventually into the waste liquid reservoir

(iii) Valve system: directs the flow of injected sample and buffer solution into the sensor while the excess is channelled into the waste liquid reservoir

(iv) Quartz crystal sensor: this is the component in which sensing of analyte occurs

2.3.4 Methods of Bio-Recognition Element Immobilization

In order for bio-recognition elements such as antibodies to be integrated with the biosensor, they need to be immobilized onto the transducer surface. Immobilization of the bio-recognition elements onto the transducer surface ensures that one cohesive biosensor unit is formed. The most useful immobilization techniques for biosensor application are (i) physical adsorption and (ii) chemical adsorption. Important considerations that need to be made when choosing an immobilization technique include the type of transducer or substrate surface to be used in the biosensor such as silver, gold, silicon or polymers. The kind of bio-recognition elements to be immobilized also needs to be considered. Biomolecules such as antibodies can be immobilized using both physical adsorption as well as chemical adsorption. Others such as nucleic acids and enzymes require immobilization on functionalized polymers, that is, polymers whose surface has been treated with compounds that possess reactive functional groups. For example avidin, streptavidin and biotin. The two main immobilization methods are presented.

2.3.4.1 Physical Adsorption

Physical adsorption is attraction or adherence of atoms or molecules to the surface of a solid to which they are in close proximity. Physical adsorption is the easiest technique available for biomolecule immobilization. It depends on physical interactions between the biomolecule and the transducer surface via ionic, Van der Waals, hydrogen bonding or hydrophobic forces without any need for pre-treatment with reagents. Physical adsorption does not alter the conformation of the biomolecule structure and is therefore advantageous in this regard. The binding interactions that occur between the transducer and the biomolecule are relatively weak and require substantially long periods of incubation in order to yield sensor layers that are useful for application (Scouten, Luong and Stephen Brown, 1995). Adsorption on solid surfaces is the easiest technique used for immobilization of biomolecules. Physical adsorption, as shown in Figure 2.10, relies

mainly on hydrogen bonding and hydrophobic interactions between the solid surface and the biomolecule (Jung, Jeong and Chung, 2008).

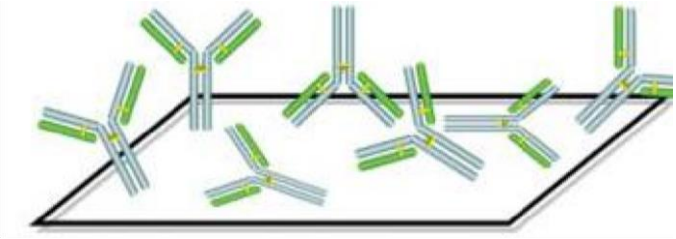

Figure 2.10: Random orientation of antibodies after physical adsorption (Jung, Jeong and Chung, 2008)

Physical adsorption of antibodies has the disadvantage of giving randomly oriented antibody layers that have vastly reduced antigen binding capacity. This method of antibody immobilization can in some cases result in only 10% of the antibodies showing antigen binding activity (Butler et al., 1993). Immobilization by physical adsorption via ionic bonding is shown in Figure 2.11.

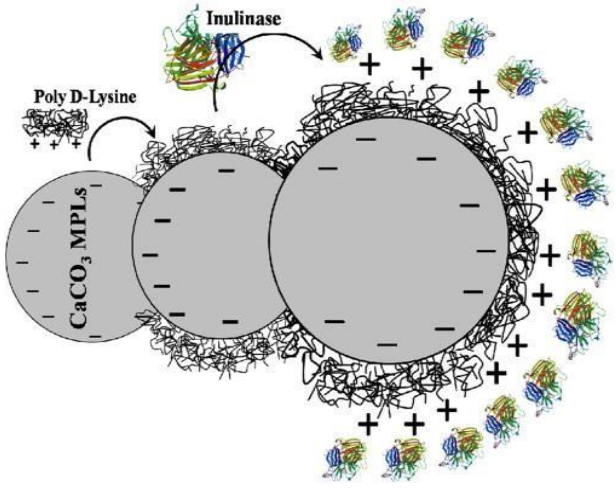

Figure 2.11: Immobilization by physical adsorption of endo-inulinase on poly-D-lysine coated $CaCO_3$ micro-particles via electrostatic interactions (Karimi et al., 2014)

In contrast to the reduced activity seen when antibodies are immobilized by physical adsorption, enzymes such the one shown in Figure 2.11 exhibit improved activity and specificity when immobilized using the physical adsorption method (Karimi et al., 2014). The performance of such enzymes can be improved through immobilization via ionic bonding on small immobilization supports (Gill, Manhas and Singh, 2006).

2.3.4.2 Chemical Adsorption

Chemical adsorption of biomolecules involves the formation of chemical bonds between the surface and the biomolecule in question. Chemical adsorption of biomolecules relies mainly on covalent bonding between the biomolecule and the transducer surface. This form of immobilization provides sensor layers that are very stable. This is due to the chemical modification that occurs between reactive functional groups present in both the biomolecules and on the transducer surface. If the biomolecule being used is a protein then the available functional groups are numerous. A few of these groups are:

- Amino: ($-NH_2$)
- Thiol: (-SH)
- Disulphide: (-S-S-)
- Phenolic groups:

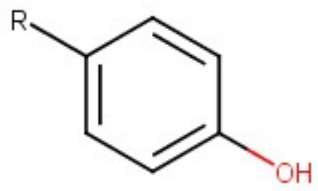

- Guanidine groups:

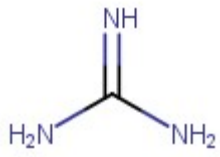

- Thioester groups:

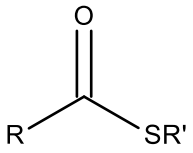

- Hydroxyl groups: (-OH)

- Imidazole's:

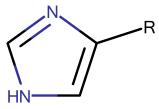

- Indole's:

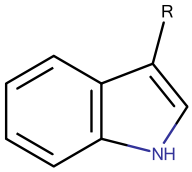

In order for chemical adsorption to be effective, the functional groups targeted for immobilization should not be in the active site of the protein. Immobilization via functional groups located in the active site leads to loss of biological activity that renders the biosensor ineffective in its intended application. However, protein immobilization via sites that are near the active site of enzymes may be advantageous in certain cases because it may lead to hyper-activation of the enzyme and therefore better sensor performance (Hernandez and Fernandez-Lafuente, 2011).

Antibodies are usually chemically adsorbed onto surfaces by covalent bonding. The surfaces are chemically activated prior to immobilization to make the process more

efficient. The F_c fragments of antibodies contain carboxylic acid groups through which coupling with reactive groups in activated surfaces is made possible. Antibodies also have amino groups in the F_{ab} fragments which can interact with groups such as epoxy, aldehyde and *N*-hydroxysuccinimide in activated surfaces (Jung, Jeong and Chung, 2008). It is more desirable to immobilize antibodies via their F_c fragments to ensure that the antigen binding F_{ab} fragments are free and oriented in a manner that allows ease of access to antigens in sample solutions. The disulphide bridges present in both F_{ab} and F_c region have also been used for immobilization as have the carbohydrates present in the F_c region (Jung, Jeong and Chung, 2008). Figure 2.12 shows an illustration of chemical adsorption immobilization of proteins.

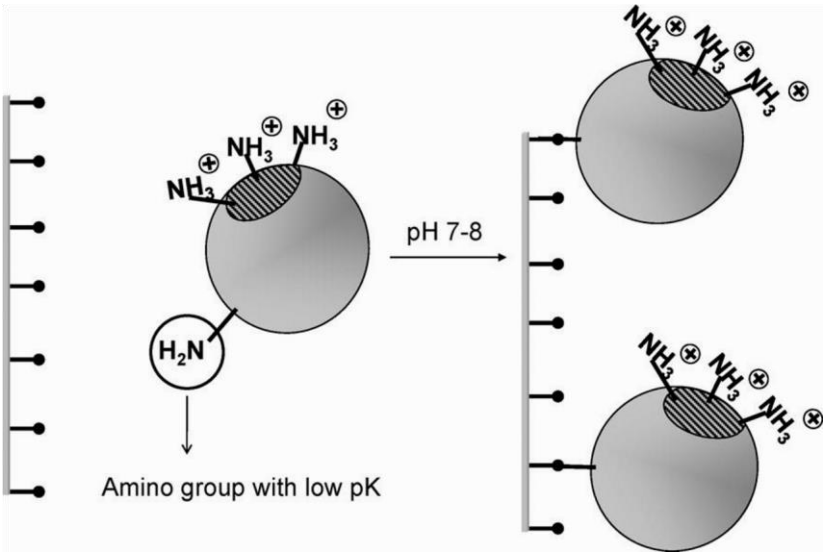

Figure 2.12: Chemical adsorption immobilization of proteins via reactive amino groups (Hernandez and Fernandez-Lafuente, 2011)

The graphic image above depicts site-directed immobilization of a protein. Site directed immobilization is used to control the orientation of immobilized biomolecules as this plays a critical role in their function. Control of immobilization using such conditions as, for example, high ionic strength can help to give highly oriented immobilized proteins (Pessela et al., 2006).

2.4 Biosensor Detection Methods

A variety of detection methods are available for application to biosensor systems. Generally, no more than one method of detection is appropriate for deployment in a biological assay used in a biosensor setup. The following detection methods are representative of the types of techniques used in antibody based biosensor devices:

2.4.1 Fluorescence Detection

This method of detection is widely used in antibody based biosensors. Fluorescence detection is also used in nucleic acid/protein detection and quantification. Fluorescent detection systems typically consist of the components highlighted in Figure 2.13.

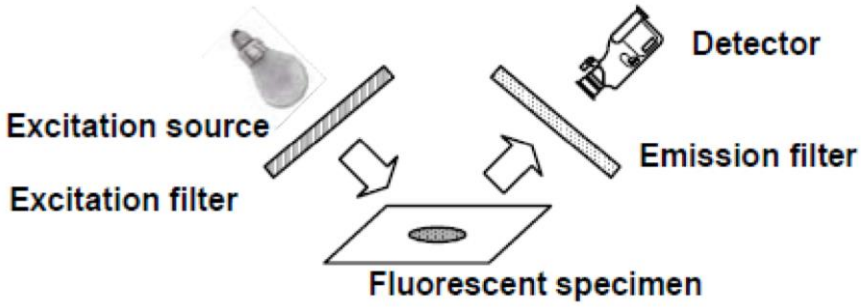

Figure 2.13: Basic Components of Fluorescence Detection System (Agah et al., 2005)

Molecules in a sample at room temperature occupy the lowest vibrational level of the ground state (V_1 in Figure 2.14). When energy in the form of heat, light or electrical energy is applied to the sample, the molecules are elevated to states of higher energy known as the excited state (S_1-S_3 in Figure 2.14). Once in the excited state, the molecules can undergo vibrational relaxation to lower energy excited states shown by the curved yellow arrow in Figure 2.14. When the molecule in excited state S_1 relaxes back to the lowest vibrational level in the ground state, a photon of light is emitted as fluorescence. The emission occurs in all directions and the wavelengths of light emitted corresponds to the

difference in energy between the excited state and the ground state. The scheme for fluorescence emission is shown in Figure 2.14.

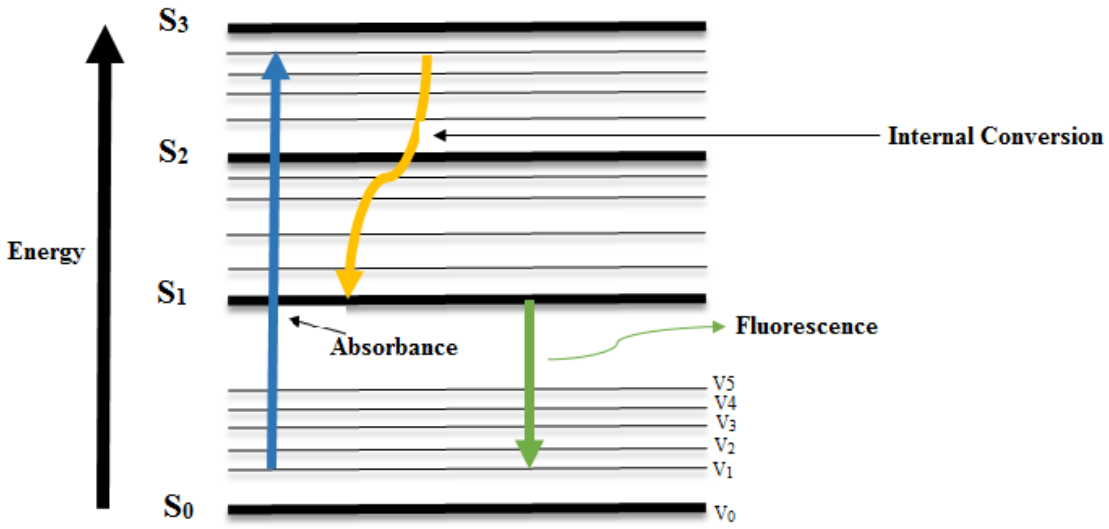

Figure 2.14: Jablonski diagram showing fluorescence emission

In fluorescence detection the excitation source produces a single frequency excitation as it passes through a sample. The sample then emits a photon of different frequency which is detected by the fluorescent detector. Two main types of fluorescence detection systems are available. One such system uses a photomultiplier tube as the detector. In this system, the light from the excitation source is passed through the sample and a photomultiplier tube detects the emitted light. The other type of fluorescence system uses a monochromatic light source for excitation and the emitted fluorescence is measured using a two dimensional detector such as a Charge-coupled device (CCD) cameras (Agah et al., 2005).

2.4.2 Bioluminescence Detection

The emission of light by living organisms or by a biochemical reaction is known as bioluminescence. Bioluminescence occurs when there is a conversion of chemical energy

to light with little or no heat evolved in the process. Most bioluminescence involve reactions catalyzed by the enzyme luciferase which oxidizes luciferin to oxyluciferin with the emission of light as shown in Figure 2.15.

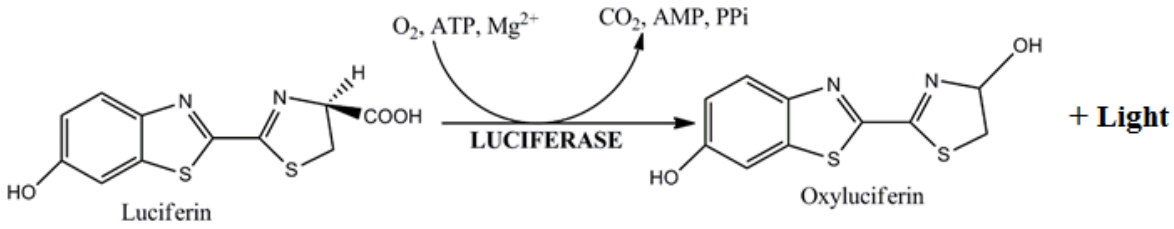

Figure 2.15: Bioluminescent reaction catalysed by Luciferase (Marques and Esteves da Silva, 2009)

In the initial stage of the reaction shown in the diagram above, adenosine triphosphate (ATP) reacts with the luciferase and luciferin in the presence of magnesium ions. Pyrophosphate and a complex of luciferase-luciferyl-adenylate are formed in the reaction. This complex then reacts with molecular oxygen and is raised from the ground state of low energy to an excited high energy state. The complex then loses energy by emission of a photon of light while returning to the ground state (Encyclopedia Britannica, 2014).

The amount of light emitted from bioluminescence is usually very small and cannot be detected with the naked eye. It therefore, requires special equipment such as ultra-sensitive CCD cameras to image the bioluminescence to an external visual system or an equally sensitive photo-detector. Figure 2.16 shows a bioluminescence biosensor.

The important components of the bioluminescence biosensor are:

(i) Micro-fluidic Channel: the sample containing the analyte of interest is injected through this channel which directs the flow of sample solution in the reaction chamber.

(ii) Micro-Reaction Chamber: this chamber contains luciferase producing bacteria fixed to a matrix formed from numerous tiny rods. The chamber has an inlet from the micro-fluidic channel allowing sample solution in and an outlet channel to allow the exit of waste liquid.

(iii) Photo-Detector: the photo-detector detects any bioluminescence emitted by the bacteria reacting with the sample in the reaction chamber.

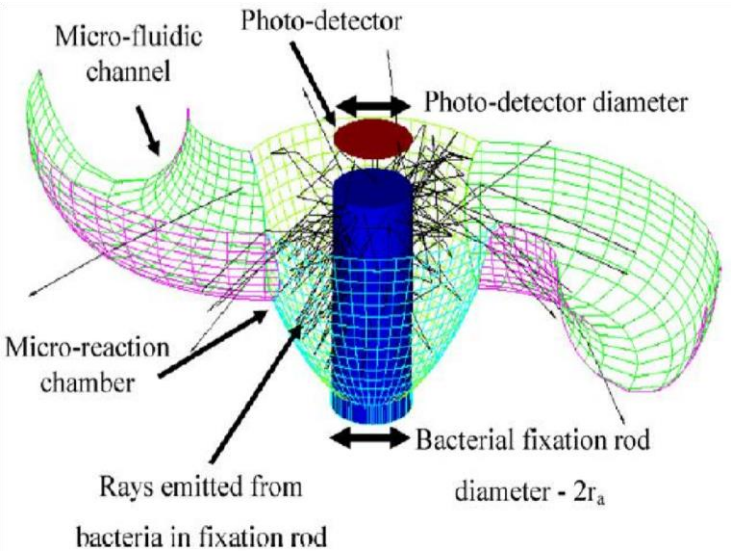

Figure 2.16: A schematic of a bioluminescence based biosensor (Ben-Yoav et al., 2009)

Bioluminescence detection is a relatively cheap method of detecting microorganisms in samples. The sensor is usually designed as a single chip that requires a low power input which is beneficial for use in field testing far from the laboratory (Ben-Yoav et al., 2009).

2.4.3 Light Scattering and Absorption Detection

Light scattering involves the detection and measurement of light scattered from a source while absorption detection measures the changes in intensity of the excitation source that passes through the sample solution due to such factors as reflection, scattering and absorption. The intensity of a beam of monochromatic light passing through a sample containing absorbing molecules reduces with increasing concentration of the molecules as shown in Figure 2.17.

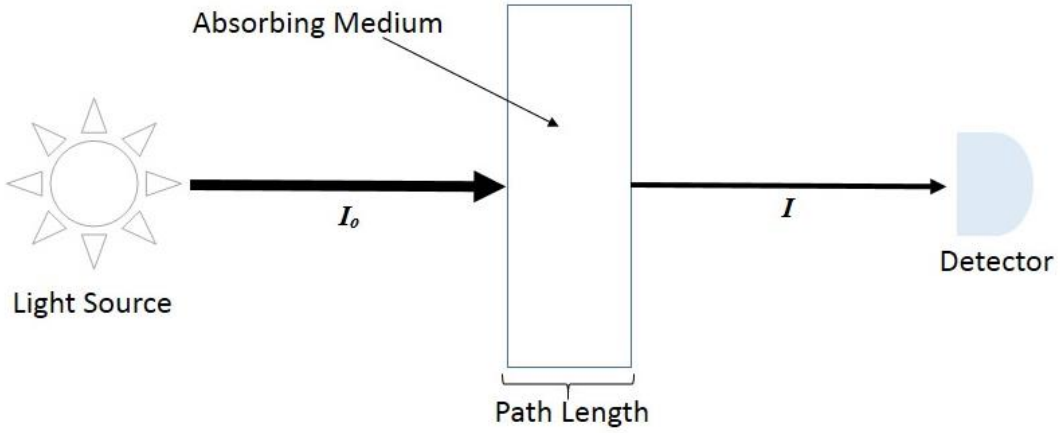

Figure 2.17: Attenuation of an absorbed light beam

Where I_o and I are incident and emergent beam respectively.

The intensity of the light decreases because energy is transferred from the incident beam of light to the absorbing molecules resulting in reduction in the emergent beam intensity. An increase in the length of the path through which the light must travel leads to greater reduction in the intensity of the light while a decrease in the path length has the opposite effect. The law that governs this absorption process is the Beer-lambert law shown in Equation 2.2 (Skoog, West, Holler and Crouch, 2004):

$$A = \varepsilon bc \qquad \textbf{Equation 2.2}$$

Where *A* is the absorbance, ε is the molar absorptivity in $Lmol^{-1}cm^{-1}$, b is the path length in cm and *c* is the concentration in gL^{-1}.

The change in intensity that occurs when light passes through absorbing species can be exploited to measure antigen-antibody reactions in solution. Antigen-antibody reactions form precipitates in solution that absorb light in the same concentration dependent manner highlighted above. Figure 2.18 shows an absorption detector.

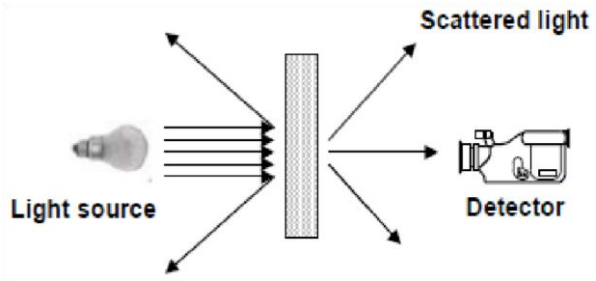

Figure 2.18: Basic Absorption Detector (Agah et al., 2005)

A scattering optical analysis system is shown in Figure 2.19. The most common detectors used in absorption and scattering systems are photodiodes and photomultiplier tubes. Photodiodes are made of semi-conductor material that converts photons of light energy into current through the photoelectric effect. Photomultiplier tubes on the other hand consist of a series of vacuum phototubes that can multiply the current produced by incident photons of light energy striking a photocathode and generating electrons.

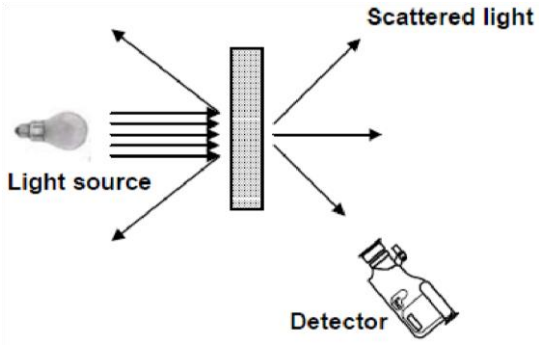

Figure 2.19: Basic Scattering Optical Analysis Systems (Agah et al., 2005)

2.4.4 Electrochemical Detection

This involves electrochemical detection of residues of biological entities and is based on detecting the change in electrical quantity such as voltage, current impedance or charge. Electro-active polymer systems play a major role in the design of electrochemical biosensor systems and they are suitable for integration into such devices due to their ability to conduct current. The current results from chemical reactions that occur between substances imbedded into their surfaces and specific substances in their environment (Agah et al., 2005). Bio-electrochemical reactions that are detected by electrochemical biosensors generate either current, accumulation of charge or may change the conductivity of the media in which electrodes are suspended. Electrochemical detection requires a reference electrode, a counter electrode and a working electrode. The bio-electrochemical reactions usually occur near the working electrode surface which in turn acts as the transduction element in the reaction while the counter electrode acts as a connector to the solution where the electrolysis occurs. Conducting stable material such as gold, platinum, silicon and carbon are popular for use as electrodes in electrochemical detection based biosensors (Grieshaber, MacKenzie, Vörös and Reimhult, 2008).

2.4.5 Surface Plasmon Resonance

Surface plasmon resonance is the process that occurs when polarized light hits a metal film under conditions of total internal reflection (Frischeisen et al., 2008). Light passing through a prism tends to bend towards the plane of the interface especially when passing from a relatively dense medium to a comparatively less dense one. If a circular prism is used and the incidence angle of the light changed, the light going out reaches a critical angle at which all the light entering the circular prism is all reflected in a phenomenon known as total internal reflection (TIR). When TIR occurs, no light entering the prism will be able to exit but an electric field of photons is formed that extends outside the surface of reflection (Daghestani and Day, 2010). Surface Plasmon resonance phenomena is shown in Figure 2.20. Thin films of gold with one surface functionalized with antibodies against a specific analyte of interest and facing away from the polarised light while the other surface is fused to a thin film of polymer are normally used (Lee, Goodrich and Corn, 2001).

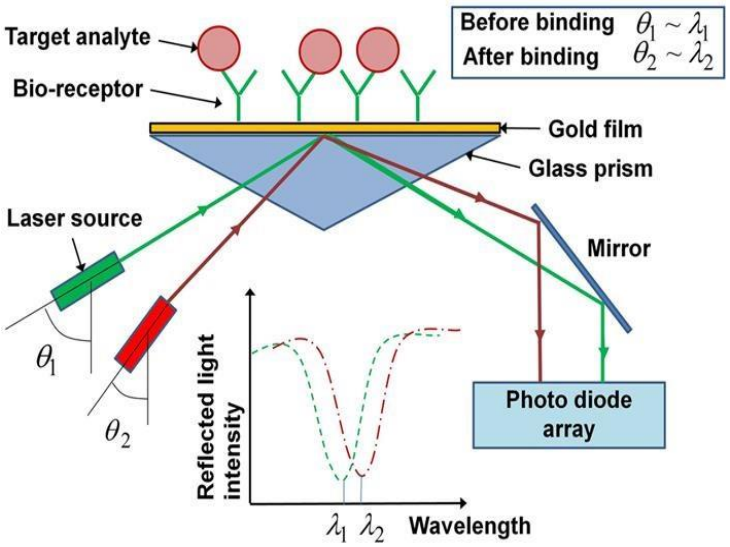

Figure 2.20: Graphic representation of surface Plasmon resonance (http://www.bionavis.com/en/)

Aluminium films have also been used in devices that use UV light to generate surface Plasmon's due to its more favourable cost compared to gold films (Gryczynski et al., 2004).In surface Plasmon resonance, the polarised light generates a photon electric field that interacts with free conduction band electrons on the surface of the metal. Once the photons of light are absorbed by these electrons, they are excited by the energy transfer and are converted into surface Plasmon's. Photons of light and electrons both have wave and particle behavioural properties and a Plasmon is generally described as the particle name for electron density waves. When photons are transformed into Plasmon's, there is a conservation of momentum and energy. When the momentum of a photon equals that of the Plasmon's, resonance occurs. Photons and Plasmon's both possess vector functions that have magnitude plus direction. Any time either the angle of incidence of the light or the wavelength is changed the magnitude of the vector functions changes as well. In the case of metal films the vector quantity is parallel to the reflecting surface and the incident light energy must correspond to the angle of incidence in order for SPR to be observed. An electric field results from the reflected photons on one side of the metal film surface while a similar electric field forms on the other side of the metal film that radiates into the micro fluidic environment of the other side of the film. The second electric field is known as an evanescent wave due to the fact that its amplitude reduces with an increase in distance from the metal film surface (Nagata and Handa, 2000). Factors that affect surface Plasmon resonance angle are (i) the wavelength of incident light (ii) properties of the metal film (iii) the refractive index of the medium on the side of the metal film opposite to the incident light (Markey, 1999). In cases where the media interfaced with the metal film (that is, on the side functionalised with antibodies) changes due to bio-molecular reactions such as antigen-antibody interactions, the refractive index of the medium is altered and this affects the velocity of the Plasmon's. Therefore, this change in the sensor surface consequently leads to changes in the angle of the incident light at which the surface Plasmon resonance is observed. This provides an opportunity for accurate measurements of bio-molecular interactions to be made (Akimoto, Sasaki, Ikebukuro and Karube, 2000).

The angle at which resonance occurs when the medium undergoes changes is called the Resonant Angle though in most cases it is known as the Angular Surface Plasmon Resonance. The wavelength of the light can be varied while maintaining the same angle of incidence until SPR is observed (Quinn et al., 2000).

2.4.6 Fourier Transform Infrared Spectroscopy (FTIR)

Fourier transform infrared (FTIR) spectroscopy has recently become prominent as a technique used for the detection of bacteria in samples. This technique employs the use of infrared radiation (λ = 2.5-25 μm) as the source of energy in order to excite molecules in samples. When a molecule absorbs infrared light, it undergoes changes in its vibrational motions. Two or more atoms that are bonded together via covalent bonds are generally not motionless in space but the bonds between them tend to stretch and bend. The bending and stretching vibrations are synonymous with the vibrational modes that a given molecule can undergo (Smith, 2010). The available modes of vibration in the IR region for molecules is shown in Figure 2.18.

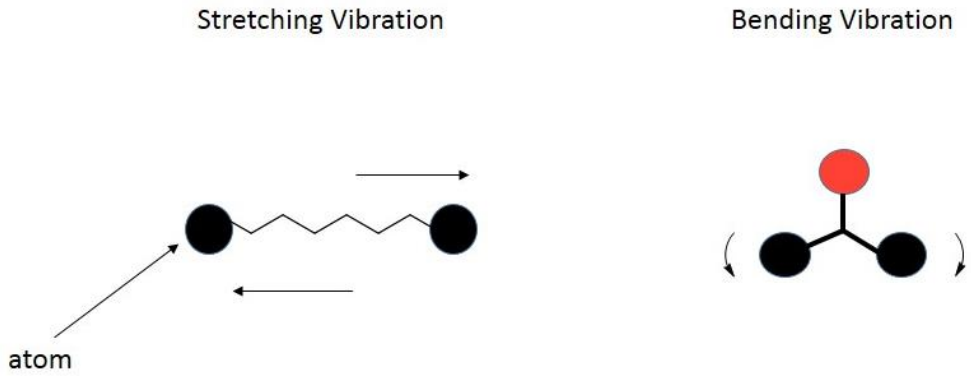

Figure 2.21: Vibrational modes available to molecules in the IR region

Since the vibrations are quantized, they are observed only at defined frequencies of infrared light. Any time the frequency of the infrared light and the frequency of a given vibrational mode match, the light is absorbed leading to an increase in the magnitude of a

bond stretching or bond bending vibration. Bonds of different types tend to vibrate at different frequencies and will hence absorb different frequencies of infrared light. Therefore, infrared spectroscopy is able to differentiate between different types of bonds in a molecule thus making it possible to ascertain the functional group that may be present in a given molecule under examination. In infrared spectroscopy, the functional group region occurs at wavenumber ≥ 1500 cm^{-1} while the fingerprint region occurs at < 1500 cm^{-1}. The functional group region will usually contain peaks for functional groups that absorb infrared light at a given frequency. The fingerprint region contains a complex number of peaks that are unique for every compound and are useful in determining the identity of a given compound (Smith, 2010).

CHAPTER 3: CONDUCTING POLYMERS FOR BIOSENSOR APPLICATION - POLYANILINE

3.1 Introduction

Polyaniline is a conducting polymer widely used in many applications that has gained interest for application in biosensors. This is due to its favourable optical and electrical properties plus its ease of synthesis and use (Davis and Higson, 2007). Davis and Higson (2007) report that the use of polymers as thin films in biosensors can improve selectivity of sensors by hindering adulterants from reaching the active sites of the sensor. Polyaniline is also biocompatible and can be used in sensor surfaces that have integrated biomolecules such as antibodies. The method most widely used for preparation of polyaniline is chemical polymerization of aniline monomers with a wide range of oxidizing agents though catalysts have been used as an alternative for preparation. Thin films of polyaniline can be made either by in situ polymerization on suitable substrates such as glass or metal, dip coating or by spin coating. The film thickness in *in situ* polymerization depends on the polymerisation time of the substrate while it depends on the spin rate and time of rotation for spin coating. Dip time affects the thickness of films prepared by dip coating method. Optimal film thickness of polyaniline for biosensor applications is essential. Other than good biocompatibility, polyaniline thin films also have good environmental properties coupled with excellent electrical and chemical stability (Stejskal, Kratochvíl and Jenkins, 1996). The physicochemical properties of polyaniline depend on the form in which it exists. The protonated (conducting) and non-protonated (insulating) forms of polyaniline are shown in Figure 3.1.

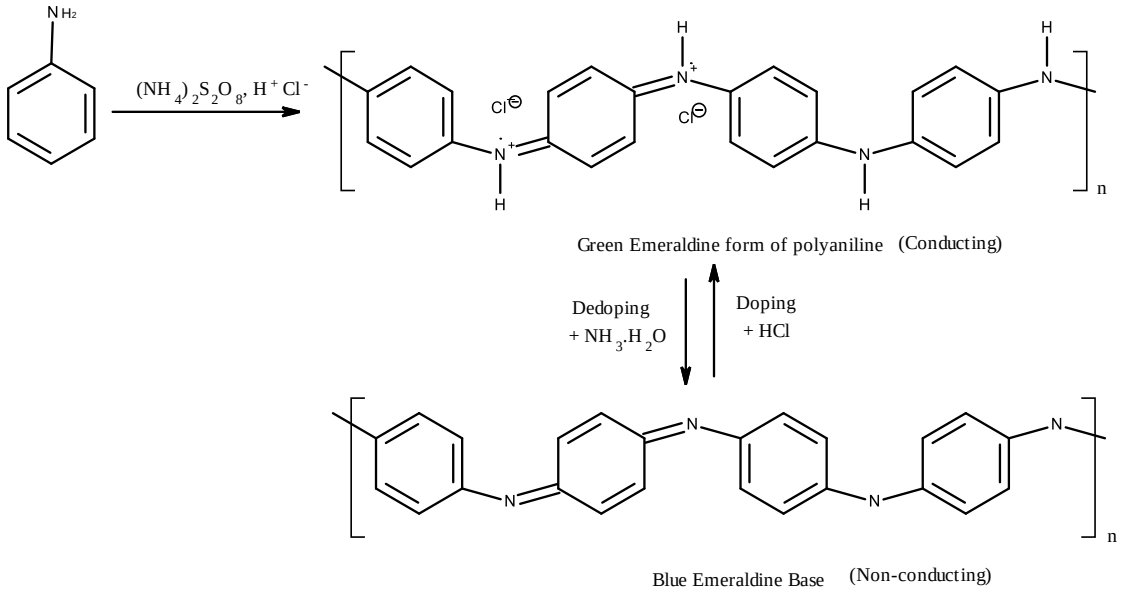

Figure 3.1: The green (protonated) and blue forms of polyaniline (Srinivas et al., 2012)

The emeraldine green polyaniline is the predominant form in which this polymer exists after completion of polymerisation. Emeraldine green polyaniline is the protonated form of the polymer and has conductivity that is much like that of semiconductors, that is, 10 S/cm. This conductivity is much higher than that of most conducting polymers which generally have a conductivity of $< 10^{-9}$ S/cm. Metals, however, have higher conductivities than polyaniline (usually > 104 S/cm) (Stejskal, Kratochvíl and Jenkins, 1996).

3.1.1 Synthesis of Polyaniline

Stejskal (2002) in his IUPAC technical report, described the standard preparation of polyaniline. In his method aniline hydrochloride was oxidized with ammonium peroxydisulphate in aqueous conditions. The polymerization was then allowed to continue for 24 hours after which the precipitated polymer was collected (Stejskal and Gilbert, 2002). Sapurina and Shishov (2012) report that the oxidative polymerization of aniline is achieved through two closely related mechanisms one of which involves the aniline monomer being subjected to a chain reaction leading to the formation of well-arranged

macromolecules while the other involves the growing chains of polyaniline (PANI) being arranged into interlinked supramolecular structures (Sapurina & Shishov, 2012). The structures formed are further reported by Sapurina and Shishov (2012) to appear as either one-dimensional, two-dimensional, that is, planar in nature or as three-dimensional structures. The one-dimensional structures may be nanofibers, nanorods or nanotubes while the two and three-dimensional structures may be ribbons, nanobelts, nanoplates and microspheres, nanospheres or granules respectively. These structures have been noted to grow in increasing complexity as the polymerization process continues (Stejskal and Gilbert, 2002). Initiation of aniline polymerization relies on the oxidant used and the pH of the reaction medium. Single-electron oxidation forms an anilinium dication radical (**E**) and a neutral aniline radical (**F**). Two-electron oxidation forms an aniline dication (nitrenium cation or nitrene) (Ciric-Marjanovic, 2013). Figure 3.2 illustrates these electron oxidations.

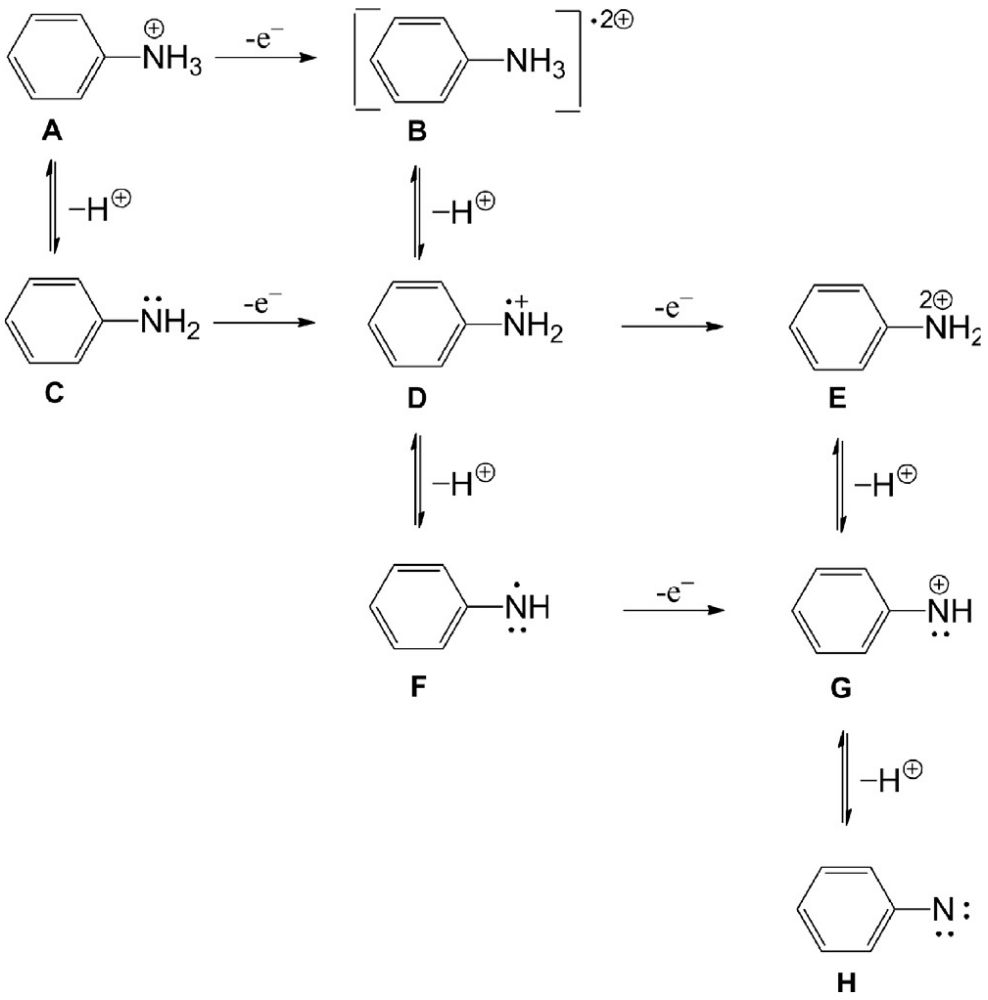

Figure 3.2: Electron Oxidations of Polyaniline (Ciric-Marjanovic, 2013)

It has been proposed that the deprotonation and electron transfer steps shown in Figure 3.2 may follow either C → D → E → G if conditions are acidic or C → D → F → G if reaction conditions are basic. The reactive species of PANI dimerise to form oligomers and polymeric structures via the following mechanisms shown in Figure 3.3.

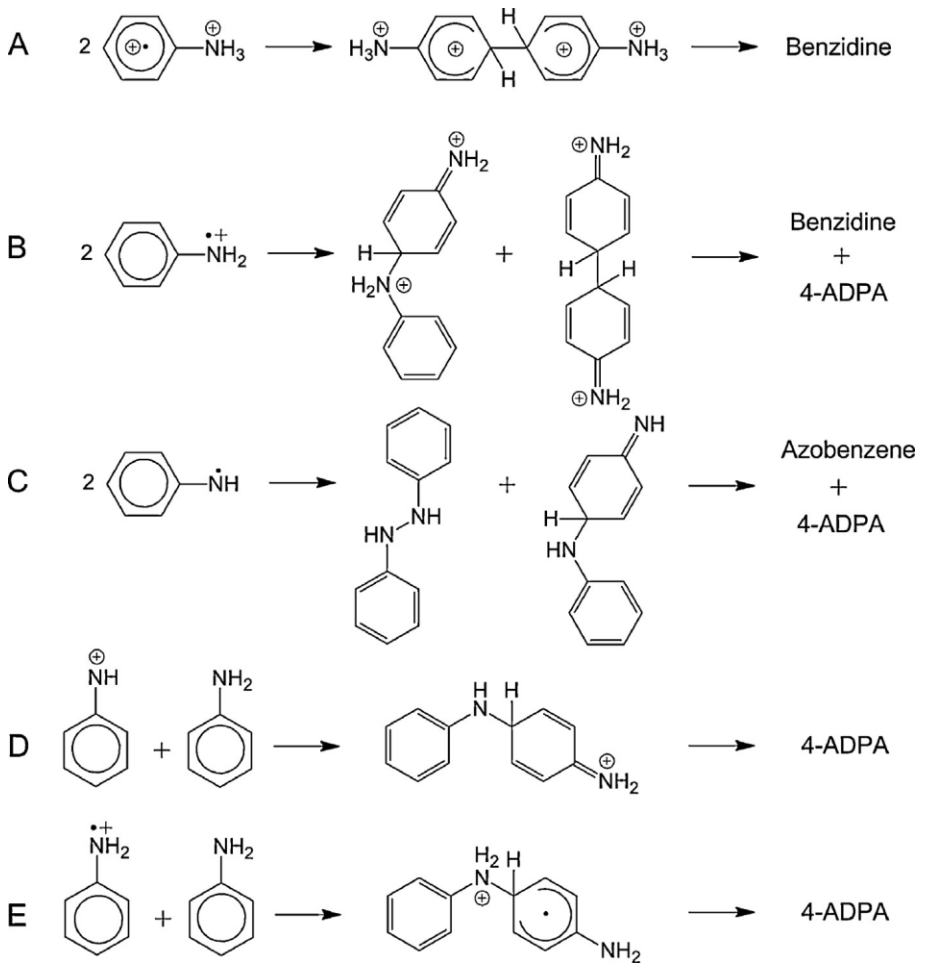

Figure 3.3: PANI Dimerization Products where 4-ADPA is 4-aminodiphenylamine (Ciric-Marjanovic, 2013)

The products obtained from the polymerisation scheme shown in Figure 3.3 indicate the complexity of the polymerisation of aniline that leads to the formation of complex supramolecular structures.

3.1.2 In Situ Polymerization of Polyaniline

This is a process used in the preparation of polyaniline thin films where the polymerization occurs on glass or other suitable support surfaces immersed in the reaction vessel. The substrates thus immersed in the aqueous acidic solution containing aniline and an oxidant

undergoes an in-situ adsorption of polymerized aniline on their surfaces and eventually become covered by a thin film of polyaniline (Stejskal, Sapurina, Prokeš and Zemek, 1999). Stejskal et al (1999) further report that glass supports removed from the reaction mixture after the polymerization process is completed have a layer of pernigraniline (the non-conducting emeraldine base) which is reduced to the emeraldine salt (conducting form) with the help of acidic solution of aniline. PANI films produced by this process are said to have smooth portions, globular deposits seen as granular micro-particles and portions with fibrous PANI Chain deposits (Armes et al., 1991). The mechanism of film formation was reported by Stejskal and Sapurina (2005) in their IUPAC Technical report where they demonstrated that the initial phase of film formation involved production of aniline oligomers that possessed lower solubility than the original anilinium cations present in the reaction vessel. The oligomers are said to be hydrophobic and tended to separate from the aqueous medium and readily adsorb onto any surface present in the reaction mixture. It was also found that the adsorbed oligomers had greater reactivity in initiating polyaniline chain growth due to their different electron density distribution compared to the original mixture (Stejskal and Sapurina, 2005). Also various reports confirm that polymerization occurs preferentially at surfaces in the reaction mixture before it occurs in the bulk mixture (Tzou and Gregory, 1992; Mazur and Blanchard, 2004). Figure 3.4 shows the three stages of thin film formation.

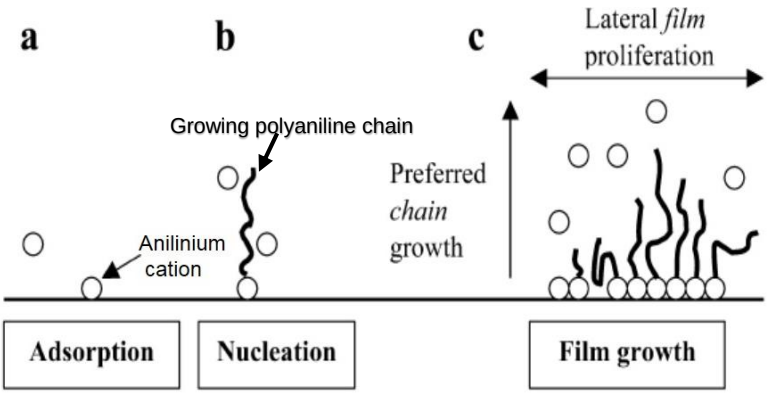

Figure 3.4: The Three Stages of Polyaniline Film Formation (Stejskal and Sapurina, 2005)

The electrical conductivity of the films produced by in-situ polymerization is comparable to that of the bulk polymer except where acid concentrations higher than 1 Molar are used. In such instances the conductivity of the thin films is higher than that of the bulk polymer (Stejskal et al., 1999). Electrical conductivity of polyaniline thin films can be measured by a four-point-probe coupled to a source meter where the film conductivity (σ_f) is calculated using conductivity of a hypothetical sample (σ_1) with a thickness of 1 cm and the actual thickness (d_f) shown in Equation 3.1.

$$\sigma = \sigma_1/d_f \qquad \textbf{Equation 3.1}$$

The conductivity of polyaniline at different voltages varies in a linear manner showing the direct proportionality in relationship between voltage and conductivity. Conductivity of polyaniline increases with increasing voltage especially in crystalline samples with highly ordered chain arrangements (Vivekanandan, Ponnusamy, Mahudeswaran and Vijayanand, 2011). Crystallinity of polyaniline can be improved by increasing the level of doping of the polymer and such films will consequently have a higher direct current (DC) electrical conductivity (Nath and Kumar, 2012; Ciric-Marjanovic, 2013; Ziadan and Saadon, 2012).

3.1.2.1 Properties of Polyaniline

The unique properties of polyaniline are not restricted to its good electrical conductivity but also extend to its optical properties. Polyaniline is reported by Ciric-Marjanovic (2013) to have high optical transparency in the UV-Visible region of the electromagnetic spectrum. Polyaniline also exhibits excellent transmittance (85%) in the infrared region especially around 550 nm (Lee, Park, Back and Lee, 2011). The interaction of polyaniline with light is governed by absorption coefficients (α) that are estimated after correction for losses due to reflection are made. The absorption coefficient for polyaniline is shown in Equation 3.2.

$$\alpha = (2.303 \div d) * A' \qquad \textbf{Equation 3.2}$$

Where d is the sample thickness and A' is the absorption of the sample and given by the expression $A' = A - A^o$ where A is the absorbance and A^o is the correction for reflection. Photon energy was shown by Ali et al (2008) to be directly proportional to both the absorption coefficient and the band gap energy ($\alpha h\nu$) of the polymer.

The properties highlighted above have made polyaniline a suitable polymer for both electrochemical and optical biosensor platforms among others.

CHAPTER 4: LITERATURE REVIEW

4.1 Polyaniline in Biosensor Application

A lot of interest has been generated in conducting polymers and their potential applications to biosensors. Shinohara et al (1988) reported an enzyme micro-sensor for the detection of glucose that utilized a glucose oxidase entrapped-polyaniline thin film on a platinum fibre film. This sensor showed excellent glucose oxidase activity due to the good permeability of the polyaniline to oxygen. The pore size of the polyaniline was also suitable for keeping out larger molecules that would have interfered with the biosensor performance thus the polyaniline imparted good selectivity and sensitivity enabling the sensor to detect glucose concentrations in samples at concentrations between 10^{-4} M to 5×10^{-3} M (Shinohara, Chiba and Aizawa, 1988).

Karyakin et al (1996) reported another biosensor based on polyaniline thin films. This sensor could detect *N*-benzoyl-L-arginine ethyl ester (BAEE) and organophosphate. As a BAEE biosensor, Trypsin was immobilized on the polyaniline thin films by physical adsorption. The thin films were incubated in trypsin solution overnight in a refrigerator set at 4 ^{o}C. This sensor was able to detect protons formed during the hydrolysis of BAEE by trypsin and had a response range of 5×10^{-5} – 10^{-2} M. PANI thin films without immobilized trypsin were used as a control and these showed no potentiometric response when compared to the trypsin-PANI electrodes. The BAEE biosensor showed cathode redox responses in potential that were independent of pH in weakly acidic solutions while at the same time showing anode responses in potential that were dependent on pH in the range 1-5. Based on these findings it was predicted that this biosensor would show a linear response in potential when used to detect BAEE in physiological solutions. Another biosensor with organophosphate hydrolase (OPH) immobilized on PANI thin films in the same manner as the trypsin was also reported by Karyakin et al (1996). This sensor was used for environmental monitoring. The OPH immobilized on PANI films catalysed the

hydrolysis of ester functional group in organophosphates. OPH was selected for its high selectivity for organophosphates. The OPH-PANI electrode showed a detection limit of 10^{-7} M which was the lowest for all biosensors based on potentiometric detection. The sensor had an excellent response time of 1-2 minutes but despite the low detection limit, it was not sensitive enough for use in environmental monitoring (Karyakin, Bobrova, Lukachova and Karyakina, 1996).

Polyaniline was used as a transducer in an amino acid biosensor reported by Langer and co-workers (2004). In this sensor choline oxidase was entrapped in nanoporous polyaniline such that electrons would be generated and transmitted through the polymer when the enzyme catalysed the breakdown of choline. The sensitivity of this sensor was increased when a fluctuating potential was passed through the polyaniline. This sensor showed sensitivities of 5 µA mmol/L when measured in amperometric mode and 10 mV mmol/L when measured in the potentiometric mode. Its detection limit was 20 mmo/L (Langer et al., 2004). Other polyaniline based biosensors such as the vitamin sensor, DNA sensor have been reported (Castelletti et al., 2002; Gooding, 2002).

An amperometric biosensor for detection of lactate was reported by Malhotra et al (2006). This sensor consisted of polyaniline thin films developed by electrochemical deposition on which was immobilized lactate oxidase (LOD) and lactate dehydrogenase (LDH). The enzymes where immobilized on PANI by physical adsorption method. This biosensor showed a linear response between the concentrations 0.1-1.0 mM of lactate with a detection limit of 5×10^{-5} M. The lactate sensor electrode composite of LOD/LDH/PANI was quite stable and could be used for three weeks when stored at temperatures ranging from 4 to 10 ^{o}C (Malhotra, Chaubey and Singh, 2006).

Barton et al (2009) reported a label-free impedimetric biosensor for the detection of bovine serum albumin (BSA). The sensitivity of this sensor was in the pg/ml range. The important components of this biosensor were carbon-polyaniline composite electrodes

with entrapped anti-BSA antibodies, an auto alternating current (AC) frequency response analyser and a potentiometer. Entrapment of anti-BSA antibodies in the carbon-polyaniline composite electrodes was achieved by electro-polymerisation of aniline-antibody acetate buffer mixture. When a sample of BSA in the range 0-100 ng/ml was introduced, the biosensor showed a linear response. However, when concentrations exceeding 100 ng/ml were used a plateau was observed in the calibration curve. The plateau was characteristic of biosensor binding site saturation. The biosensor had better sensitivity for bovine serum albumin than the previously reported 10 µg/ml. Despite the biosensor showing outstanding sensitivity, its low concentration saturation was a serious limiting factor because any BSA levels exceeding 100 ng/ml could not be accurately determined. However, it had a good lifespan of about 12 weeks with loss of sensitivity only seen after a further 4 weeks (Barton et al., 2009).

A review conducted by Dhand et al (2011) reported a number of other biosensors based on polyaniline. These biosensors included (a) PANI based peroxidase biosensor (b) PANI based glucose biosensor (c) PANI based cholesterol biosensor (d) PANI based DNA biosensors (Dhand, Das, Datta and Malhotra, 2011).

Prathap et al (2012) reported a polyaniline-based biosensor for the selective detection of γ-hexachlorocyclohexane (γ-HCH), an organochlorine pesticide commonly known as lindane. The biosensor consisted of genetically engineered *E.coli* immobilized on polyaniline thin films. The *E. coli* possessed γ-hexachlorocyclohexane (γ-HCH) dehydrochlorinase (LinA2), an enzyme involved in the hydrolysis of lindane. When samples containing lindane where injected into the biosensor, rapid hydrolysis with evolution of hydrochloric acid occurred. A change in the conductivity of the polyaniline films was also observed and this was detected amperometrically. The biosensor had excellent sensitivity and could detect lindane present in parts-per-trillion (ppt) concentration. Additionally, at concentration of lindane between 2 and 45 ppt, linear calibration graphs were obtained showing a direct proportionality between lindane

concentration and conductivity. The sensor was also highly selective for lindane and did not show any conductivity changes when other pesticides such as trichlorobenzene, dichlorodiphenyltrichloroethane (DDT) and 1, 1-dichloro-2, 2-bis (p-chlorophenyl) ethylene (DDE) (Anu Prathap, Chaurasia, Sawant and Apte, 2012).

It is important to re-state that polyaniline use in biosensor applications has been used due to its good conductivity, ease of synthesis, good stability to heat, high biocompatibility and good electrochemical and environmental stability (Chiang and MacDiarmid, 1986).

4.2 Polyaniline-Based Biosensors for Pathogen Detection

Tahir and Alocilja (2003) reported a polyaniline-based conductimetric biosensor. This sensor incorporated anti-*E. coli* and anti-*salmonella* polyclonal antibodies as opposed to monoclonal ones. The antibodies were immobilized on polyaniline with interconnecting silver electrodes on either side. Polyaniline was used in this biosensor as the vehicle through which electron transport could occur across the silver bridges. Whenever antigen-antibody complexes were formed the conductance increased resulting in an increased signal output. The layout of the biosensor is Figure 4.1**.**

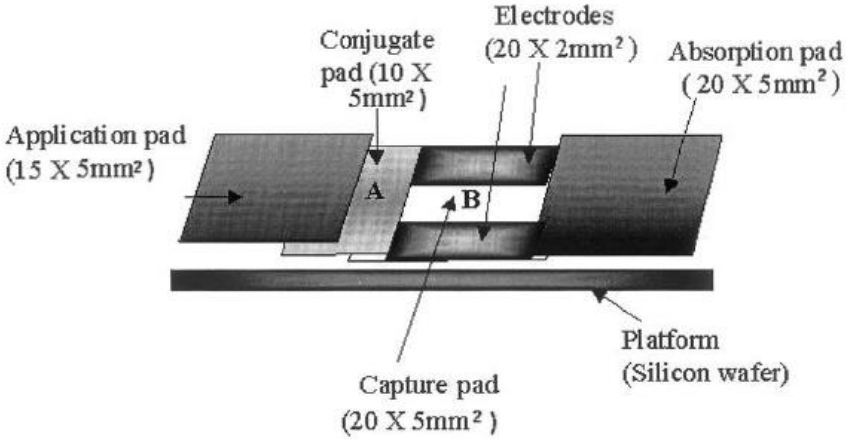

Figure 4.1: Tahir and Alocilja's Biosafety Biosensor (Muhammad-Tahir and Alocilja, 2003)

Figure 4.1 shows the important components of the biosafety biosensor described by Tahir and Alocilja (2003). The antibody-polyaniline conjugate pad is shown as (A) in the diagram while the capture pad is shown in (B). An expanded view of the capture membrane is shown in the Figure 4.2. This particular biosensor was developed for the detection of *E. coli* 0157:H7 and *Salmonella* species, two bacteria implicated as biosecurity hazards. The sensor showed a linear response in in the concentration range between 10 to 10^3 CFU/ml, 10 to 10^4 CFU/ml and 10 to 10^5 CFU/ml.

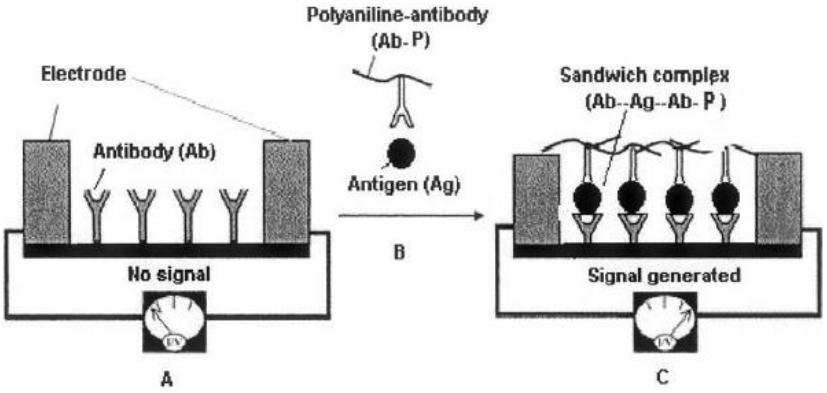

Figure 4.2: An overview of the capture membrane (A) before and (C) after antigen capture (B) shows introduction of antigen (Muhammad-Tahir and Alocilja, 2003)

The concentration of bacteria in these ranges were directly proportional to the change in conductance. However, at bacteria concentrations higher than 10^5 CFU/ml the change in conductance was found to be inversely proportional to the concentration. The biosensor showed remarkable specificity and did not show any change in conductance when other bacteria other than *E. coli* and *Salmonella* were used. In fact, the other bacteria showed a response similar to that of a blank, that is, no change in conductance.

Tahir and co-workers (2005) subsequently reported a conductimetric biosensor for the detection of bovine viral diarrhoea virus (BVDV). This biosensor had the same design as the device reported in their earlier work shown in Figure 4.1. The sensor consisted of anti-BVDV monoclonal antibodies physically adsorbed on PANI which was synthesised by

oxidative polymerisation. The PANI-immobilized antibody film was then adsorbed on cellulose membranes and another antibody nitrocellulose membrane was prepared. The antibody-PANI membrane was then sandwiched between the nitrocellulose membrane and a copper wafer while a silicon wafer was used as the support. The antibody-nitrocellulose membrane was connected to an ohmmeter and computer via two silver electrodes. The detection limit of the biosensor was 10^3-10^4 cell culture infective dose per millilitre (CCID/ml). When phenylphosphonic acid and 4-hydroxybenzenesulphonic acid doped PANI were used in the biosensor, the detection limit increased to 10^5 CCID/ml. Thus the sensitivity of the sensor was dependent on the dopant used on PANI and careful selection was required to develop a biosensor which was very sensitive for BVDV. The sensor was also highly specific for BVDV due to its incorporation of monoclonal antibodies (Tahir, Alocilja and Grooms, 2005).

Pal and co-workers (2007) reported another biosensor for pathogen detection. This biosensor consisted of polyaniline nanowires with immobilized polyclonal anti-*Bacillus cereus* antibodies in a conjugate layer. The biosensor also had three other layers, that is, the cellulose sample layer, secondary antibody capture layer and the absorption layer. All three layers were placed on a copper platform as shown in Figure 4.3.

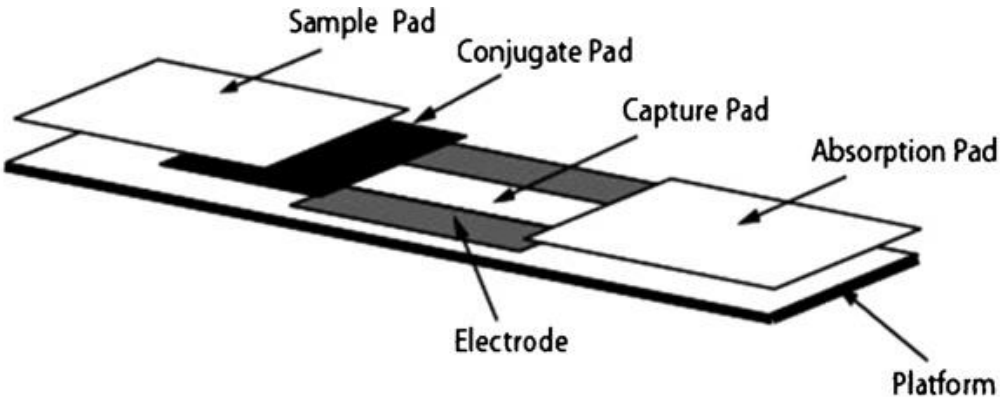

Figure 4.3: Membrane layer arrangement in the Bacillus cereus biosensor (Pal, Alocilja and Downes, 2007)

The capture layer was connected to silver electrodes on both sides as shown in the diagram above. The sample was applied to the active layer and flowed to the conjugate layer where the primary antigen-antibody interaction would occur. After the primary reaction, the complex formed reacted further with the secondary antibodies on the capture layer and transmitted electrons through the polyaniline nanowires to the silver electrodes to complete the circuit as shown in Figure 4.4.

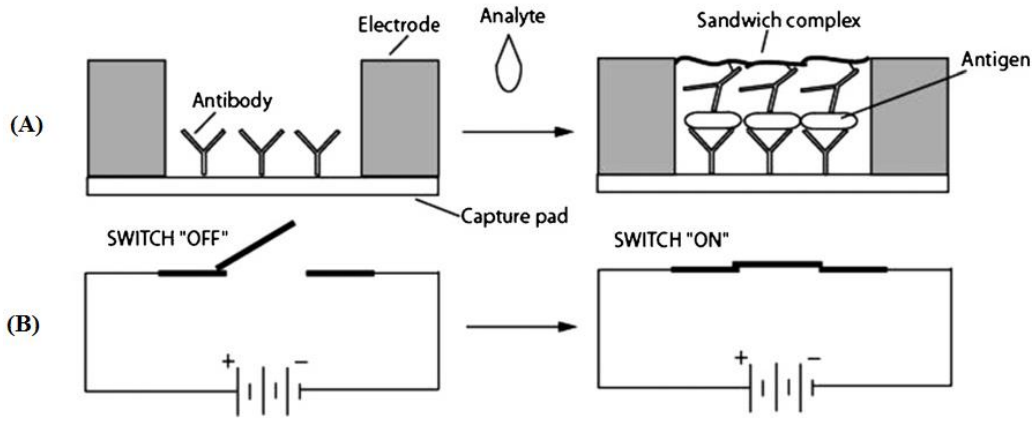

Figure 4.4: Shows the capture layer before and after antigen binding (B) Shows the analogous circuit formed before and after antigen binding (Pal, Alocilja and Downes, 2007)

The current produced was then read out on a multimeter. The biosensor had a sensitivity of 10^1-10^2 CFU/ml and detection limits ranging from 1.2×10^1 to 4.4×10^2 CFU/ml. The *B. cereus* biosensor performance was affected mainly by the concentration of antibody versus the amount of polyaniline used in the biosensor. It was found that when a higher concentration of PANI than antibody was used, the sensor response was reduced while the use of more antibodies than PANI weakened the sensor response further. Therefore, optimal concentrations of both antibodies and PANI were essential for obtaining the best response from the biosensor.

Liu et al (2008) described a biowire-based biosensor device for detection of several pathogens at the same time. The biosensor used a configuration that was previously

developed by Tahir and Alocilja (2003). This biosensor consisted of two important components, that is, (a) mixed antibodies immobilized on polyaniline nanowires for antigen binding and (b) multi-channel potentiostat for conductance measurements. The mixed anti-*E.coli* and anti-*B. cereus* antibodies were immobilized on polyaniline nanowires by physical adsorption. The antibody-polyaniline conjugates were the precipitated by centrifuging and the resulting pellets formulated into a conjugate pad which were integrated into the biosensor. When a sample containing the pathogen of interest was injected into the biosensor, there was a conversion of the antigen-antibody reaction into an electrical signal with the aid of the polyaniline nanowires, which acted as transducers. Due to the presence of antibodies specific to *E. coli* and *B. cereus,* this biosensor was able to detect both pathogens simultaneously when present in samples. The biosensor was calibrated using concentrations of 6×10^7 CFU/ml and 5×10^7 CFU/ml for *B. cereus* and *E. coli* respectively. The conductance readings obtained for concentrations of bacteria ranging from 10^2-10^5 CFU/ml were 15-18 µS. The sensor was highly sensitive for the detection of the bacterial pathogens as exhibited by its micro-Siemen detection range as well as possessing excellent selectivity for the analyte of interest due to the presence of specific antibodies (Liu, Gore, Chakrabartty and Alocilja, 2008).

Pal et al (2008) in further work reported the development of a conductimetric biosensor for the detection of *B. cereus* in food matrices. The biosensor consisted of primary anti-*B-cereus* antibodies immobilized on a polyaniline transducer (conjugate pad), a capture pad with immobilized secondary anti-*B. cereus* antibodies, a sample application pad, an absorption pad, and two silver electrodes. All these components were placed on a copper support. This biosensor utilised a similar sandwich immunoassay and membrane pads as that reported by Muhammad-Tahir and Alocilja (2003) and shown in Figure 4.1. The biosensor construction followed the procedure that was developed by Pal et al (2007). Food samples previously inoculated with *B. cereus* were used to test the sensitivity of the biosensor while cross-reactivity and selectivity tests were done using *Bacillus magaterium*

and *E. coli*. When food samples containing *B. cereus* were introduced into the biosensor, the detection limit was found to range between 35-88 CFU/ml while the resistance signal ranged between 25.6-122 kΩ. The resistance signals for the control were significantly higher than the test sample, ranging between 93.3-178.1 kΩ. The reduction in resistance signals observed with the *B. cereus* inoculated test samples when compared to the controls was due to the electrons generated by the antigen-antibody binding event increasing the conductance of the biosensor (Pal, Ying, Alocilja and Downes, 2008). The biosensor did not show any difference in resistance signals between the control and the bacteria used in the cross-reactivity test. The sensitivity of the majority of biosensors is reported to be in the range 10^2-10^6 CFU/ml, therefore, this biosensor had a superior sensitivity than most available biosensors (Subramanian, Irudayaraj and Ryan, 2006). However, the biosensor was unable to correlate bacteria concentration directly to resistance values because there was a non-linear variation of resistance signals in relation to bacteria concentrations. This meant that the concentration of bacteria in samples could not be determined based on the resistance values obtained.

A label-free biosensor for the detection of a *Listeria monocytogenes* surface protein known as Internalin B (InlB) was reported by Tully and co-workers (2008). The biosensor was made up of electro-polymerised polyaniline-carbon composite electrodes with immobilised biotinylated anti-InlB antibodies coupled to a potentiostat for electrochemical readings and an auto frequency response analyser for impedance measurements. Biotinylated antibodies were immobilised by chemical adsorption to neutravidin treated polyaniline films. The frequency response analyser operating at a varied frequency range of 10,000 to1 Hertz (Hz) yielded a detection limit of 4.1 pg/ml for InlB surface protein. Both detection and quantification of the InlB surface protein was possible with this biosensor due to the consistent calibration curves obtained from different concentrations of bacteria at the same frequency of 1 Hz (Tully, Higson and O'Kennedy, 2008). The use of anti-InlB antibodies was also advantageous because it

ensured that cross-reactivity with other pathogens was limited and biosensor specificity was maintained.

Langer et al (2009) reported a polyaniline based "ON-OFF" nanobiosensor for the detection of up to four bacterial pathogens. This biosensor was made up of two gold electrodes on a glass support with polyaniline nanofibrils in close contact with the gold coupled to a conductivity meter. The biosensor was useful for the detection of *Klebsiella pneumoniae*, *Pseudomonas aeruginosa*, *Escherichia coli* and *Enterococcus faecalis*. When a sample containing any of the four bacteria was injected separately into the biosensor, an increase in the conductivity of the polyaniline nanofibrils was observed. Conductivity increases after introduction of bacteria were due to an increase in the flow of charge carriers in the polymer backbone when sufficient bacteria were lodged into the polymer matrix. This increase was proportional to the number of bacterial cells injected and a linear graph characteristic for each bacteria was obtained when conductivity values were plotted against bacterial cell concentration. The conductivity increases were observed when the concentration of bacteria injected into the biosensor was between 0.44×10^6 CFU/ml and 2.50×10^6 CFU/ml. Saturation of the conductivity signal due to high concentration of bacteria was observed only for *P. aeruginosa*. This was undesirable because it limited the range over which bacteria could be detected reliably (Langer et al., 2009).

The use of direct-charge transfer for the detection of *E. coli* 0157:H7 and bovine viral diarrhoea virus (BVDV) was reported by Luo et al (2010). The biosensor that was developed was composed of three membranes, that is, a sample application membrane, a capture membrane and an adsorption membrane connected to the other two membranes through two silver electrodes. Magnetic iron oxide-polyaniline nanoparticles with immobilized anti-*E. coli* 0157:H7 and anti-BVDV antibodies were used for analyte capture in the sample solution. The nanoparticles were separated from the sample solution after analyte capture with the aid of a magnet after which they were injected on the

biosensor application membrane. A sandwich assay similar that described by Tahir and Alocilja (2003) was formed on the capture membrane. Electrons generated during the sandwich antigen-antibody reaction were transmitted through the iron oxide-polyaniline nanoparticles to the electrodes and the signal measured by a data acquisition system. The biosensor setup, antigen capture and signal generation are shown in Figure 4.5. This biosensor showed a linear response with increasing BVDV and *E. coli* concentrations respectively. For *E. coli*, the response was linear over the concentration range 0 to 10^4 CFU/ml which was superior to the 0 to 10 CFU/ml seen with other methods while the detection limit of the biosensor was at a concentration of 61 CFU/ml. The detection limit for the BVDV was 10^3 CCID/ml with a linear response in the concentration range of 0 to 10^3 CCID/ml (Luo et al., 2010). The direct-charge transfer biosensor had the advantage of offering fast, selective and sensitive detection which was superior to conventional methods of detecting *E. coli* and BVDV (Black, 2002). The biosensor also did not show any saturation plateau at higher pathogen concentrations seen with other devices reported by Barton et al (2009) and Langer et al (2009) respectively.

Besides other biosensors for the detection of *E. coli* highlighted above, Setterington and Alocilja (2011) also developed an electrochemical biosensor for the detection of polyaniline-labelled *E. coli* 0157:H7. Monoclonal anti-*E. coli* 0157:H7 antibodies were immobilized on the polyaniline nanoparticles by physical adsorption. The biosensor had a screen printed carbon electrode on which the polyaniline-labelled *E. coli* was deposited and a potentiostat used for the detection of PANI by cyclic voltammetry. In order to magnify the signal, an external magnetic field was applied to the carbon electrode with deposited polyaniline-*E. coli*. Decreases in the peak intensities of the cyclic voltammogram of PANI indicated that the analyte, *E. coli*, was present in the sample. The detection limit of the electrochemical biosensor was 70 CFU/ml and the current versus bacteria concentration graphs showed linearity over the concentration range of 10^1-10^5 CFU/ml. Though the biosensor was easy to carry due to its small size, it was only able to

provide a result after 1 hour 10 minutes. This was better than most conventional methods but was by no means as impressive as the biosensor reported by Karyakin et al (1996) which could provide results within 2 minutes.

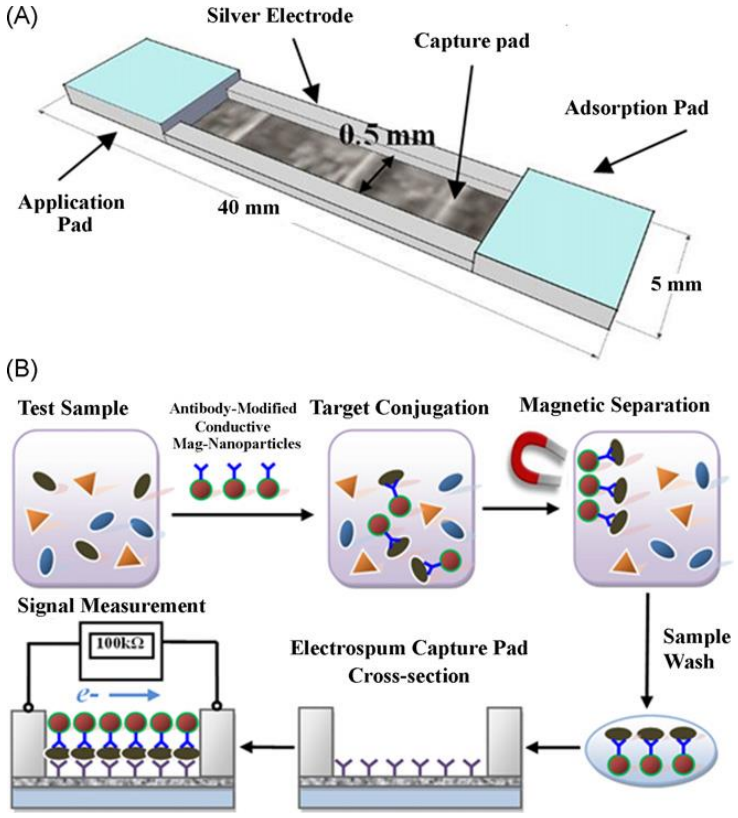

Figure 4.5: The direct-charge transfer biosensor developed by Luo and co-workers (Luo et al., 2010)

Setterington and Alocilja (2012) reported another electrochemical biosensor for the detection of *B. cereus* and *E. coli* 0157:H7. This biosensor was developed using the same strategy as their earlier work published in 2011 and had similar architecture (Setterington and Alocilja, 2011). The detection limits of the sensor were 40 CFU/ml and 6 CFU/ml for *B. cereus* and *E. coli* 0157:H7 respectively (Setterington and Alocilja, 2012). Because the biosensor incorporated bacteria specific antibodies, it was highly selective for the detection of only the bacteria of interest.

Another polyaniline-based biosensor for the detection of *E. coli* was reported by Chowdhury and co-workers (2012). The biosensor had a detection limit of 10^7 CFU/ml and reasonable selectivity for *E. coli* when other bacteria were tested. However, the specificity of this device was not comparable with other biosensors such as the one reported by Setterington and Alocilja (2011). Also, the relatively high detection limit was a major disadvantage of this biosensor as lower concentrations of bacteria in samples would pass testing as false negative results (Chowdhury et al., 2012).

The detection of *Mycobacterium tuberculosis* using a DNA biosensor was reported by Liu and co-workers (2014). The sensing layer of the biosensor was composed of graphene oxide-gold nanoparticles and gold-polyaniline nanoparticles on which the IS6110 DNA sequence strand specific for *Mycobacterium tuberculosis* was immobilized. Samples of the bacteria in the concentration range 1.0×10^{-15} to 1.0×10^{-9} M were injected into the biosensor, a linear response was observed. Additionally, the biosensor was highly stable and was very selective for *Mycobacterium tuberculosis* only while also maintaining specificity by the IS6110 DNA strands (Liu et al., 2014).

More work on *E. coli* was reported in a review by Singh et al (2014). They described a nucleic acid biosensor based on polyaniline. The biosensor consisted of an *E. coli* DNA probe immobilized on polyaniline with the aid of avidin and biotin. The biosensor showed good sensitivity and was able to electrochemically detect *E. coli* DNA at a concentration of 0.01ng/µl and 11 cells/ml of *E. coli*. Complementary strands of DNA in samples were detected at a concentration of 0.009 ng/ml and the entire detection process took between 1 to 14 minutes to complete. Apart from rapid sensor response and good detection limit, other pathogens in samples did not interfere with tests due to the high specificity of the DNA probe used (Singh et al., 2014).

More recently, Thakur et al (2015) reported a polyaniline nanoparticle colorimetric biosensor for monitoring the growth of *E. coli*. The polyaniline nanoparticles were coated

with pectin (Pec) and agarose and deposited on polyethylene terephthalate (PET) supports to form films of PANI-Pec nanoparticles. A PANI-Pec film was then dipped in lysogeny broth (LB) containing a known amount of bacteria and the UV-Vis spectra of the film recorded. This was repeated at equal intervals of time and the UV-Vis spectra read each time. The growth of the bacteria was monitored visually by monitoring colour changes in the PANI-Pec film and also by using UV-Vis spectroscopy. When monitored visually, a blue to green transition in the colour of the polyaniline was noted. This was due to an increase in acidic by-products of bacterial metabolism such as lactic acid and acetic acid that acted as dopants for the PANI. The initial UV-Vis spectra showed two peaks at 325 nm and 620 nm that were characteristic for the blue non-conducting emeraldine base of PANI at a pH of 8. This was before sufficient metabolism of pectin by the bacteria leading to the production of acidic by products had occurred. The UV-Vis spectra that was done after the film turned green showed two peaks at 420 nm and 800 nm that were characteristic of the green emeraldine salt of PANI. Signal production took 100 and120 minutes and the biosensor had a detection limit of 10^6 cells/ml. Sensor response was dependent on the time required for the measurement to be taken. Better responses were obtained only after a prolonged wait for bacterial metabolism to be sufficient. This was a drawback because long waiting times were not desirable for positive responses to be obtained were bacterial monitoring was concerned (Thakur, Amarnath, Mangoli and Sawant, 2015). The detection limit was also relatively high at 10^6 cells/ml compared to other sensors reviewed such as the device reported by Luo et al (2010).

The literature shows that though a reasonable amount of work has been done concerning the use of polyaniline in biosensors for pathogen detection, not much has been done to develop a biosensor for the specific detection of *P. aeruginosa*, an organism that not only causes serious infections but also takes more than 48 hours to detect using conventional methods (Black, 2002).

The versatility of polyaniline for application in biosensors for pathogen detection has been demonstrated in the previous section. Chapter 5 of this dissertation presents the design and evaluation of the sensing characteristics of a polyaniline-biotinylated antibody *Pseudomonas aeruginosa* biosensor for the real-time detection of *P. aeruginosa*.

CHAPTER 5: EXPERIMENTAL

The development of the polyaniline-biotinylated antibody *Pseudomonas aeruginosa* biosensor required a number of experimental methods to be undertaken. These methods are presented in the sections that follow.

5.1 Synthesis of Polyaniline

Polyaniline was synthesized by the oxidative polymerization of anilinium sulfate (0.2 M) with ammonium peroxydisulphate (0.25 M) in aqueous medium at room temperature. The anilinium sulfate was prepared in 1 M H_2SO_4 in a 50 ml volumetric flask. The 0.25 M ammonium peroxydisulphate was prepared in a 50 ml volumetric flask with distilled water. Both solutions were left to stand at room temperature for 1 hour, then mixed in a beaker, and stirred using a magnetic stirrer for 2 minutes. The solution mixture was left to polymerize at 25 ^oC and was monitored over the course of 1 hour.

5.2 Thin Film Development

5.2.1 *In situ* Polymerisation of Polyaniline on Glass Slides

Four Cole-Parmer® Pre-Cleaned Frosted glass slides 75 × 25 × 1.0 mm were used to develop thin films of PANI. The glass slides were cleaned by washing in chemical baths of 1 M HCl and 1 M H_2SO_4 and then rinsing with distilled water. The clean glass substrates were then dried for 2 hours at 25^o C. One side of the dry glass slides was covered with adhesive tape and suspended in a beaker. Two solutions, one being a 50 ml solution of anilinium sulphate (0.2 M) and the other being a 50 ml solution of Ammonium peroxydisulphate (0.25 M) were sequentially added to the beaker with the suspended slides until they were completely submerged and polymerization initiated. To ensure the two solutions were thoroughly mixed, they were stirred for 2 minutes using magnetic

stirrer and then allowed to stand for 1 hour. The suspended glass slides were removed from the reaction mixture one by one at intervals of 15, 30, 45 and 60 minutes, rinsed with 100 ml portions 1 M sulfuric acid, then with 100 ml portions of acetone, and dried.

5.2.2 Effect of Polymerisation Time on Film Morphology and Thickness

The effect of polymerization time on film morphology was studied using a Nanosurf® Atomic Force Microscope (AFM) while the film thickness of the films prepared at different polymerization times were determined spectroscopically using a Shimadzu IRAffinity® Fourier Transform Infrared (FTIR) spectroscopy.

5.3 Characterisation of Thin Films

5.3.1 Spectroscopic Analysis

(a) Ultraviolet/Visible (UV-Vis) Spectroscopy:

UV/Vis spectroscopy was used for characterization of the optical properties of PANI thin films. This was done to study the absorption characteristics and the UV-Vis transitions of the prepared thin films. The optical absorption spectra of the PANI were recorded using a computerized Shimadzu UV-2600® UV-Vis Spectrophotometer interfaced to a computer. The spectra were recorded at normal incidence at 25 ^{o}C in the spectral range of 1000-200 nm and the speed used was 1000 nm/min.

(b) FTIR Spectroscopy:

The FTIR spectra of the PANI thin films were recorded with a computerized Shimadzu IRAffinity-1® Fourier Transform Infrared Spectrophotometer interfaced to a computer. The infrared spectra were recorded in the range 400-2000 cm^{-1} at 20 scans per spectrum with a resolution of 16 cm^{1}. The recorded spectra were corrected for the presence of moisture and carbon dioxide.

5.3.2 Conductivity Measurements

Conductivity of the thin films was measured with the aid of the four-point probe coupled to a source meter. A four point probe consisting of two outer current and two inner voltage probes with electrode distances of 0.8 mm was pressed onto the PANI thin films. The current measurements were recorded in the range of 5-20 mA, the corresponding voltage was measured and recorded across the two inner probes. A Jandell® Model RM3000 Test Unit with a constant current source and digital voltmeter was used as the source meter for these measurements and is shown in Figure 5.1.

Figure 5.1: Jandell® Model RM3000 Test Unit and four point probe

5.3.3 Surface Morphology Analysis

The morphology and roughness were obtained from images collected with the aid of a Nanosurf Easy Scan® Atomic Force Microscope. The images were collected in contact mode with a Tap 190 Al-G Long Cantilever. The cantilever was 225µm in length with a resonance frequency of 190 kHz and tip radius of < 10 nm. All the images were obtained at a scan rate of 5 seconds/line. Prior to reading the films, the AFM was calibrated with an HS-100MG Calibration Grid.

5.4 Thermal Treatment of Thin Films

Five PANI thin films were developed at 30 minutes dip time and thermally treated on a temperature controlled hot plate in a fume hood for 10 minutes each at different temperatures. The temperatures used for the films were 50 ^{o}C, 100 ^{o}C and 150 ^{o}C respectively. The thermal treatment experiments were done in order to study the effect of temperature on the PANI thin film morphology, conductivity, UV-Vis, and FTIR spectral properties.

5.4.1 Characterisation of Thermally Treated Thin Films

The effect of thermal treatment on film morphology was evaluated using a Nanosurf Easy Scan® Atomic Force Microscope set to the same parameters as in section 5.33 above. The conductivity and spectral properties of the treated thin films were studied as was done in section 5.32 and section 5.31 respectively.

5.5 Ethical Approval

This study was approved by ERES Converge IRB, an independent research Board (Lusaka, Zambia) specifically to obtain permission to conduct the animal studies involving rabbits (*Leporidae lagomorpha*).

5.6 *Pseudomonas aeruginosa* Subculture

P. aeruginosa was sub-cultured from a bacterial isolate stored in peptone water at 4 ^{o}C obtained from the Microbiology Department, School of Medicine University of Zambia (UNZA) at the University Teaching Hospital UTH. The Nutrient Agar used for the first subculture was prepared by suspending 5.6 g of agar in 200 ml of distilled water in an Erlenmeyer flask. This suspension was mixed thoroughly with a clean glass rod and then brought to boil in a microwave oven for about 2 minutes until the agar had completely dissolved in the water. This resulted in a golden yellow solution signifying complete

dissolution of the agar. The golden yellow solution of agar was then autoclaved for 60 minutes at 121^{o}C and 1.03 bar pressure after which it was allowed to cool. The cooled agar solution was poured onto eight bacterial culture plates after the mouth of the Erlenmeyer flask was flamed with a Bunsen burner. This was done in a Dalton® Laminar Flow Hood, which provided a sterile environment for this stage of the plate preparation in order to prevent contamination. The poured plates were left to congeal for 10 minutes after which they were placed in an incubator for 15 minutes at 45^{o}C to ensure complete drying. The plates were removed from the incubator and were ready for use to subculture the bacteria.

Blood Agar plates were provided by the Department of Clinical Studies and Disease Control, School of Veterinary Medicine, UNZA. One of these plates together with two nutrient agar plates were used to prepare bacterial subcultures of *P. aeruginosa* while the rest of the plates were stored at 4 ^{o}C for later use.

A clean platinum loop sterilized in a Bunsen flame was used to streak the Blood Agar plate and the two Nutrient Agar plates with the stock *P. aeruginosa* stored in the peptone water. Streaking was done using standard bacteriological techniques (Black, 2002). The three streaked plates were incubated at 37 ^{o}C for 24 hours. The plates were removed from the incubator the following day and observed for bacterial growth. The three plates showed excellent growth with the Nutrient Agar plates showing yellowish green streaks characteristic of *P. aeruginosa* and the Blood Agar plate showing black streaks of growth. The three plates were all labelled "Sub 1" to denote the first subculture plates of *P. aeruginosa.* These plates were then stored in a sealed transparent plastic bag at 4 ^{o}C for later use.

5.6.1 Preparation of Mueller Hinton Agar for Bacterial Sensitivity Test

Mueller Hinton Agar for bacterial sensitivity testing was prepared by dissolving 7.6 g of agar powder in 200 ml of distilled water in an Erlenmeyer flask and mixing well with a

glass rod. The resulting suspension was boiled for 2 minutes in a microwave oven to ensure that the agar dissolved completely in the water. A clear golden yellow solution resulted after 2 minutes of microwaving the sample suspension symbolizing complete dissolution of the agar in solution. The agar solution was then placed on a bench top, capped with aluminium foil and tied loosely with a piece of string after which it was autoclaved at 121 ^{o}C for 60 minutes at 1.03 bar pressure. The autoclaved agar solution was allowed to cool to 50 ^{o}C for 10 minutes before it was poured onto four bacterial culture plates in a Dalton® Laminar Flow Hood. The poured Mueller Hinton Agar plates were allowed to dry for 10 minutes and then incubated at 45 ^{o}C for 15 minutes to complete the drying process. These plates were then stored at 4 ^{o}C in a refrigerator until required for the bacterial sensitivity test.

5.6.2 Standardization of Bacterial Suspensions by Nephelometry

One percent solutions of barium chloride ($BaCl_2$) and sulphuric acid (H_2SO_4) were prepared by dissolving 0.5 g of barium chloride in 50 ml of distilled water and adding 1 g (0.54 ml) of concentrated sulphuric acid (98 %) to 100 ml of distilled water respectively. The two one percent solutions were mixed in varying proportions as shown in Table 5.1 to yield suspensions whose turbidity closely correlated with the concentration of suspended bacteria in samples of similar volumes, that is, all samples were made up to a final volume of 10 ml. Table 5.1 illustrates the outcome of the Nephelometry standardization using the McFarland Scale.

Table 5.1: Nephelometry Standardisation using the McFarland Scale

McFarland Scale	1% $BaCl_2$ (ml)	1% H_2SO_4 (ml)	Number of bacteria represented (value listed, × 10^8)
0.5	0.05	9.95	1.5
1	0.1	9.9	3
2	0.2	9.8	6
3	0.3	9.7	9
4	0.4	9.6	12
5	0.5	9.5	15
6	0.6	9.4	18

5.6.3 Antibiotic Sensitivity Testing

The sensitivity test of *Pseudomonas aeruginosa* isolates obtained from UTH Microbiology laboratory was carried out on previously prepared Mueller Hinton Agar plates using disk diffusion method. A sterile swab was used to transfer bacteria in suspension from 0.5 the McFarland Scale test tube (1.5×10^8 colony forming units/ml (CFU/ml)) onto an agar plate. The plate was gently swabbed uniformly and the GV-Minus Octodisc® sensitivity disc placed on the agar. The GV-Minus Octodisc® contained ampicillin, ticarcillin, gentamicin, cephalexin, trimethoprim, sulphamethoxazole, tetracycline and sulphonate respectively.

The control strain of *Pseudomonas aeruginosa* (ATCC 27853) was sub-cultured from bacterial stock obtained from the School of Veterinary Medicine, Department of Disease Control, UNZA. The swabbing of bacteria onto the plate of Mueller Hinton Agar was done according to standard bacteriological methods (Cockerill et al., 2012).

5.6.4 Preparation of Live *Pseudomonas aeruginosa* Crude Vaccine

Preparation of the live *Pseudomonas aeruginosa* vaccine was done by suspending previously cultured bacteria with a sterile loop into two sterile 50 ml Vacutainer® bottles containing 20 ml of sterile normal saline solution each. The two bacterial suspensions were standardized to 0.5 on the McFarland Scale by addition of two loops of bacteria from a plate and homogenizing the mixture on a Vortex® Mixer. The resulting suspension corresponded to 1.5×10^8 CFU/ml. The bacterial suspension meant for intravenous injection had no aluminium hydroxide added to it after standardization while the other 20ml suspension meant for subcutaneous and intramuscular injection was mixed with 10 ml of 2% aluminium hydroxide as adjuvant. The adjuvant was prepared by dispersing 2 g of aluminium hydroxide gel into 100 ml of distilled water and autoclaving the resulting colloid at 121 ^oC for 60 minutes at 1.03 bar pressure. The allowed (working concentration) ratios of the aluminium hydroxide colloid to the antigen solution should range between

1:1 to 1:9 (Jones et al., 2005). The ratio used for this research was 1:2. After mixing the aluminium hydroxide colloid with the antigen solution, the resulting mixture was allowed to stand for 5 minutes to ensure that antigen adsorption by the aluminium was complete. The two solutions of live *Pseudomonas aeruginosa* vaccine were then ready for immediate use.

5.6.4.1 Rabbit Immunization

All animal studies were done in conformity to the guidelines established by the School of Veterinary Medicine, UNZA. Two 8 week old rabbits were immunized subcutaneously and intramuscularly with 2 % aluminium hydroxide adjuvant conjugated with live *P. aeruginosa* in a 1:2 ratio respectively, while a third 8 week old rabbit was given only live *P*. aeruginosa intravenously. A fourth rabbit was used as the control and was not immunized. Two subsequent immunizations were administered at 2 week intervals in the same manner as the first one. One week after the third immunisation, the test bleed was carried out and the last booster immunization was administered 1 week later. The terminal bleed was carried out 1 week after the test bleed. The full immunization protocol is presented in Appendix III.

5.6.5 Serum Agglutination Test and Antibody Purification

The serum agglutination test (SAT) was used to detect for antibodies to *P. aeruginosa* outer core lipopolysaccharide (O) antigens. An overnight bacteria culture plate was used to suspend about 1.5×10^8 cells of *P. aeruginosa* in phosphate buffered saline in a test tube as described in section 5.62 above. A portion of the pooled sera was diluted to 1 in 20 with normal saline and tested for agglutinins. Another portion of the pooled sera was sequentially diluted to 1 in 40, 1 in 80 and 1 in 160 in normal saline. A 1 ml volume of the antigen suspension was mixed with 1 ml of each of the diluted samples of sera and the mixture placed in a test tube rack for 5 minutes. After 5 minutes the tube that gave the highest agglutination was noted.

A stock solution containing 100 % saturated ammonium sulphate was prepared and from this, a working solution of 60 % saturated ammonium sulphate was made. Mixing this working solution with equal volumes of rabbit serum yielded mixtures of 35 % ammonium sulphate. The justification for using ammonium sulphate precipitation alone and not in combination with caprylic acid has been reported (Mohanty and Elazhary, 1989). The precipitated crude antibody mixture was then fractionated and desalted in a column of Sephadex G25 after which it was resolubilized in phosphate buffered saline solution before use in the biotinylation step.

5.7 Antibody Biotinylation and Immobilization onto PANI Thin Films

In order to properly orient the antibodies in an organized manner on the polyaniline thin film and improve sensor performance, a biotinylation process was done. About 10 mg of biotin was dissolved in 1 ml DMSO and mixed with the crude antibody solution. After thorough mixing, the solution was wrapped in aluminium foil and incubated with mild shaking for 4 hours at 23 ^{o}C. The excess biotin that did not react with antibody was then removed by dialysis against four changes of phosphate buffered saline at 4^{o} C for 24 hours. The biotin tagged antibody solution was gently poured into a 100 ml beaker. Polyaniline thin films that had been prepared beforehand and incubated in avidin for 5 hours and dried were placed into the biotinylated antibody solution and incubated at 4^{o} C for 5 hours after which the films were then ready for sensing characterization. The characterisation was carried out using Atomic Force Microscopy in the manner described in section 5.3.3.

5.8 Biosensor Setup and Testing

The biosensor was setup using the circuitry shown in Figure 5.2 integrated with a Helium-Neon® NIR Laser whose operating wavelength was 632.8 nm. Various volumes of 0.5 McFarland Scale standardised *Pseudomonas aeruginosa* suspended in phosphate buffered saline (PBS) were injected onto the biotinylated anti-*P. aeruginosa* antibody-polyaniline thin film. The resistance readings were obtained from the integrated multimeter. PBS was

used as the control for this initial biosensor test. *P. aeruginosa* was then suspended in sterile bovine, sheep, goat and rabbit sera and standardized to 0.5 on the McFarland scale. The varying volumes of standardized serum samples were sequentially injected onto biotinylated anti-*P. aeruginosa* antibody-polyaniline thin films and the resistance read on the multimeter. Serum devoid of the bacteria was used as the control in each case.

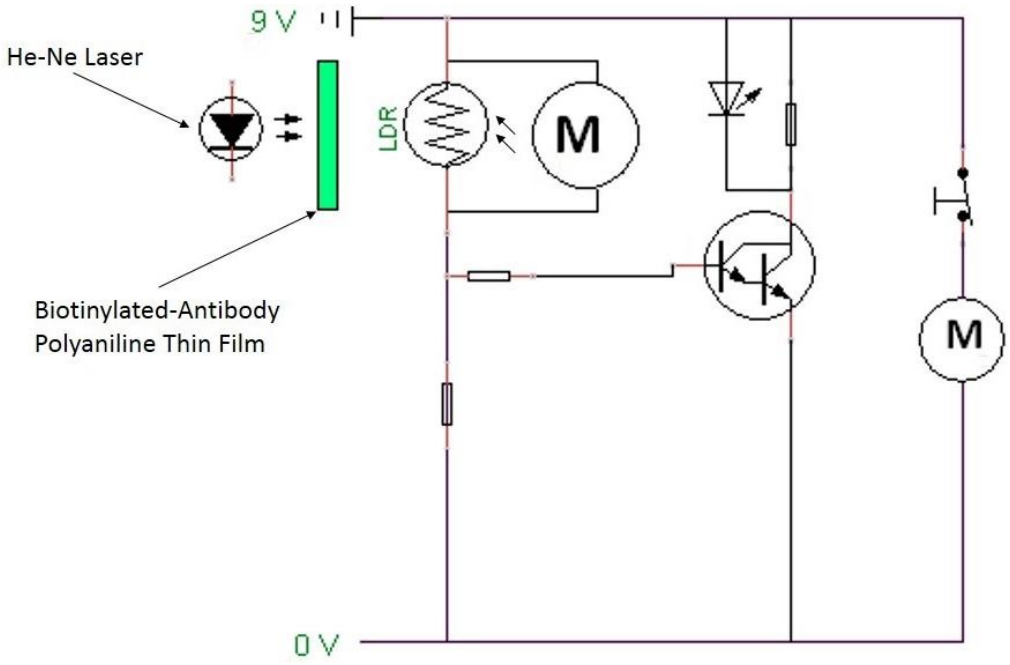

Figure 5.2: Polyaniline-biotinylated antibody *Pseudomonas aeruginosa* biosensor setup

5.8.1 Bacterial Cross-Reactivity Test

Escherichia coli (0157) bacteria were used to test for the cross-reactivity performance of the biosensor. The test was conducted under the same conditions as that of the *P. aeruginosa* detection experiment. The 0.5 McFarland Scale of *E. coli* was used for these tests with the bacteria suspended in PBS buffer solution.

CHAPTER 6: RESULTS AND DISCUSSION

This chapter presents the results of the preceding experimental procedures described in the previous chapter and their discussion.

6.1 Synthesis of Polyaniline and Film Development

Polyaniline was synthesized by the oxidative polymerization of aniline using the standard preparation method adapted from Stejskal and Gilbert (2002). The changes that were observed during the synthesis of PANI are shown in Figure 6.1.

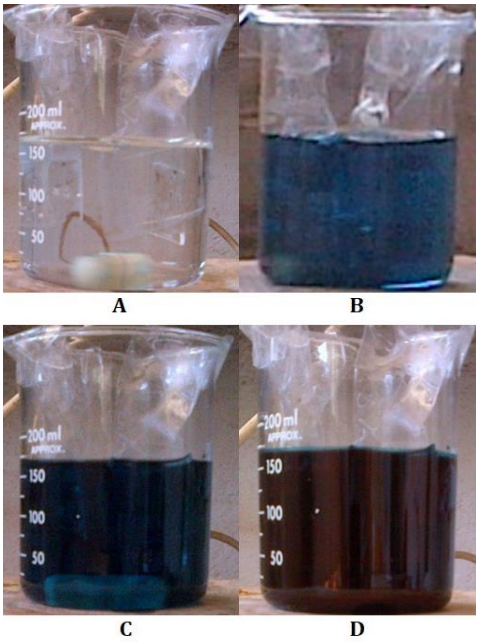

Figure 6.1: Synthesis of polyaniline showing (A) Initiation; Time 0 Minutes (clear solution) (B) 20 Minutes after Initiation (blue solution) (C) 40 Minutes after Initiation (green solution) (D) 60 Minutes after Initiation (dark green solution)

During the polymerization process, the reaction medium went through visible colour changes that were indicative of the various stages of polymerization. Figure 6.1 (B) shows formation of the blue non-conducting emeraldine form of polyaniline. The structure of

this form of polyaniline is shown in Figure 3.1, Section 3.1 in Chapter 3. Figure 6.1 (C) and (D) shows the formation of the green emeraldine conducting form of polyaniline whose structure is also shown in Figure 3.1. Structural analysis was done on the green emeraldine form of polyaniline using FTIR and UV-Vis. The results of the UV-Vis analysis are presented in Figure 6.2.

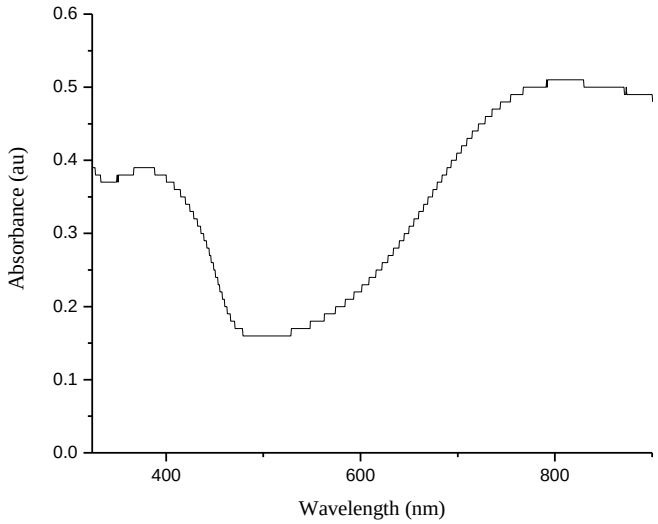

Figure 6.2: UV Spectrum of Polyaniline

The UV/Vis spectrum of polyaniline showed two intense absorption bands; one at 375 nm and another at 800 nm. These two absorption bands are reported by Stejskal et al (1993) to be characteristic of the green protonated form of polyaniline that is conducting. The absorption band seen at 375 nm is attributed to the л→л* transition of electrons from the valence band to the absorption band while the band seen at 800 nm is the quinoid – benzenoid transition (Stejskal, Kratochvíl and Radhakrishnan, 1993; Gopalakrishnan, Elango and Thamilselvan, 2012). The results of the FTIR spectroscopic analysis of polyaniline are shown in

Figure 6.3 and the important peaks are highlighted in Table 6.1.

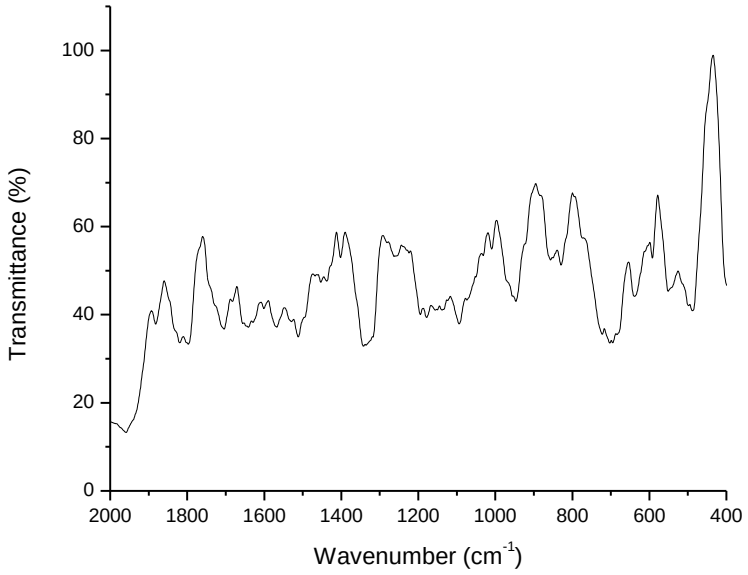

Figure 6.3: (A) FTIR Spectrum of Polyaniline (B) Insert showing important peaks

Table 6.1: FTIR absorption bands for polyaniline thin films

Type of Vibration (cm^{-1})				
N-H Scissoring or bending	Quinoid ring stretching	Benzenoid ring stretching	C=C aromatic ring stretching	C-N stretching
1621	1590	1508	1425	1364

The spectra shows peaks characteristic of PANI at 1650-1600 cm^{-1}, 1590-1510 cm^{-1}, 1480-1420 cm^{-1} and 1380-1350 cm^{-1}. The peak seen at 1621 cm^{-1} is assigned to the N-H scissoring or bending of the primary aromatic amine while a ring stretching with a contribution of the N-H scissoring is seen at 1603 cm^{-1} (the N-H peak at 3500 cm^{-1} is shown in Appendix V). The PANI quinoid ring stretching is observed at 1590 cm^{-1}, the

benzenoid ring stretching is seen at 1508 cm^{-1}. A C=C aromatic stretching is seen at 1425 cm^{-1} which is characteristic of the aromatic ring stretching in PANI. A C-N stretch characteristic of the quinoid-benzenoid-quinoid rings of PANI is seen at 1364 cm^{-1}. The results of the FTIR spectrum validated the successful synthesis of polyaniline.

6.1.1 *In situ* Polymerisation of Polyaniline on Glass Substrates

Variation of time polymerisation was done in order to establish the polymerisation time that would produce a film with the most suitable properties for the biosensor application. *In situ* polymerization of polyaniline was done on Cole-Parmer® Pre-Cleaned Frosted glass slides suspended in the reaction vessel over a period of 60 minutes. The glass slides were removed from the reaction vessel at intervals of 15, 30, 45 and 60 minutes. When glass slides or other suitable substrates are suspended in a PANI polymerization reaction vessel, *in situ* adsorption of PANI nanofibers occurs on the surface of the substrates. The thin films prepared in this way are reported to be strongly adhering (Stejskal and Sapurina, 2005). Oxidation of aniline with ammonium peroxydisulphate leads to the formation of aniline cation radicals. Due to their high reactivity, these radicals react to form dimers. Additional oxidation of the dimers and addition of more aniline cation radicals leads to the formation of aniline oligomers. The aniline oligomers are hydrophobic and tend to come out of solution and adsorb to surrounding surfaces. Since glass slides were submerged into the reaction vessel at the beginning of the reaction, the aniline oligomers preferentially adsorbed to these surfaces. The aniline oligomers are highly reactive and they act as centres of nucleation for other oligomers. Therefore, the reaction of the adsorbed aniline oligomers and those in the reaction medium leads to the growth of polyaniline nanofibers that initially form at 90 ^{o} angles to the surface in a perpendicular manner (Sapurina et al., 2002). Since the growth of the polyaniline nanofibers in initial stages of polymerisation is perpendicular to the surface, the thin film formed has a brush-like appearance of nanofibers. As polymerisation continues, the PANI nanofibers begin to

grow more parallel to the surface with complex crosslinking reactions occurring. This leads to a more closed surface which contrasts the initial more open brush-like appearance.

6.2 Effect of Polymerisation Time on Film Morphology, Thickness and Conductivity

Thin films were prepared at different polymerisation times and the effect that this had on the morphology, thickness and conductivity of the films was studied.

6.2.1 Surface Morphology Analysis

The surface morphologies of the thin films prepared at 15, 30, 45 and 60 minutes were studied with the aid of Atomic Force Microscopy. The AFM images of the films prepared *in situ* over a period of 60 minutes are shown in Figure 6.4 and conform to the mechanism of polymerization that has been highlighted in section 6.1.1. The thin film prepared at 15 minutes showed the initial stages of film formation with many brush-like nanofibers of polyaniline seen. The packing and length of these nanofibers increased at 30 minutes leading to regions of closely aggregated polyaniline nanofibers while at 45 minutes the closing up of the surface due to lateral growth was observed. The thin film prepared at 60 minutes showed a much more dense aggregation of nanofibers that was consistent with cross chain reactions of nearby polymer fibres that led to further closing up of the surface that was first observed at 45 minutes. Polyaniline thin films that are prepared by *in situ* polymerization on glass supports usually gives rise to well-ordered brush-like nanofibers at low polymerisation times. This is the result of mainly perpendicular nanofibers growth that occurs at polymerisation times of 30 minutes or less as observed from the AFM images. The polymerization mechanism of polyaniline on suitable supports consists of the three stages shown in Figure 3.4, Section 3.1.2 (Chapter 3). The mechanism proposes three stages required for successful thin film growth on support surfaces such as glass. These three stages occur after the initial formation of aniline cation radicals. The first step of the mechanism involves adsorption of aniline oligomers to the support surface as they

come out of solution due to their higher hydrophobicity when compared with anilinium cations. Due to their high reactivity, the aniline oligomers adsorbed to the surface will then initiate polyaniline chain growth. This is the second step of chain growth and is known as nucleation. The third step involves growth of nanofibers from centres of nucleation which leads to film growth and spreading over the exposed surface (Stejskal and Sapurina, 2005).

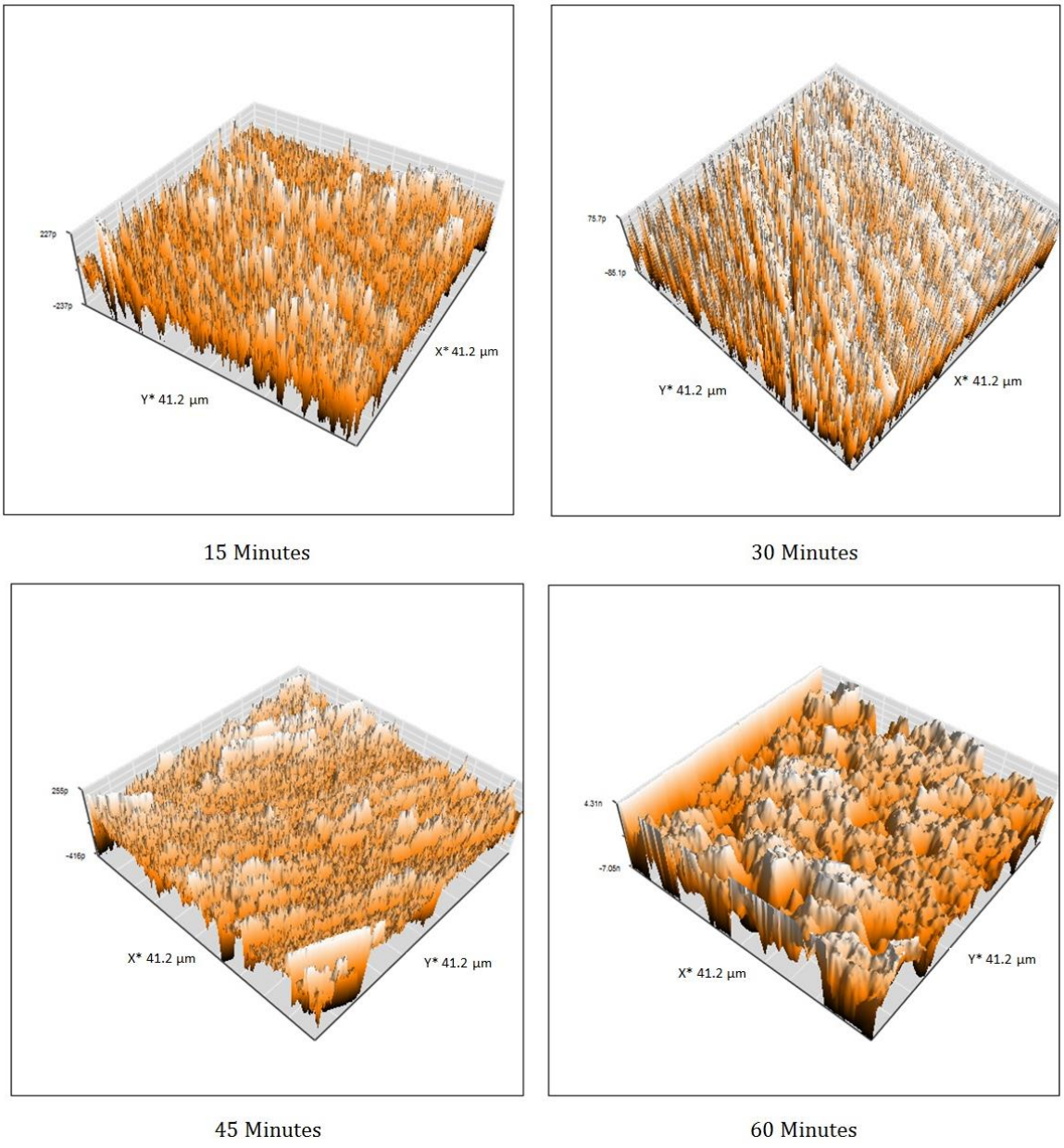

15 Minutes

30 Minutes

45 Minutes

60 Minutes

Figure 6.4: AFM image showing surface morphology of thin films polymerized at 15, 30, 45 and 60 Minutes

The evaluation of the surface morphology of thin films is useful in determining their surface roughness, which is an important consideration in their application. The surface

roughness and root mean square roughness of the PANI thin films prepared at different polymerisation times are shown in Table 6.2.

Table 6.2 : Average surface roughness and average mean square roughness for in situ polymerized thin films

Polymerisation Time	Average Surface Roughness (Ra, nm)	Root Mean Square Roughness (Rq, nm)
15	2.4	3
30	2.7	3.7
45	2.8	4.3
60	2.9	4.8

From the values obtained in the table above, it was observed that both the average surface roughness and the root mean square roughness of the polyaniline thin films increased with increasing polymerisation time. The largest increase in surface roughness and root mean square roughness was seen between 15 minutes and 30 minutes polymerisation time respectively. Only marginal increases in both surface roughness and root mean square roughness were observed between 30 and 60 minutes polymerisation time. This could be explained by an examination of the mechanism of film formation discussed in section 6.1.1. The first 30 minutes of thin film formation revealed that film growth was predominantly perpendicular which accounted for the higher increase in roughness in this timeframe. Beyond 30 minutes, film formation was observed to be mostly lateral to the support surface. This meant that in the later stages of polymerisation the perpendicular growth of the polyaniline nanofibers, which predominantly accounted for the roughness parameters, was less than the lateral film growth that contributed less to roughness. The AFM images in Figure 6.4 confirmed these observations.

6.2.2 Effect of Polymerization Time on Film Thickness

The thicknesses of the polyaniline thin films were obtained by FTIR spectroscopy. The polymerization time of the thin films and their corresponding thicknesses are shown in Table 6.3.

Table 6.3: Polymerisation time and film thickness

Polymerization Time (min)	Film Thickness (nm)
15	9
30	13
45	19
60	21

The film thickness were found to increase in increasing polymerization time. The increase was highest between 30 and 45 minutes followed by the increase between 15 and 30 minutes. Only a marginal increase was observed between 45 and 60 minutes. Polyaniline thin film formation in the initial stages involves mainly perpendicular growth of nanofibers. This is in the later stages of film growth superseded by more lateral proliferation of nanofibers. Thus, in the early stages it is expected that the film thickness would increase by larger values as seen between 15 and 45 minutes than in the later phase of film formation that predominate the period between 45 and 60 minutes. The result showing that film thickness of polyaniline thin films increases in a linear fashion with polymerization time was also demonstrated by Sapurina et al., 2002. Varying the polymerisation time of a thin film can therefore be used to control the thickness of films intended for various applications.

From the surface morphology studies it was determined that the thin film prepared *in situ* at 30 minutes polymerisation time was ideal for biosensor application due to its better uniformity when examined with Atomic Force Microscopy. This film together with the

films prepared at 15, 45 and 60 minutes are shown in Figure 6.4 above. In addition, the studies of the effect of polymerisation time on film thickness revealed that the film prepared at 30 minutes had a thickness of 13 nm and this film thickness was determined to be the most ideal for the biosensor application.

6.2.3 Conductivity Measurements

The results of the conductivity study carried out on the thin films polymerized *in situ* are shown in Table 6.4.

Table 6.4: Polymerization time and conductivity of polyaniline

Polymerization Time (min)	Conductivity (S/cm)
15	0.33
30	0.28
45	0.23
60	0.2

The relationship between conductivity and polymerization time is shown in Figure 6.5.

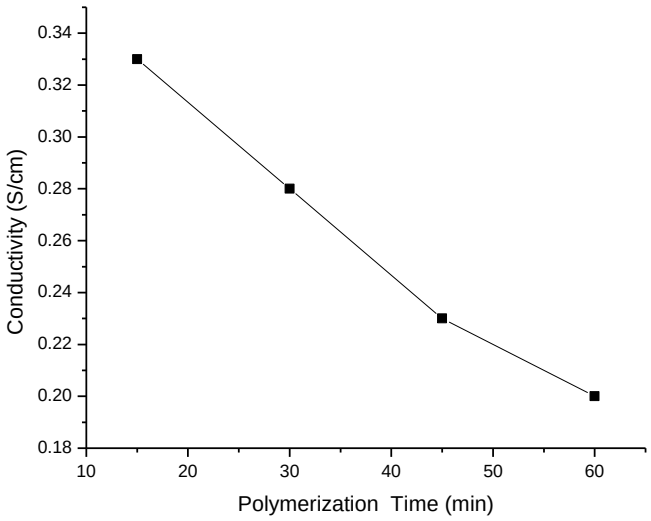

Figure 6.5: Conductivity vs. polymerisation time of in situ polymerized thin films

The polyaniline thin films prepared over a period of 60 minutes showed a decrease in conductivity with increasing polymerization time. The AFM images in Figure 6.4 above show the morphological changes that occur in the polyaniline thin films with increasing polymerisation time. In the first 15 minutes, the polyaniline nanofibers form a network of brush-like structures. These structures are still visible at 30 minutes, however due to continued film growth it is observed that the initial orderly packing of polyaniline nanofibers seen at 15 minutes is reduced. The reduction in orderly packing of nanofibers is further seen at 45 minutes with increased appearance of more amorphous looking regions. At 60 minutes the amorphous regions predominate the film surface and are due to the increase in lateral growth of nanofibers and cross-linking that is predominant in the later stages of thin film growth. The brush-like nanofibers seen in the early stages of film growth which are well ordered are said to be crystalline in nature (Sapurina et al., 2002). Orderly packing of polyaniline nanofibers increases conductivity by ensuring that the polymer nanofibers are in close proximity to each other thereby reducing the distance that electrons need to jump in the conduction mechanism (Arshak et al., 2009). As polymerisation continues more complex supramolecular structures that have a tendency to disrupt the initial well ordered packing of polyaniline chains with the formation of more globular domains that are less crystalline and more amorphous in nature (Sapurina and Shishov, 2012). The overall result of these changes in the morphology of the films deposited on the glass slide with increasing polymerisation time is a reduction in conductivity observed in these results.

6.3 Thermal Treatment of Thin Films

6.3.1 Characterisation of Thermally Treated Thin Films

6.3.1.1 Spectroscopic Analysis

(a) Ultraviolet/Visible (UV-Vis) Spectroscopy

The UV/Vis spectra of the thin films that were thermally treated at different temperatures and the spectrum of a non-treated film are shown in Figure 6.6.

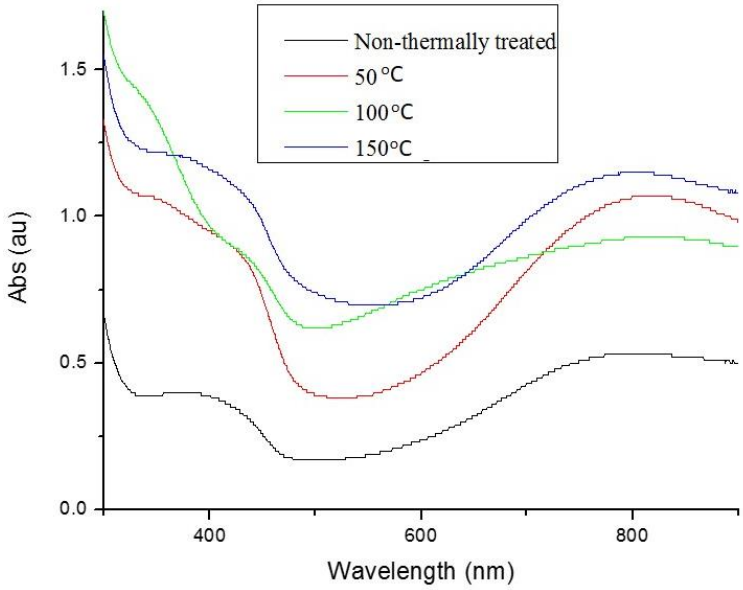

Figure 6.6: UV/Vis spectra of non-treated and films thermally treated at 50 ^{o}C, 100 ^{o}C, and 150 ^{o}C

The two main transitions at 375 nm and at 800 nm in the PANI UV/Vis spectra were still present as the films were thermally treated at increasing temperatures. However, bathochromic and hyperchromic shifts for both transitions were noted for all films treated at different temperatures. The non-treated thin film had a UV/Vis spectrum showing the л→л* transition at 375 nm and the quinoid-benzenoid transition at 800 nm. The absorption maxima for the two transitions in the non-treated film occurred at 0.4 and 0.5 respectively. Upon thermal treatment at 50 ^{o}C the л→л*, the quinoid-benzenoid transition

shifted to 390 nm and 824 nm while the absorption maxima for both transitions shifted to 1.0 and 1.07 respectively. The thin film treated at 100 ^{o}C had the л→л* and quinoid-benzenoid transition shift to 432 nm and 824 nm with the absorption maxima shifting to 0.99 and 0.95 respectively. When the thin film of PANI was thermally treated at 150 ^{o}C the shifts in transition for the л→л* and quinoid-benzenoid moved to 409 nm and 822 nm. The absorption maxima shifted to 1.16 and 1.15 respectively.

Thermal treatment of polyaniline leads to changes in the structure of the polymer. The main change being an increase in oxidation and crosslinking of the polymer structure. In addition to the change in polymer structure, there is also increased removal of dopant and moisture at higher temperatures. The reduction in dopant coupled with increased cross-linking increases the surface roughness of polyaniline. Since an increase in surface roughness improves the photon trapping characteristics of the polymer by reducing reflection of incident photons of light, an increase in absorption intensities manifesting as the hyperchromic shift is observed in the UV-Vis spectra of thermally treated polyaniline (Bhadra and Khastgir, 2008). In addition to increasing the surface roughness, the cross-linking that occurs during thermal treatment introduces an *N, N''*-diphenylphenazine moiety at the site of cross-linking. The greater conjugation that is brought about by the *N, N''*-diphenylphenazine also increases the absorption intensities and introduces the bathochromic shift that is seen in the UV-Vis spectrum of thermally treated polyaniline (Mathew, Mattes and Espe, 2002; Nobrega, Silva, Constantino and Temperini, 2012).

(b) FTIR Spectroscopy

The FTIR spectra of PANI thin films thermally treated at 50 ^{o}C, 100 ^{o}C, and 150 ^{o}C are shown in Figure 6.7 and the important transitions are presented in Table 6.5**.**

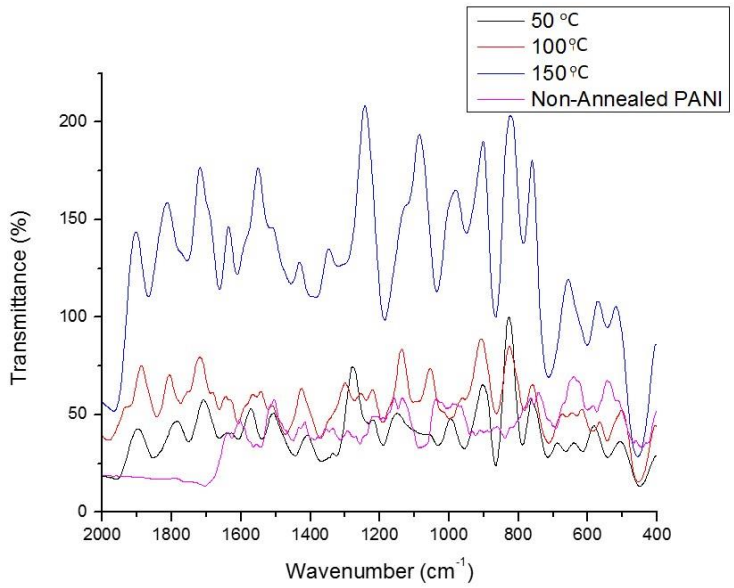

Figure 6.7: FTIR Spectra of non-thermally treated and films treated at 50 °C, 100 °C, and 150 °C

Table 6.5: FTIR Spectra of a non-treated and thermally treated PANI thin films shows the FTIR absorption peaks their assignments

Types of Vibration (cm^{-1})							
Thin Film	N-H Scissoring or bending	Quinoid ring stretching	Benzenoid ring stretching	C=C stretching; aromatic ring stretching	C-N stretching	C-H bending vibration	C-H stretching
Non-Thermally Treated	1621	1590	1508	1425	1364	1152	1052
50 °C	1621	1590	1508	1425	1364	1152	1052
100 °C	1613	1554	1525	1463	1375	1119	1030
150 °C	1613	1536	1503	1453	1380	1191	1041

The FTIR spectra of the thermally treated thin films revealed that there was a decrease in the intensity of the stretching values of each spectrum. The intensity decrease was observed with increase in treatment temperature of the thin films. The transmittance of the films was also seen to increase with greater temperature. The successive increase in the

transmittance of the thin films with greater treatment temperatures was consistent with the findings of Begum et al (2013). Thermal treatment of PANI thin films causes a change in the quinoid to benzenoid peak intensity ratio which is observed as an increase in transmittance or reduction in absorbance in the FTIR spectra. This is caused by chain scission and cross linking leading to conversion of some quinoid rings into benzenoid rings (Traore et al., 1991; Begum et al., 2013).

The FTIR spectral data of the non-thermally treated thin film and those of films treated at 50, 100 and 150 ^{o}C were then multiplied by a factor of 50 and displaced. This was done to examine whether any of the important peaks had shifted. The result is shown in Figure 6.8.

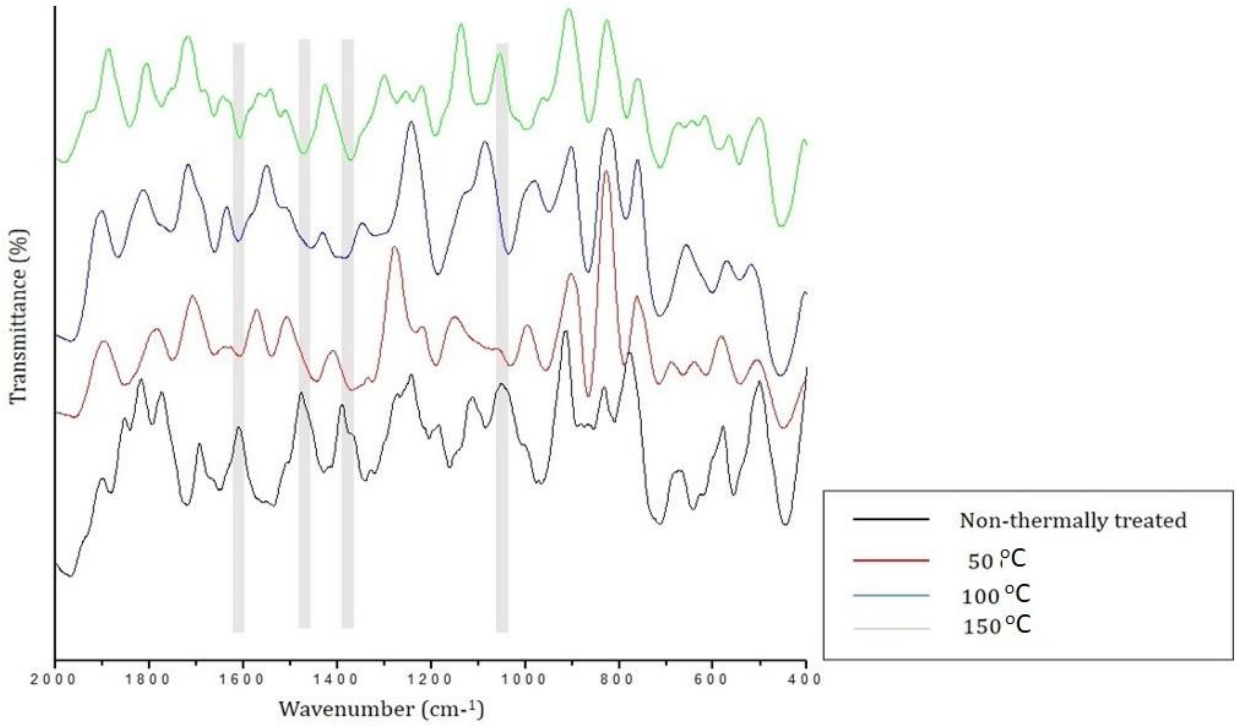

Figure 6.8: FTIR Composite Spectra for non-treated and thermally treated thin films

The FTIR composite spectra in figure 6.8 revealed that a blue shift had occurred for some of the peaks of PANI. The C-H bending vibration seen at 1152 cm^{-1} and the C-N stretching vibration at 1364 both underwent blue shifts. Further blue shifts were observed for the C=C aromatic ring stretching at 1364 and the N-H scissoring at 1621 cm^{-1}. The blue shifts occurred with increasing thermal treatment temperature and were as a result of the progressive destruction of the conjugated pathways of polyaniline with increasing temperature. The reduction in the amount of dopant in the polymer at elevated temperatures due to evaporation also contributed to the blue shifts seen in the spectra (Tang et al., 2014).

6.3.1.2 Conductivity Measurements

Thermal treatment temperature and conductivity results are presented in Table 6.6 and the relationship between treatment temperatures and conductivity is shown in Figure 6.9.

Table 6.6: Thermal Treatment Temperature and Thin Film conductivity

Thermal Treatment Temperature (^{o} C)	Conductivity (S/cm)
50	1.89
100	1.75
150	1.57

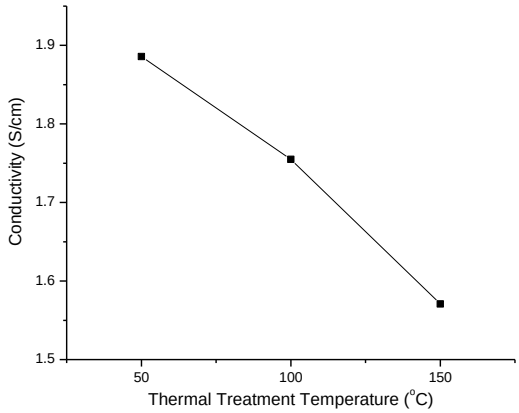

Figure 6.9: Thin Film Conductivity vs. Thermal Treatment Temperature

Thermal treatment of the polyaniline thin films led to a reduction in conductivity from 1.89 S/cm to 1.57 S/cm. The loss of dopant by evaporation was the major cause of this loss in conductivity. Deprotonation of the polymer chains leads to an overall reduction in the number of available charge carriers which in cases of complete deprotonation is seen as a reduction of conductivity from 100 S/cm to 10^{-9} S/cm (Trchová, Šeděnková, Tobolková and Stejskal, 2004). The loss in conductivity from 50-150 ^{o}C is reversible while thermal treatment with temperatures exceeding 150 ^{o}C leads to irreversible conductivity loss. Thermal treatment may also lead to irreversible changes in the morphology and structure of polyaniline. The structural changes are the result of cross-linking reactions that have been implicated in reducing the re-protonation of thermally treated polyaniline. This further contributes to a loss in conductivity (Ansari and Keivani, 2006). Additionally, thin films of PANI exhibit faster thermal degradation than that seen in bulk samples (Trchová et al., 2004). Thermal treatment of polyaniline at elevated temperatures has also been linked to the destruction of conjugated pathways in the polymer backbone by direct degradation of the polymer chains. The net result of which impact negatively on the conductivity of the polymer. Moisture loss also reduces conductivity and is mostly observed at about 100 ^{o} C (Prokeš, Trchová, Hlavatá and Stejskal, 2002).

6.3.1.3 Surface Morphology Analysis

The results of the AFM imaging of a non-thermally treated thin film and films thermally treated at different temperatures are presented in Figure 6.10. The non-thermally treated film predominantly showed the morphology of the films consisted of polyaniline nanofibers. Since this film was prepared at 30 minutes polymerization time, that is, relatively early in the polymerization process before more complex structures that form (Sapurina and Shishov, 2012). The thin film thermally treated at 50 ^{o}C showed

smoothening when compared with the non-annealed film. This smoothening is attributed to polymer chain relaxation as the temperature of annealing is raised above the glass-rubber transition temperature (T_g) of polyaniline. The T_g of polyaniline ranges between 30-40 ^oC (Bhadra and Khastgir, 2009). Thermal treatment above the T_g improves polymer chain packing of tangled segments of the polymer leading to the smoothening effect observed in the film (Lin et al., 2013). The thin films treated at 100 ^oC and 150 ^oC both showed a marked increase in elevated regions on their surfaces when compared to the film treated at 50 ^oC. These raised regions resulted in an increase in the average surface roughness of the two films. The observation is confirmed by the results of the average surface roughness shown in

Table 6.7. The change in roughness between the non-treated thin film prepared *in situ* at 30 minutes and the film treated at 50 ^oC was marginal. However, the roughness of the film treated at 100 ^oC increased by almost double that of the film treated at 50 ^oC. A dramatic increase in the average surface roughness was observed for the film treated at 150 ^oC when compared with the film treated at 100 ^oC. The major cause of the increases in surface roughness that were observed after thermal treatment were due to a gradual loss of bound water and dopant from the polymer matrices (Bhadra, Singha, Chattopadhyay and Khastgir, 2007). In addition to the dehydration of the polymer, crosslinking reactions around 150 ^oC and beyond are also possible (Ansari and Keivani, 2006). Crosslinking of polyaniline causes changes in the structural arrangements within the polymer, which also lead to an increase in the observed surface roughness.

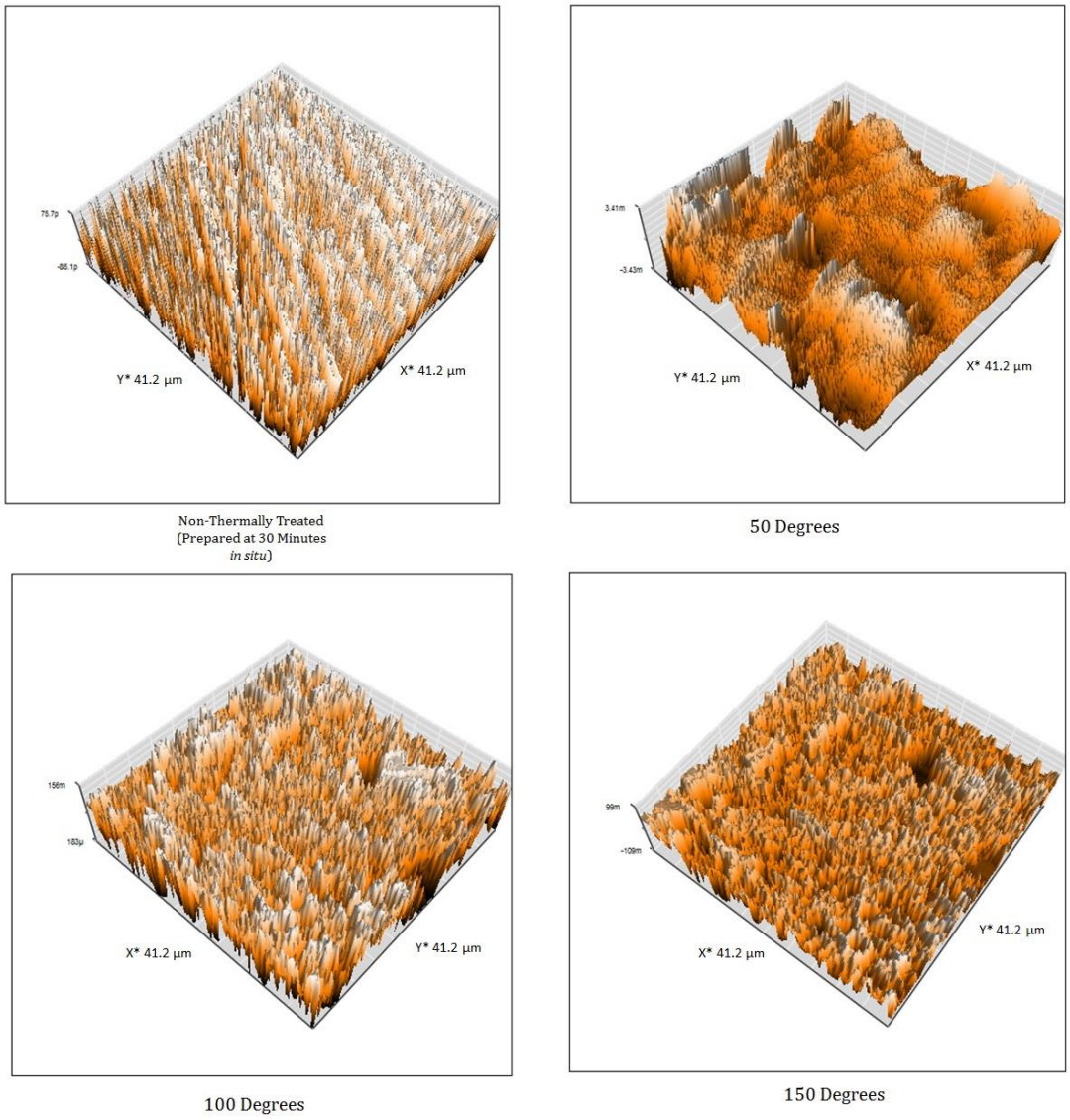

Figure 6.10: AFM images of a non-treated thin film and films thermally treated at 50 ºC, 100 ºC and 150 ºC

Table 6.7: Average surface roughness and root mean square roughness of a non-treated thin film and thin films thermally treated at 50, 100 a nd 150

		Average Surface Roughness (*Ra* , nm)	Root Mean Square Roughness (*Rq* , nm)
Non-Treated (30 minutes)		2.7	3.7
Temperature (°C)	50	2.9	3.8
	100	5.5	6.8
	150	210	260

6.4 Antibody Purification and Immobilization

6.4.1 Bacterial Antibiotic Sensitivity Testing

Bacterial antibiotic testing of the *Pseudomonas aeruginosa* isolate and the control strain of *Pseudomonas aeruginosa* (ATCC 27853) were done simultaneously on GV-Minus Octodisc® sensitivity discs to ascertain the sensitivity of the bacterial isolate in comparison to the control strain. The results of the sensitivity tests are presented in Table 6.8 and Table 6.9. The *Pseudomonas aeruginosa* isolate showed sensitivity to only Tetracycline (TE, 25µg), while for all the other antibiotics, it was resistant. On the other hand, the control strain of *Pseudomonas aeruginosa* was sensitive to Ticarcillin (Ti, 75µg), Gentamicin (Gen, 10µg), Sulphonate (CL, 25µg) and showed intermediate sensitivity to Tetracycline (TE, 25µg). The criterion used to ascribe the results was based on the antibacterial susceptibility test interpretive category described by Cockerill et al., 2012. The sensitivity profile of the *Pseudomonas aeruginosa* was important to note before the rabbit vaccine was prepared and used. This precaution was necessary in case aggressive infection ensued after immunization, the rabbit would quickly be effectively treated with the appropriate antibiotic with little time lost. The sensitivity profile of the *P. aeruginosa* isolate is shown in Table 6.8.

Table 6.8: Antibiotic Susceptibility of *Pseudomonas aeruginosa* isolate

Antibiotic	Dose (µg)	Reaction
Ampicillin (Amp)	10	R
Ticarcillin (Ti)	75	R
Gentamicin (Gen)	10	R
Cefalexin (CN)	30	R
Trimethoprim (TR)	1.25	R
Sulphamethoxazole (SX)	25	R
Tetracycline (TE)	25	S
Sulphonate (CL)	25	R

Note that "R" denotes Resistant while "S" denotes Sensitive

The sensitivity profile of the *P. aeruginosa* control strain is shown in Table 6.9.

Table 6.9: Antibiotic Susceptibility of *Pseudomonas aeruginosa* control strain (ATCC 27853)

Antibiotic	Dose (µg)	Reaction
Ampicillin (Amp)	10	R
Ticarcillin (Ti)	75	S
Gentamicin (Gen)	10	S
Cefalexin (CN)	30	R
Trimethoprim (TR)	1.25	R
Sulphamethoxazole (SX)	25	R
Tetracycline (TE)	25	I
Sulphonate (CL)	25	S

Note that "I" denotes Intermediate sensitivity

6.4.2 Serum Agglutination Test

The result of the serum agglutination test is shown in Figure 6.11. Addition of the particulate antigen, that is, *Pseudomonas aeruginosa* suspended in phosphate buffered

saline resulted in the formation of the milky coloured agglutinations seen in Figure 6.11. An interaction between antibodies and antigens in suspension produces clumping that is visible to the naked eye. Agglutination reactions are highly dependent on the crosslinking of polyvalent antigens via antibodies resulting in the effect observed (Kindt, Goldsby and Osborne, 2007).

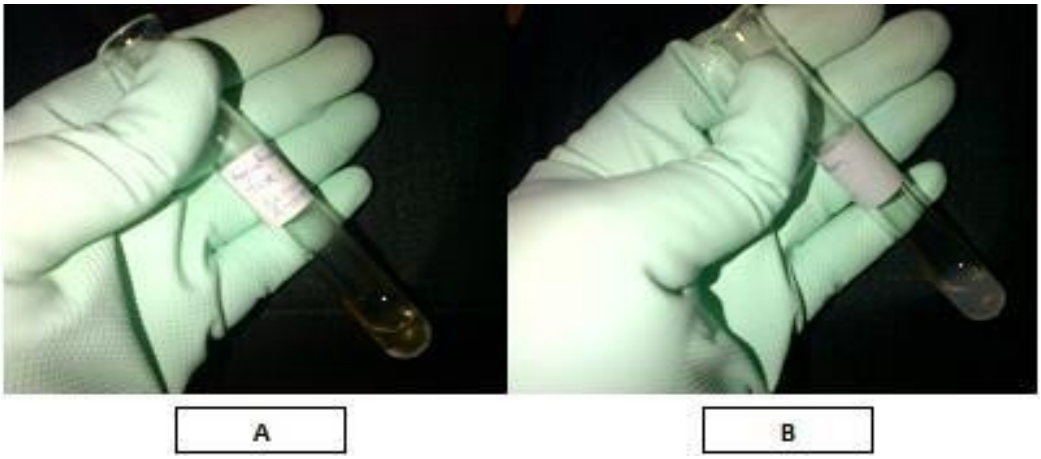

Figure 6.11: Serum agglutination test result (A) before addition of antigen and (B) after addition of antigen showing visible agglutination for anti-*P. aeruginosa* antibodies

6.5 Characterisation of Polyaniline-Biotinylated Antibody Chip

The polyaniline-biotinylated antibody films were characterised using Atomic Force Microscopy before and after injection of *P. aeruginosa* into the biosensor. This was done to ascertain whether any antigen binding event occurred when *P. aeruginosa* was injected onto the thin films. The result of the morphology analysis is presented in Figure 6.12 and shows the change that occurred to film surface after treatment with avidin and immobilisation of the biotinylated antibodies and injection of bacteria.

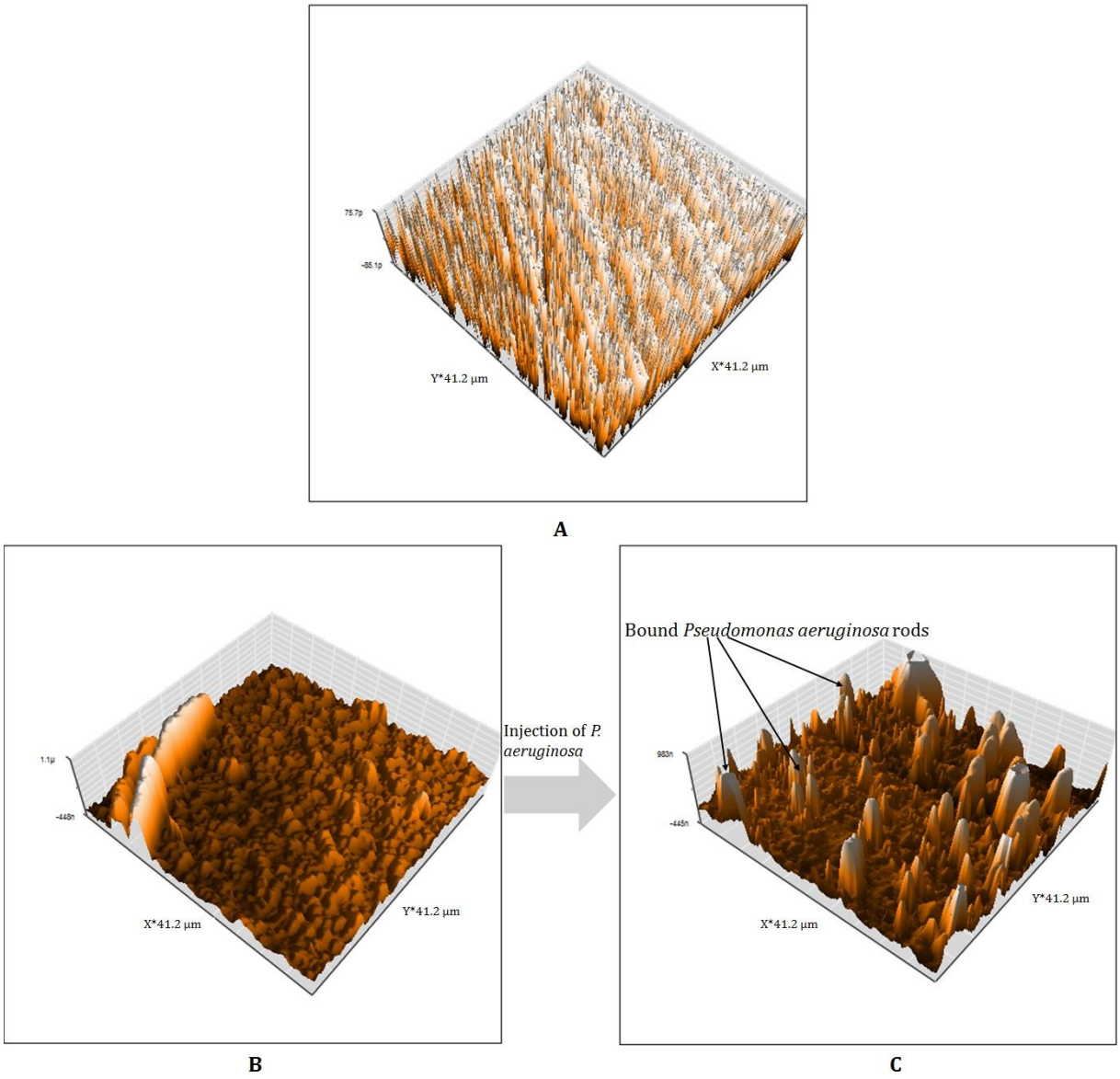

Figure 6.12: AFM images showing (A) Neat PANI thin film prepared at 30 minutes (B) PANI-biotinylated antibody thin film and (C) Bound Pseudomonas aeruginosa on polyaniline-biotinylated antibody thin film

The PANI thin film in Figure 6.12 (A) shows the brush-like nanofibers that are formed at 30 minutes polymerisation time. Treatment of the thin film with avidin and biotinylated antibodies resulted in the surface morphology seen in Figure 6.12 (B). The film showed notable disappearance of the brush-like nanofibers and appearance of numerous mound-

like structures. The structures were as a result of the presence of the globular proteins (avidin and antibodies) immobilized on the polyaniline thin film surface. Injection of *Pseudomonas aeruginosa* into the biosensor resulted in the film morphology shown in the AFM image in Figure 6.12 (C). The AFM image shows the rod-shaped *P. aeruginosa* bacteria bound to the polyaniline-biotinylated antibody thin film surface to form an antigen-antibody complex. The antigen-antibody complex formed is able to absorb light to a greater extent than the polyaniline with immobilized antibodies alone. This property of the antigen-antibody complex was useful in implementing the biosensor setup outlined in Figure 5.2, Section 5.8 (Chapter 5). The binding of *P. aeruginosa* to the thin film thus confirmed allowed the biosensor tests to be carried out as described in the next section.

6.6 Evaluation of Sensing Characteristics

The biosensor that was designed and used in this research was based on a light dependent resistor (LDR) as the light detector connected to a circuit. A light source (He-Ne Laser operating at 632.8 nm) was shone on the sensor chip injected with various concentrations of bacteria. Since the sensor chip had immobilized polyclonal antibodies on the surface, the bacteria was selectively bound on the surface of the chip leading to a reduction in the amount of light passing through the sensor chip to reach the detector. The reduction in the amount of light reaching the detector was because the bacteria bound on the surface of the chip absorbed some of the light. This would eventually manifest as changes in the resistance across the LDR. The resistance across the LDR increased with increasing bacteria concentration bound on the chip.

The results of the biosensor test carried out with *Pseudomonas aeruginosa* suspended in phosphate buffered saline and the cross reactivity test with *E. coli* are presented in Figure 6.13**.** The biosensor was tested with different known concentrations of *P. aeruginosa* (ATCC 27853) suspension in the range 9.0×10^5- 3.0×10^6 CFU. The resistance was observed to increase with increasing concentration of *P. aeruginosa.* The relationship

between resistance (in KΩ) and number of bacteria cells was found to be linear while PBS in the control experiment and PBS plus *E.coli* in the cross-reactivity experiment did not yield significant resistance values. Further tests were carried out to check the response of the biosensor when the *P. aeruginosa* was suspended in various types of serum. Sterile rabbit, goat, bovine and sheep sera were used and the various results are presented in Figure 6.14, Figure 6.15, Figure 6.16 and Figure 6.17 respectively.

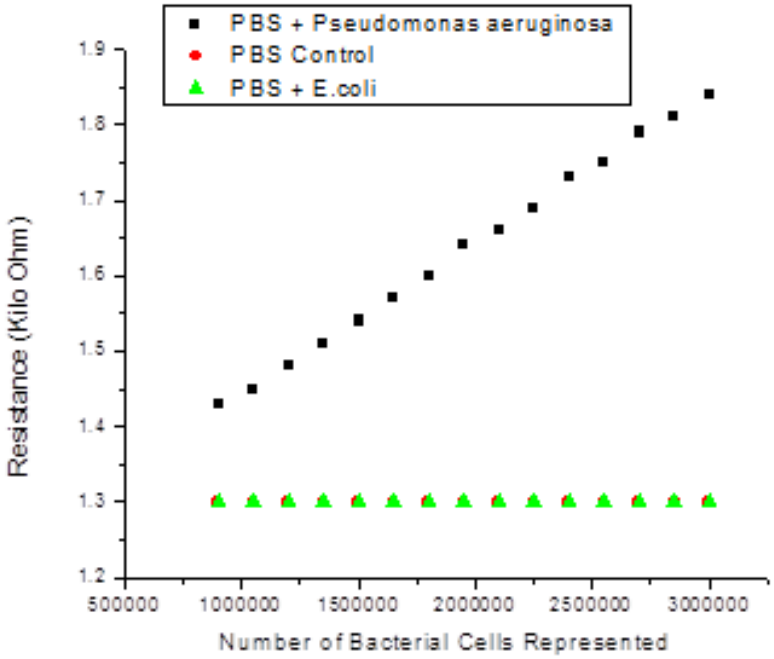

Figure 6.13: The calibration curve showing the relationship of Resistance vs. Number of Pseudomonas aeruginosa cells (in Phosphate Buffered Saline)

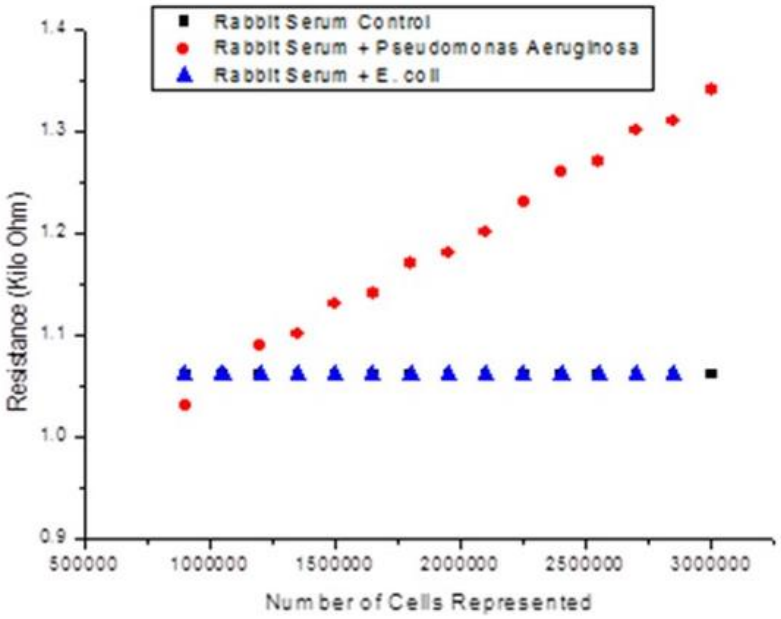

Figure 6.14: The calibration curve of Resistance vs. Rabbit Serum + *Pseudomonas aeruginosa*

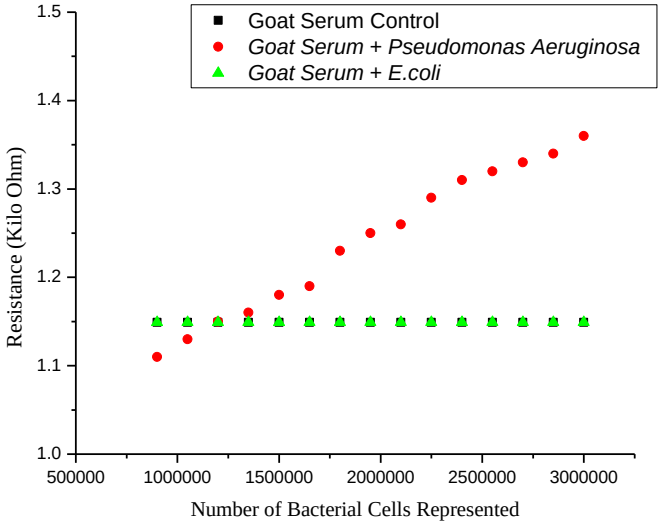

Figure 6.15: The calibration curve of Resistance vs. Goat Serum + *Pseudomonas aeruginosa*

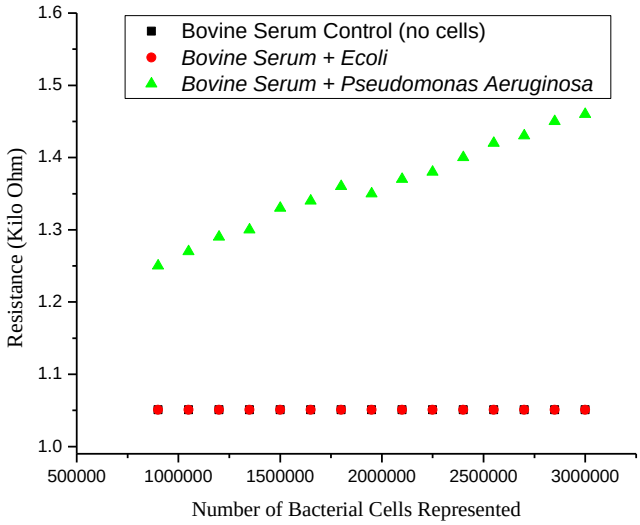

Figure 6.16: The calibration curve of Resistance vs. Bovine Serum + *Pseudomonas aeruginosa*

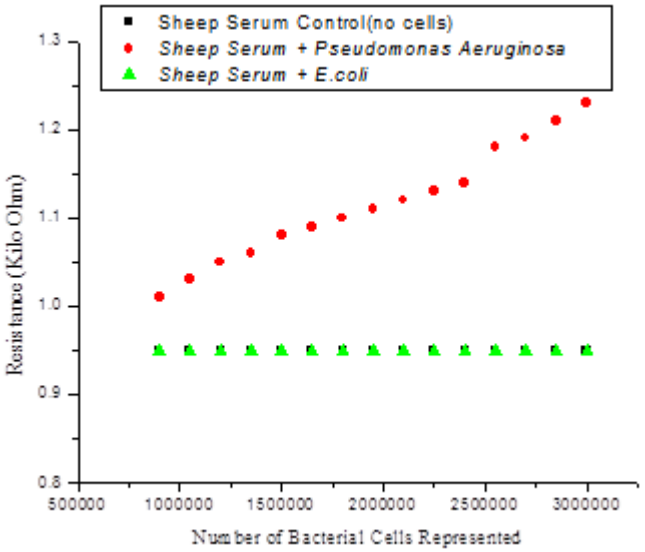

Figure 6.17: The calibration curve of Resistance vs. Sheep Serum + *Pseudomonas aeruginosa*

Figure 6.14 shows the results of the biosensor test with a rabbit serum control, rabbit serum with suspended *P. aeruginosa* and rabbit serum with suspended *E.coli*. Though the

relationship between resistance and bacterial concentration remained linear, it was noticed that the resistance values reduced drastically for all serum samples tested compared to the sample suspended in PBS.

The resistance value for PBS was 1.3 KΩ; 1.061 KΩ for rabbit serum; 1.149 KΩ for goat serum; 1.051 KΩ for bovine serum; and 0.96 KΩ for sheep serum. The composite graph for all the samples tested is shown in Figure 6.18.

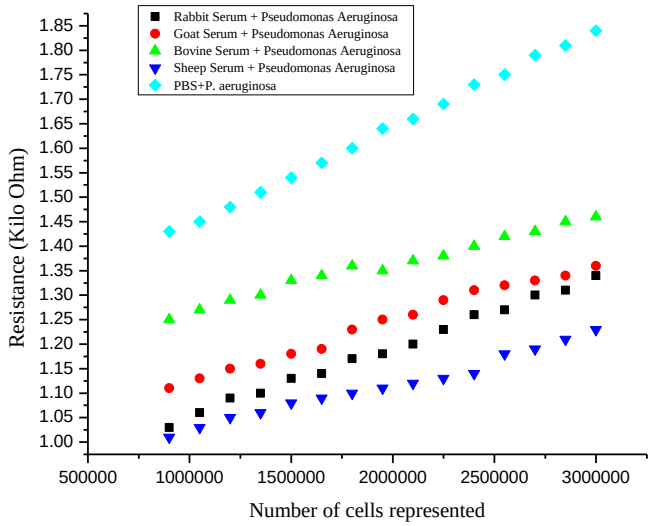

Figure 6.18: The graph of resistance vs. *P. aeruginosa* concentration suspended in PBS and various sera

Figure 6.18 shows that the various calibration curves were generally linear; although where serum was used, the graphs seemed to deviate slightly from this linear behaviour. The calibration curve for PBS + *P. aeruginosa* not only gave the highest resistance responses for given concentrations of bacteria but also gave the most linear relationship when compared to the four serum calibration curves. Bovine serum showed the next highest resistance responses followed by goat, rabbit and sheep sera respectively. The differences in resistance responses seen with the different types of serum resulted from differences in ion, protein, lipid and hormone content. These differences result in variable

serum viscosity in different species of animals that further lead to differences in the extent to which the sera absorbs or transmits light when used as a diluent.

From the experimental results, the limit of detection of the biosensor for *P.* aeruginosa was 9×10^5 CFU/ml while the detection range was 9×10^5 to 3×10^6 CFU/ml. Diagnosis of infection depends on the amount of bacteria present in clinical samples. For instance, bacteriuria is usually diagnosed when there are bacteria greater than 10^5 CFU/ml of urine although about 30 %-50 % of patients who develop acute urinary infection may have colony counts below 10^5 CFU/ml (Stamm et al., 1982; Smith, 1983). In other cases, especially involving sputum samples, diagnosis of infection involves detection of a minimum of 10^4 CFU/ml of sputum of for example tubercle bacilli to confirm infection (Baron, 1996). The number of colony forming units of *P. aeruginosa* required to cause infection in 50 % of test animals was reported by Hendricks et al (2001) to be 4.8×10^5 CFU. A study conducted by Rusin et al (1997) found that the infectious dose of *P. aeruginosa* in human subjects ranged from 10^8-10^9 CFU (Shalit, McKee, Beauchamp and Waner, 1985; Rusin, Rose, Haas and Gerba, 1997; Hendricks et al., 2001). The sensitivity of the biosensor correlated well with the cited literature sources. Crude polyclonal antibodies were used in the sensor chips and these could have limited the sensitivity seen in the biosensor output. Shalit et al (1985) demonstrated precisely this fact when they compared polyclonal and monoclonal antibodies when they found that monoclonal antibodies had a higher sensitivity of 69 % versus 46 % for polyclonal in detecting Influenza A. Monoclonal antibodies also showed a slightly higher accuracy of 86 % versus 75 % for polyclonal antibodies (Abcam, 2015). Lowering the detection limit of the biosensor would have required the use of pure antibodies rather than crude ones because the concentrations of antibodies on the sensor chips would be more easily controlled and increasing chances that lower concentrations of bacteria would be bound and detected. Monoclonal antibodies could also have lowered the detection limit due to their higher

specificity in binding antigens when compared to polyclonal antibodies (Lazcka, Del Campo and Muñoz, 2007).

CHAPTER 7: CONCLUSION AND FUTURE WORK

7.1 Conclusion

The polyaniline thin films were successfully prepared by *in situ* polymerization on glass supports and the most optimal film thickness for the biosensor application was found to be 13 nm. Spectral analysis using UV-Vis and FTIR revealed the key transitions and peaks that were characteristic of PANI. The absorption maxima's in the UV spectra were observed at 375 nm and 800 nm respectively and were characteristic of doped polyaniline. The FTIR spectra analysis revealed peaks characteristic of PANI at 1621 cm^{-1}, 1590 cm^{-1}, 1508 cm^{-1}, 1425 cm^{-1}, and 1364 cm^{-1}. Together, the two spectral methods validated the successful synthesis of polyaniline. It was further found that film thickness was not only affected by polymerization time but also determined the conductivity of prepared films. The conductivity of the polyaniline thin films decreased with increasing polymerization time. It was also found that thermal treatment of thin films at 50 ^{o}C, 100 ^{o}C and 150 ^{o}C resulted in increased surface roughness and reduced the conductivity of the thin films but also dramatically increased their average surface roughness. Spectral studies using UV-Vis and FTIR showed that thermal treatment increased thin film absorbance in the UV region while increasing transmittance in the IR region. Subsequently, it was found that the thin films thermally treated at 150 ^{o}C had the best optical properties for incorporation into the biosensor because they were able to trap and transmit more light thus favorably influencing the biosensors sensitivity profile. Antibodies were generated from rabbits via multiple immunizations that mounted an immune response in the animals. The polyaniline-biotinylated antibody *Pseudomonas aeruginosa* biosensor that was developed showed a concentration dependent linear response to the presence of *P. aeruginosa* in samples. The biosensor was selective for *Pseudomonas aeruginosa* as seen from the cross-reactivity tests carried out with *E. coli.* The detection limit of the biosensor was 9.0×10^{5} CFU, which was sensitive enough to detect clinically relevant *P. aeruginosa* infections that generally ranged from 10^{5}-10^{9} CFU. Therefore, the biosensor could be used

clinically to determine both the presence and concentration of offending pathogen in *P. aeruginosa* infections.

7.2 Future Work

Having demonstrated that the polyaniline-biotinylated antibody *Pseudomonas aeruginosa* biosensor could both detect and quantify the offending pathogen, there is need to consolidate knowledge on its performance in clinical settings. Studies on human subjects with both differential diagnoses of suspected or confirmed infections caused by *P. aeruginosa* would be invaluable in generating information on the biosensor performance in real world scenarios. Furthermore, studies relating to the reversibility and stability of the biosensor should be carried out. These studies would give a better impression of the overall biosensor performance and additional material properties consideration for the optimization of the biosensor stability.

The work that has been described in the previous chapters is one step in the design, development and testing of a low cost, sensitive and specific polyaniline-based biosensor for the detection of *Pseudomonas aeruginosa*.

REFERENCES

Abcam, 2015. *A comparison between polyclonal and monoclonal*. [online] Available at: <http://www.abcam.com/protocols/a-comparison-between-polyclonal-and-monoclonal> [Accessed 8 Feb. 2016].

Agah, a,, Hassibi, a,, Plummer, J.D.,, Griffin, P.B., and Systems, I., 2005. Design requirements for integrated biosensor arrays. *Proceedings of SPIE*, 5699(650), pp.403–413.

Akimoto, T.,, Sasaki, S.,, Ikebukuro, K., and Karube, I., 2000. Effect of incident angle of light on sensitivity and detection limit for layers of antibody with surface plasmon resonance spectroscopy. *Biosensors & bioelectronics*, 15(7-8), pp.355–62.

Ansari, R., and Keivani, M.B., 2006. Polyaniline Conducting Electroactive Polymers Thermal and Environmental Stability Studies. *E-Journal of Chemistry*, 3(4), pp.202–217.

Anu Prathap, M.U.,, Chaurasia, A.K.,, Sawant, S.N., and Apte, S.K., 2012. Polyaniline-based highly sensitive microbial biosensor for selective detection of lindane. *Analytical chemistry*, 84(15), pp.6672–8.

Armes, S.P.,, Aldissi, M.,, Hawley, M.,, Beery, J.G., and Gottesfeld, S., 1991. Morphology and structure of conducting polymers. *Langmuir*, 7(7), pp.1447–1452.

Arshak, K.,, Velusamy, V.,, Korostynska, O.,, Oliwa-Stasiak, K., and Adley, C., 2009. Conducting polymers and their applications to biosensors: Emphasizing on foodborne pathogen detection. *IEEE Sensors Journal*, 9(12), pp.1942–1951.

Baron, S., 1996. *Medical Microbiology*..

Barton, A.C.,, Collyer, S.D.,, Davis, F.,, Garifallou, G.-Z.,, Tsekenis, G.,, Tully, E.,, O'Kennedy, R.,, Gibson, T.,, Millner, P.A., and Higson, S.P.J., 2009. Labeless AC

impedimetric antibody-based sensors with pgml(-1) sensitivities for point-of-care biomedical applications. *Biosensors & bioelectronics*, 24(5), pp.1090–5.

Begum, A.N.,, Dhachanamoorthi, N.,, Saravanan, M.E.R.,, Jayamurugan, P.,, Manoharan, D., and Ponnuswamy, V., 2013. Influence of annealing effects on polyaniline for good microstructural modification. *Optik*, 124(3), pp.238–242.

Bentley, A.,, Atkinson, A.,, Jezek, J., and Rawson, D.M., 2001. Whole cell biosensors — electrochemical and optical approaches to ecotoxicity testing. *Toxicology in Vitro*, 15(4–5), pp.469–475.

Ben-Yoav, H.,, Elad, T.,, Shlomovits, O.,, Belkin, S., and Shacham-Diamand, Y., 2009. Optical modeling of bioluminescence in whole cell biosensors. *Biosensors & bioelectronics*, 24(7), pp.1969–73.

Bhadoria, R., and Chaudhary, H.S., 2011. Recent advances of biosensors in biomedical sciences. *International Journal of Drug Delivery*, 3(4), pp.571–585.

Bhadra, S., and Khastgir, D., 2008. Extrinsic and intrinsic structural change during heat treatment of polyaniline. *Polymer Degradation and Stability*, 93, pp.1094–1099.

Bhadra, S., and Khastgir, D., 2009. Glass–rubber transition temperature of polyaniline: Experimental and molecular dynamic simulation. *Synthetic Metals*, 159(12), pp.1141–1146.

Bhadra, S.,, Singha, N.K.,, Chattopadhyay, S., and Khastgir, D., 2007. Effect of different reaction parameters on the conductivity and dielectric properties of polyaniline synthesized electrochemically and modeling of conductivity against reaction parameters through regression analysis. *Journal of Polymer Science, Part B: Polymer Physics*, 45(15), pp.2046–2059.

Bhavana Gupta, S.S.S.M. and R.P., 2010. *Biosensors*. InTech.

Black, J.G., 2002. Microbiology : Principles and Explorations. In: *Microbiology: Principles and Explorations*. pp.292–293.

Bodey, G.P.,, Bolivar, R.,, Fainstein, V., and Jadeja, L., 1983. Infections caused by Pseudomonas aeruginosa. *Reviews of infectious diseases*, 5(2), pp.279–313.

Butler, J.E.,, Ni, L.,, Brown, W.R.,, Joshi, K.S.,, Chang, J.,, Rosenberg, B., and Voss, E.W., 1993. The immunochemistry of sandwich ELISAs--VI. Greater than 90% of monoclonal and 75% of polyclonal anti-fluorescyl capture antibodies (CAbs) are denatured by passive adsorption. *Molecular immunology*, 30(13), pp.1165–75.

Castelletti, L.,, Piletsky, S.A.,, Turner, A.P.F.,, Righetti, P.G., and Bossi, A., 2002. Development of an integrated capillary electrophoresis/sensor for L-ascorbic acid detection. *Electrophoresis*, 23(2), pp.209–14.

Castillo, J.,, Gáspár, S.,, Leth, S.,, Niculescu, M.,, Mortari, a.,, Bontidean, I.,, Soukharev, V.,, Dorneanu, S. a.,, Ryabov, a. D., and Csöregi, E., 2004. Biosensors for life quality - Design, development and applications. *Sensors and Actuators, B: Chemical*, 102(2), pp.179–194.

Chambers, J.P.,, Arulanandam, B.P.,, Matta, L.L.,, Weis, A., and Valdes, J.J., 2008. *Biosensor recognition elements*. *Current Issues in Molecular Biology*, Available at: <http://oai.dtic.mil/oai/oai?verb=getRecord&metadataPrefix=html&identifier=ADA541989\nhttp://www.dtic.mil/cgi-bin/GetTRDoc?Location=U2&doc=GetTRDoc.pdf&AD=ADA541989>.

Chaplin, M.F., and Bucke, C., 1990. *Enzyme Technology*. CUP Archive.

Chiang, J.-C., and MacDiarmid, A.G., 1986. 'Polyaniline': Protonic acid doping of the emeraldine form to the metallic regime. *Synthetic Metals*, 13(1-3), pp.193–205.

Chowdhury, A.D.,, De, A.,, Chaudhuri, C.R.,, Bandyopadhyay, K., and Sen, P., 2012. Label free polyaniline based impedimetric biosensor for detection of E. coli O157:H7 Bacteria. *Sensors and Actuators B: Chemical*, 171-172, pp.916–923.

Ciric-Marjanovic, G., 2013. Recent advances in polyaniline research: Polymerization mechanisms, structural aspects, properties and applications. *Synthetic Metals*, 177(3), pp.1–47.

Clark, L.C., and Lyons, C., 1962. Electrode systems for continuous monitoring in cardiovascular surgery. *Annals Of The New York Academy Of Sciences*, 102(1), pp.29–45.

Cockerill, F.R.,, Wikler, M. a.,, Alder, J.,, Dudley, M.N.,, Eliopoulos, G.M.,, Ferraro, M.J.,, Hardy, D.J.,, Hecht, D.W.,, Hindler, J. a.,, Patel, J.B.,, Mair Powell, MD, F.,, Swenson, J.M.,, Jr., R.B.T.,, Traczewski, M.M.,, Turnidge, J.D.,, Weinstein, M.P., and Zimmer, B.L., 2012. Performance standards for antimicrobial disk susceptibility tests ; approved atandard. *Clinical and Laboratory Standars Institute - NCCLS*, 32(1), p.76.

De Corcuera, J.I.R., and Cavalieri, R.P., 2003. Biosensors. *Encyclopedia of Agricultural, Food, and Biological Engineering*, pp.119–123.

D'Orazio, P., 2003. Biosensors in clinical chemistry. *Clinica chimica acta; international journal of clinical chemistry*, 334(1-2), pp.41–69.

D'Souza, S.F., 2001. Microbial biosensors. *Biosensors and Bioelectronics*, 16(6), pp.337–353.

Daghestani, H.N., and Day, B.W., 2010. Theory and applications of surface plasmon resonance, resonant mirror, resonant waveguide grating, and dual polarization interferometry biosensors. *Sensors*, 10(11), pp.9630–9646.

Darsanaki, R.K.,, Azizzadeh, A.,, Nourbakhsh, M.,, Raeisi, G., and Aliabadi, M.A., 2013. Biosensors: Functions and Applications. 2(1), pp.53–61.

Davis, F., and Higson, S., 2007. Polymers in biosensors. *biomedical polymers*, pp.1–42.

Devanaboyina, S.C.,, Lynch, S.M.,, Ober, R.J.,, Ram, S.,, Kim, D.,, Puig-canto, A.,, Breen, S.,, Kasturirangan, S.,, Fowler, S.,, Peng, L.,, Zhong, H.,, Jermutus, L.,, Wu, H.,, Ward, E.S.,, Gao, C.,, Kim, D.,, Puig-canto, A.,, Breen, S.,, Kasturirangan, S.,, Fowler, S.,, Zhong, H.,, Jermutus, L.,, Wu, H.,, Webster, C.,, Ward, E.S.,, Gao, C.,, Devanaboyina, S.C.,, Lynch, S.M.,, Ober, R.J.,, Ram, S.,, Kim, D., and Puig-canto, A., 2013. The effect of pH dependence of antibody-antigen interactions on subcellular trafficking dynamics The effect of pH dependence of antibody-antigen interactions on subcellular trafficking dynamics. 0862(February 2016).

Dhand, C.,, Das, M.,, Datta, M., and Malhotra, B.D., 2011. Recent advances in polyaniline based biosensors. *Biosensors & bioelectronics*, 26(6), pp.2811–21.

Didenko, V. V, 2001. DNA probes using fluorescence resonance energy transfer (FRET): designs and applications. *BioTechniques*, 31(5), pp.1106–16, 1118, 1120–1.

Emerson, D.,, Agulto, L.,, Liu, H., and Liu, L., 2008. Identifying and Characterizing Bacteria in an Era of Genomics and Proteomics. *BioScience*, 58(10), p.925.

Encyclopedia Britannica, 2014. *Britannica Online Encyclopedia*. [online] Ralph J. Smith. Available at: <http://www.britannica.com/>.

Frischeisen, J.,, Reinke, N.,, Ostermayr, C.,, Neumann, J.,, Nowy, S., and Brütting, W., 2008. Surface Plasmon sensor based on a planar polychromatic OLED light source. *Proc. of SPIE*, 7003, p.70031B–70031B–11.

Geise, R.J.,, Adams, J.M.,, Barone, N.J., and Yacynych, A.M., 1991. Electropolymerized Films to Prevent Interferences and Electrode Fouling in Biosensors. *Biosensors & bioelectronics*, 6(2), pp.151–160.

Gill, P.K.,, Manhas, R.K., and Singh, P., 2006. Hydrolysis of inulin by immobilized thermostable extracellular exoinulinase from Aspergillus fumigatus. *Journal of Food Engineering*, 76(3), pp.369–375.

Gonsalves, K.E.,, Halberstadt, C.R.,, Laurencin, C.T., and Nair, L.S., 2007. *Biomedical Nanostructures*. *Biomedical Nanostructures*.

Gooding, J.J., 2002. Electrochemical DNA Hybridization Biosensors. *Electroanalysis*, 14(17), pp.1149–1156.

Gopalakrishnan, K.,, Elango, M., and Thamilselvan, M., 2012. *Optical studies on nano-structured conducting Polyaniline prepared by chemical oxidation method*. [online] Scholars Research Library Archives. Available at: <http://scholarsresearchlibrary.com/APR-vol3-iss4/APR-2012-3-4-315-319.pdf> [Accessed 30 Jan. 2016].

Grieshaber, D.,, MacKenzie, R.,, Vörös, J., and Reimhult, E., 2008. Electrochemical Biosensors - Sensor Principles and Architectures. *Sensors*, 8(3), pp.1400–1458.

Gryczynski, I.,, Malicka, J.,, Gryczynski, Z.,, Nowaczyk, K., and Lakowicz, J.R., 2004. Ultraviolet surface plasmon-coupled emission using thin aluminum films. *Analytical chemistry*, 76(14), pp.4076–81.

Hahnefeld, C.,, Drewianka, S., and Herberg, F.W., 2004. Determination of kinetic data using surface plasmon resonance biosensors. *Methods in molecular medicine*, 94, pp.299–320.

Hall, G.S., 2013. Bailey & Scott's Diagnostic Microbiology, 13th Edn. *Laboratory Medicine*, 44(4), pp.e138–e139.

Hendricks, K.J.,, Burd, T.A.,, Anglen, J.O.,, Simpson, A.W.,, Christensen, G.D., and Gainor, B.J., 2001. Synergy between Staphylococcus aureus and Pseudomonas aeruginosa in a rat model of complex orthopaedic wounds. *The Journal of bone and joint surgery. American volume*, 83-A(6), pp.855–61.

Hernandez, K., and Fernandez-Lafuente, R., 2011. Control of protein immobilization: coupling immobilization and site-directed mutagenesis to improve biocatalyst or biosensor performance. *Enzyme and microbial technology*, 48(2), pp.107–22.

Hock, B., 1997. Antibodies for immunosensors a review. *Analytica Chimica Acta*, 347(1-2), pp.177–186.

Houpikian, P., and Raoult, D., 2002a. Diagnostic methods current best practices and guidelines for identification of difficult-to-culture pathogens in infective endocarditis. *Infectious disease clinics of North America*, 16(2), pp.377–92, x.

Houpikian, P., and Raoult, D., 2002b. Traditional and molecular techniques for the study of emerging bacterial diseases: one laboratory's perspective. *Emerging infectious diseases*, 8(2), pp.122–31.

Jones, L.S.,, Peek, L.J.,, Power, J.,, Markham, A.,, Yazzie, B., and Middaugh, C.R., 2005. Effects of adsorption to aluminum salt adjuvants on the structure and stability of model protein antigens. *The Journal of biological chemistry*, 280(14), pp.13406–13414.

Jönsson, M.,, Anderson, H.,, Lindberg, U., and Aastrup, T., 2007. Quartz crystal microbalance biosensor design. II. Simulation of sample transport. *Sensors and Actuators, B: Chemical*, 123(1), pp.21–26.

Jung, Y.,, Jeong, J.Y., and Chung, B.H., 2008. Recent advances in immobilization methods of antibodies on solid supports. *The Analyst*, 133(6), pp.697–701.

Justin Gooding, J., 2006. Nanoscale biosensors: Significant advantages over larger devices? *Small*, 2(3), pp.313–315.

Karimi, M.,, Chaudhury, I.,, Jianjun, C.,, Safari, M.,, Sadeghi, R.,, Habibi-Rezaei, M., and Kokini, J., 2014. Immobilization of endo-inulinase on non-porous amino functionalized silica nanoparticles. *Journal of Molecular Catalysis B: Enzymatic*, 104, pp.48–55.

Karyakin, A.A.,, Bobrova, O.A.,, Lukachova, L. V., and Karyakina, E.E., 1996. Potentiometric biosensors based on polyaniline semiconductor films. *Sensors and Actuators B: Chemical*, 33(1-3), pp.34–38.

Katakura, Y.,, Miyazaki, T.,, Wada, H.,, Omasa, T.,, Kishimoto, M.,, Goto, Y., and Suga, K., 2000. Control of antibody – antigen interaction using anion-induced conformational change in antigen peptide. 13(10), pp.719–724.

Kindt, T.J.,, Goldsby, R.A., and Osborne, B.A., 2007. *Kuby Immunology*. [online] *Kuby Immunology*, Available at: <http://books.google.com/books?id=oOsFf2WfE5wC&pgis=1>.

Kissinger, P.T., 2005. Biosensors - A perspective. *Biosensors and Bioelectronics*, 20(12), pp.2512–2516.

Koyun, A.,, Ahlatcıoğlu, E., and İpek, Y.K., 2012. Biosensors and Their Principles. *A Roadmap of Biomedical Engineers and Milestones*, pp.117–142.

Langer, J.J.,, Filipiak, M.,, Ke˛cińska, J.,, Jasnowska, J.,, Włodarczak, J., and Buładowski, B., 2004. Polyaniline biosensor for choline determination. *Surface Science*, 573(1), pp.140–145.

Langer, J.J.,, Langer, K.,, Barczyński, P.,, Warchoł, J., and Bartkowiak, K.H., 2009. New 'ON-OFF'-type nanobiodetector. *Biosensors & bioelectronics*, 24(9), pp.2947–9.

Lazcka, O.,, Del Campo, F.J., and Muñoz, F.X., 2007. Pathogen detection: a perspective of traditional methods and biosensors. *Biosensors & bioelectronics*, 22(7), pp.1205–17.

Lee, B.H.,, Park, S.H.,, Back, H., and Lee, K., 2011. Novel Film-Casting Method for High-Performance Flexible Polymer Electrodes. *Advanced Functional Materials*, 21(3), pp.487–493.

Lee, H.J.,, Goodrich, T.T., and Corn, R.M., 2001. SPR Imaging Measurements of 1-D and 2-D DNA Microarrays Created from Microfluidic Channels on Gold Thin Films. *Analytical Chemistry*, 73(22), pp.5525–5531.

Li, Q.,, Gordon, M.,, Cao, C.,, Ugen, K.E., and Morgan, D., 2007. Improvement of a low pH antigen-antibody dissociation procedure for ELISA measurement of circulating anti-Abeta antibodies. *BMC neuroscience*, 8(1), p.22.

Lin, Y.,, Tan, Y.,, Qiu, B.,, Shangguan, Y.,, Harkin-Jones, E., and Zheng, Q., 2013. Influence of annealing on chain entanglement and molecular dynamics in weak dynamic asymmetry polymer blends. *The journal of physical chemistry. B*, 117(2), pp.697–705.

Liu, C.,, Jiang, D.,, Xiang, G.,, Liu, L.,, Liu, F., and Pu, X., 2014. An electrochemical DNA biosensor for the detection of Mycobacterium tuberculosis, based on signal amplification of graphene and a gold nanoparticle-polyaniline nanocomposite. *The Analyst*, 139(21), pp.5460–5.

Liu, Y.,, Gore, A.,, Chakrabartty, S., and Alocilja, E.C., 2008. Characterization of sub-systems of a molecular biowire-based biosensor device. *Microchimica Acta*, 163(1-2), pp.49–56.

Lowe, C.R.,, Hin, B.F.,, Cullen, D.C.,, Evans, S.E.,, Stephens, L.D., and Maynard, P., 1990. Biosensors. *Journal of chromatography*, 510(3), pp.347–54.

Luo, Y.,, Nartker, S.,, Miller, H.,, Hochhalter, D.,, Wiederoder, M.,, Wiederoder, S.,, Setterington, E.,, Drzal, L.T., and Alocilja, E.C., 2010. Surface functionalization of electrospun nanofibers for detecting E. coli O157:H7 and BVDV cells in a direct-charge transfer biosensor. *Biosensors & bioelectronics*, 26(4), pp.1612–7.

Malhotra, B.D.,, Chaubey, A., and Singh, S.P., 2006. Prospects of conducting polymers in biosensors. *Analytica chimica acta*, 578(1), pp.59–74.

Markey, F., 1999. What is SPR anyway. *BIA journal*, [online] pp.14–17. Available at: <http://scholar.google.com/scholar?hl=en&btnG=Search&q=intitle:What+is+SPR+anyway?#0>.

Marques, S.M., and Esteves da Silva, J.C.G., 2009. Firefly bioluminescence: a mechanistic approach of luciferase catalyzed reactions. *IUBMB life*, 61(1), pp.6–17.

Mathew, R.,, Mattes, B.R., and Espe, M.P., 2002. A solid state NMR characterization of cross-linked polyaniline powder. *Synthetic Metals*, 131(1-3), pp.141–147.

Mazur, M., and Blanchard, G.J., 2004. Electroless Deposition of Poly(2-alkoxyaniline)s. *Langmuir*, 20(8), pp.3471–3476.

Mena, K.D., and Gerba, C.P., 2009. Risk assessment of Pseudomonas aeruginosa in water. *Reviews of environmental contamination and toxicology*, 201, pp.71–115.

Mohanty, J.G., and Elazhary, Y., 1989. Purification of IgG from serum with caprylic acid and ammonium sulphate precipitation is not superior to ammonium sulphate precipitation alone. *Comparative Immunology, Microbiology and Infectious Diseases*, 12(4), pp.153–160.

Moina, C., and Ybarra, G., 2012. Fundamentals and applications of immunosensors. In: N.H.L. Chiu and T.K. Christopoulos, eds., *Biochemistry, Genetics and Molecular Biology 'Advances in Immunoassay Technology'.* pp.65–80.

Muhammad-Tahir, Z., and Alocilja, E.C., 2003. A conductometric biosensor for biosecurity. *Biosensors and Bioelectronics*, 18(5-6), pp.813–819.

Nagata, K. and Handa, H. eds., 2000. *Real-Time Analysis of Biomolecular Interactions*. [online] Tokyo: Springer Japan. Available at: <http://link.springer.com/10.1007/978-4-431-66970-8> [Accessed 30 Jan. 2016].

Nath, C., and Kumar, A., 2012. Doping level dependent space charge limited conduction in polyaniline nanoparticles. *Journal of Applied Physics*, 112(9), p.093704.

Ni, X.,, Castanares, M.,, Mukherjee, A., and Lupold, S.E., 2011. Nucleic acid aptamers: clinical applications and promising new horizons. *Current medicinal chemistry*, 18(27), pp.4206–14.

Nobrega, M.M.,, Silva, C.H.B.,, Constantino, V.R.L., and Temperini, M.L.A., 2012. Spectroscopic study on the structural differences of thermally induced cross-linking segments in emeraldine salt and base forms of polyaniline. *The journal of physical chemistry. B*, 116(48), pp.14191–200.

Otto, C.,, Persing, D.H., and Tang, Y.W., 2014. Diagnostic Microbiology. In: *Reference Module in Biomedical Research*.

Padoa, C.J., and Crowther, N.J., 2006. Engineered antibodies: A new tool for use in diabetes research. *Diabetes Research and Clinical Practice*, 74(2), pp.S51–S62.

Pal, S.,, Alocilja, E.C., and Downes, F.P., 2007. Nanowire labeled direct-charge transfer biosensor for detecting Bacillus species. *Biosensors & bioelectronics*, 22(9-10), pp.2329–36.

Pal, S.,, Ying, W.,, Alocilja, E.C., and Downes, F.P., 2008. Sensitivity and specificity performance of a direct-charge transfer biosensor for detecting Bacillus cereus in selected food matrices. *Biosystems Engineering*, 99(4), pp.461–468.

Pan, H.,, Zhang, Y.,, He, G.-X.,, Katagori, N., and Chen, H., 2014. A comparison of conventional methods for the quantification of bacterial cells after exposure to metal oxide nanoparticles. *BMC microbiology*, 14(1), p.222.

Patel, P.D., 2002. (Bio)sensors for measurement of analytes implicated in food safety: A review. *TrAC - Trends in Analytical Chemistry*, 21(2), pp.96–115.

Patel, P.N.,, Mishra, V., and Mandloi, A.S., 2010. OPTICAL BIOSENSORS : FUNDAMENTALS & TRENDS. *Journal of Engineering Research and Studies*, I(I), pp.15–34.

Pessela, B.C.C.,, Fuentes, M.,, Mateo, C.,, Munilla, R.,, Carrascosa, A. V.,, Fernandez-Lafuente, R., and Guisan, J.M., 2006. Purification and very strong reversible immobilization of large proteins on anionic exchangers by controlling the support and the immobilization conditions. *Enzyme and Microbial Technology*, 39(4), pp.909–915.

Prodromidis, M.I., and Karayannis, M.I., 2002. Enzyme based amperometric biosensors for food analysis. *Electroanalysis*, 14(4), pp.241–261.

Prokeš, J.,, Trchová, M.,, Hlavatá, D., and Stejskal, J., 2002. Conductivity ageing in temperature-cycled polyaniline. *Polymer Degradation and Stability*, 78(2), pp.393–401.

Putzbach, W., and Ronkainen, N.J., 2013. Immobilization techniques in the fabrication of nanomaterial-based electrochemical biosensors: a review. *Sensors (Basel, Switzerland)*, 13(4), pp.4811–40.

Quinn, J.G.,, O'Neill, S.,, Doyle, A.,, McAtamney, C.,, Diamond, D.,, MacCraith, B.D., and O'Kennedy, R., 2000. Development and application of surface plasmon resonance-based biosensors for the detection of cell-ligand interactions. *Analytical biochemistry*, 281(2), pp.135–43.

Rechnitz, G.A.,, Kobos, R.K.,, Riechel, S.J., and Gebauer, C.R., 1977. A bio-selective membrane electrode prepared with living bacterial cells. *Analytica chimica acta*, 94(2), pp.357–65.

Reverberi, R., and Reverberi, L., 2007. Factors affecting the antigen-antibody reaction. *Blood transfusion = Trasfusione del sangue*, 5(4), pp.227–40.

Rusin, P.A.,, Rose, J.B.,, Haas, C.N., and Gerba, C.P., 1997. Risk assessment of opportunistic bacterial pathogens in drinking water. *Reviews of environmental contamination and toxicology*, 152, pp.57–83.

Sapurina, I.,, Osadchev, A.Y.,, Volchek, B.Z.,, Trchová, M.,, Riede, A., and Stejskal, J., 2002. In-situ polymerized polyaniline films 5. Brush-like chain ordering. *Synthetic Metals*, 129(1), pp.29–37.

Sapurina, I.Y., and Shishov, M. a., 2012. Oxidative Polymerization of Aniline: Molecular Synthesis of Polyaniline and the Formation of Supramolecular Structures. *New Polymers for Special Applications*, pp.251–312.

Schroeder, H.W., and Cavacini, L., 2013. Structure and Function of immunoglobulins. *Journal allergy clinical immunology*, 125(125), pp.S41–52.

Scouten, W.H.,, Luong, J.H.T., and Stephen Brown, R., 1995. Enzyme or protein immobilization techniques for applications in biosensor design. *Trends in Biotechnology*, 13(5), pp.178–185.

Setford, S.J., and Newman, J.D., 2005. Enzyme Biosensors. In: *Microbial Enzymes and Biotransformations*. pp.29–60.

Sethi, R.S., 1994. Transducer aspects of biosensors. *Biosensors and Bioelectronics*, 9(3), pp.243–264.

Setterington, E.B., and Alocilja, E.C., 2011. Rapid electrochemical detection of polyaniline-labeled Escherichia coli O157:H7. *Biosensors & bioelectronics*, 26(5), pp.2208–14.

Setterington, E.B., and Alocilja, E.C., 2012. Electrochemical biosensor for rapid and sensitive detection of magnetically extracted bacterial pathogens. *Biosensors*, 2(1), pp.15–31.

Shalit, I.,, McKee, P.A.,, Beauchamp, H., and Waner, J.L., 1985. Comparison of polyclonal antiserum versus monoclonal antibodies for the rapid diagnosis of influenza A virus infections by immunofluorescence in clinical specimens. *Journal of clinical microbiology*, 22(5), pp.877–9.

Shinohara, H.,, Chiba, T., and Aizawa, M., 1988. Enzyme microsensor for glucose with an electrochemically synthesized enzyme-polyaniline film. *Sensors and Actuators*, 13(1), pp.79–86.

Singh, A.,, Poshtiban, S., and Evoy, S., 2013. Recent advances in bacteriophage based biosensors for food-borne pathogen detection. *Sensors (Switzerland)*, 13(2), pp.1763–1786.

Singh, R.,, Mukherjee, M. Das,, Sumana, G.,, Gupta, R.K.,, Sood, S., and Malhotra, B.D., 2014. Biosensors for pathogen detection: A smart approach towards clinical diagnosis. *Sensors and Actuators B: Chemical*, 197, pp.385–404.

Singh, R.P., 2011. Prospects of Nanobiomaterials for Biosensing. *International Journal of Electrochemistry*, 2011, pp.1–30.

Skoog, D. a,, West, D.M.,, Holler, F.J., and Crouch, S.R., 2004. Fundamentals of Analytical Chemistry. *Anal. Chem.*, 398, pp.27–28.

Smith, G., 1983. Diagnosis of coliform infection in acutely dysuric women. *The New England journal of medicine*, 309(9), pp.1393–1394.

Smith, J.G., 2010. *Organic Chemistry*. 3rd Editio ed. Manoa: McGraw Hill.

Song, S.,, Wang, L.,, Li, J.,, Fan, C., and Zhao, J., 2008. Aptamer-based biosensors. *TrAC Trends in Analytical Chemistry*, 27(2), pp.108–117.

Srinivas, C.,, Srinivasu, D.,, Kavitha, B.,, Narsimlu, N., and Siva Kumar 5, K., 2012. Synthesis and Characterization of Nano Size Conducting Polyaniline. *IOSR Journal of Applied Physics*, 1(5), pp.12–15.

Stamm, W.E.,, Counts, G.W.,, Running, K.R.,, Fihn, S.,, Turck, M., and Holmes, K.K., 1982. Diagnosis of coliform infection in acutely dysuric women. *The New England journal of medicine*, 307(8), pp.463–8.

Stejskal, J., and Gilbert, R.G., 2002. Polyaniline. Preparation of a conducting polymer(IUPAC Technical Report). *Pure and Applied Chemistry*, 74(5), pp.857–867.

Stejskal, J.,, Kratochvíl, P., and Jenkins, A.D., 1996. The formation of polyaniline and the nature of its structures. *Polymer*, 37(2), pp.367–369.

Stejskal, J.,, Kratochvíl, P., and Radhakrishnan, N., 1993. Polyaniline dispersions 2. UV—Vis absorption spectra. *Synthetic Metals*, 61(3), pp.225–231.

Stejskal, J., and Sapurina, I., 2005. Polyaniline: Thin films and colloidal dispersions. *Pure and Applied Chemistry*, 77(5), pp.815–826.

Stejskal, J.,, Sapurina, I.,, Prokeš, J., and Zemek, J., 1999. In-situ polymerized polyaniline films. *Synthetic Metals*, 105(3), pp.195–202.

Stenberg, E.,, Persson, B.,, Roos, H., and Urbaniczky, C., 1991. Quantitative determination of surface concentration of protein with surface plasmon resonance using radiolabeled proteins. *Journal of Colloid And Interface Science*, 143(2), pp.513–526.

Su, L.,, Jia, W.,, Hou, C., and Lei, Y., 2011. Microbial biosensors: A review. *Biosensors and Bioelectronics*, 26(5), pp.1788–1799.

Subramanian, A.,, Irudayaraj, J., and Ryan, T., 2006. A mixed self-assembled monolayer-based surface plasmon immunosensor for detection of E. coli O157:H7. *Biosensors & bioelectronics*, 21(7), pp.998–1006.

Sungkanak, U.,, Sappat, A.,, Wisitsoraat, A.,, Promptmas, C., and Tuantranont, A., 2010. Ultrasensitive detection of Vibrio cholerae O1 using microcantilever-based biosensor with dynamic force microscopy. *Biosensors & Bioelectronics*, 26(2), pp.784–789.

Syam, R.,, Davis, K.J.,, Pratheesh, M.D.,, Anoopraj, R., and Joseph, B.S., 2012. Biosensors : A Novel Approach for Pathogen Detection. *VETSCAN*, 7(1), pp.14–18.

Tahir, Z.M.,, Alocilja, E.C., and Grooms, D.L., 2005. Polyaniline synthesis and its biosensor application. *Biosensors & bioelectronics*, 20(8), pp.1690–5.

Tan, L.-P.,, Lue, R.Y.P.,, Chen, G.Y.J., and Yao, S.Q., 2004. Improving the intein-mediated, site-specific protein biotinylation strategies both in vitro and in vivo. *Bioorganic & medicinal chemistry letters*, 14(24), pp.6067–70.

Tang, H.,, Ding, Y.,, Zang, C.,, Gu, J.,, Shen, Q., and Kan, J., 2014. *Effect of temperature on electrochemical degradation of polyaniline*. [online] International Journal of Electrochemical Science. Available at: <http://www.electrochemsci.org/papers/vol9/91207239.pdf> [Accessed 8 Feb. 2016].

Tang, Y.W.,, Ellis, N.M.,, Hopkins, M.K.,, Smith, D.H.,, Dodge, D.E., and Persing, D.H., 1998a. Comparison of phenotypic and genotypic techniques for identification of unusual aerobic pathogenic gram-negative bacilli. *Journal of Clinical Microbiology*, 36(12), pp.3674–3679.

Tang, Y.W.,, Ellis, N.M.,, Hopkins, M.K.,, Smith, D.H.,, Dodge, D.E., and Persing, D.H., 1998b. Comparison of phenotypic and genotypic techniques for identification of unusual aerobic pathogenic gram-negative bacilli. *Journal of clinical microbiology*, 36(12), pp.3674–9.

Thakur, B.,, Amarnath, C.A.,, Mangoli, S.H., and Sawant, S.N., 2015. Polyaniline nanoparticle based colorimetric sensor for monitoring bacterial growth. *Sensors and Actuators B: Chemical*, 207, pp.262–268.

Thévenot, D.R.,, Toth, K.,, Durst, R. a., and Wilson, G.S., 2001. Electrochemical biosensors: Recommended definitions and classification. *Biosensors and Bioelectronics*, 16(1-2), pp.121–131.

Traore, M..,, Stevenson, W.T..,, McCormick, B..,, Dorey, R..,, Wen, S., and Meyers, D., 1991. Thermal analysis of polyaniline Part I. Thermal degradation of HCl-doped emeraldine base. *Synthetic Metals*, 40(2), pp.137–153.

Trchová, M.,, Šeděnková, I.,, Tobolková, E., and Stejskal, J., 2004. FTIR spectroscopic and conductivity study of the thermal degradation of polyaniline films. *Polymer Degradation and Stability*, 86(1), pp.179–185.

Tully, E.,, Higson, S.P., and O'Kennedy, R., 2008. The development of a 'labeless' immunosensor for the detection of Listeria monocytogenes cell surface protein, Internalin B. *Biosensors & bioelectronics*, 23(6), pp.906–12.

Tzou, K., and Gregory, R.V., 1992. Kinetic study of the chemical polymerization of aniline in aqueous solutions. *Synthetic Metals*, 47(3), pp.267–277.

Velasco-Garcia, M.N., 2009. Optical biosensors for probing at the cellular level: a review of recent progress and future prospects. *Seminars in cell & developmental biology*, 20(1), pp.27–33.

Vivekanandan, J.,, Ponnusamy, V.,, Mahudeswaran, a, and Vijayanand, P.S., 2011. Synthesis , characterization and conductivity study of polyaniline prepared by chemical oxidative and electrochemical methods. *Applied Science Research*, 3(6), pp.147–153.

Yoo, E.-H., and Lee, S.-Y., 2010. Glucose Biosensors: An Overview of Use in Clinical Practice. *Sensors*, 10(5), pp.4558–4576.

Ziadan, K.M., and Saadon, W.T., 2012. Study of the electrical characteristics of polyaniline prepeared by electrochemical polymerization. *Energy Procedia*, 19, pp.71–79.

APPENDIX I: ETHICS APPROVAL LETTER

ERES CONVERGE
33 Joseph Mwilwa Road
Rhodes Park, Lusaka
Tel: +260 955 155 633
+260 955 155 634
Cell: +260 966 765 503
Email: eresconverge@yahoo.co.uk

I.R.B. No. 00005948
F.W.A. No. 00011697

23rd April, 2015

Ref. No. 2015-Mar-016

The Principal Investigator
Mr. Hanzooma Hatwiko
University of Zambia
School of Natural Sciences
Dept. of Chemistry
P.O. Box 32379,
LUSAKA.

Dear Mr. Hatwiko,

RE: DESIGN AND EVALUATION OF THE SENSING CHARACTERISTICS OF A POLYANILINE-BIOTINYLATED ANTIBODY *PSEUDOMONAS AERUGINOSA* BIOSENOR.

Reference is made to your corrections dated 21st April, 2015. The IRB resolved to approve this study and your participation as principal investigator for a period of one year.

Review Type	Ordinary	Approval No. **2015-Mar-016**
Approval and Expiry Date	Approval Date: 23rd April, 2015	Expiry Date: 22nd April, 2016
Protocol Version and Date	Version-Nil	22nd April, 2016
Information Sheet, Consent Forms and Dates	• N/A	22nd April, 2016
Consent form ID and Date	Version-Nil	22nd April, 2016
Recruitment Materials	Nil	22nd April, 2016
Other Study Documents	Nil	22nd April, 2016
Number of participants approved for study	N/A	22nd April, 2016

Specific conditions will apply to this approval. As Principal Investigator it is your responsibility to ensure that the contents of this letter are adhered to. If these are not adhered to, the approval may be suspended. Should the study be suspended, study sponsors and other regulatory authorities will be informed.

Conditions of Approval

- No participant may be involved in any study procedure prior to the study approval or after the expiration date.
- All unanticipated or Serious Adverse Events (SAEs) must be reported to the IRB within 5 days.
- All protocol modifications must be IRB approved prior to implementation unless they are intended to reduce risk (but must still be reported for approval). Modifications will include any change of investigator/s or site address.
- All protocol deviations must be reported to the IRB within 5 working days.
- All recruitment materials must be approved by the IRB prior to being used.
- Principal investigators are responsible for initiating Continuing Review proceedings. Documents must be received by the IRB at least 30 days before the expiry date. This is for the purpose of facilitating the review process. Any documents received less than 30 days before expiry will be labelled "late submissions" and will incur a penalty.
- Every 6 (six) months a progress report form supplied by ERES IRB must be filled in and submitted to us.
- ERES Converge IRB does not "stamp" approval letters, consent forms or study documents unless requested for in writing. This is because the approval letter clearly indicates the documents approved by the IRB as well as other elements and conditions of approval.

Should you have any questions regarding anything indicated in this letter, please do not hesitate to get in touch with us at the above indicated address.

On behalf of ERES Converge IRB, we would like to wish you all the success as you carry out your study.

Yours faithfully,
ERES CONVERGE IRB

Dr. E. Munalula-Nkandu
BSc (Hons), MSc, MA Bioethics, PgD R/Ethics, PhD
CHAIRPERSON

APPENDIX II: APPROVED PROTOCOL

Antibody Production Protocol*

The sites that have been selected for use in this study are the Materials Laboratory (Department of Chemistry, UNZA), the Microbiology Laboratory and Animal Paddocks (Department of Clinical Studies and Disease Control, School of Veterinary Medicine, UNZA). Preparation of the immunologic adjuvant, aluminium hydroxide will be conducted at the Materials Laboratory while *Pseudomonas aeruginosa* sub-culture and rabbit immunization will be carried out at the Microbiology Laboratory and Animal Paddocks respectively.

A rabbit will be used for antibody generation. Blood will be collected from the animal to test the pre-immune serum for any interfering pathogens. This will be done by tranquilizing the rabbit with an intramuscular injection of ketamine at a dose of 8mg/kg together with xylazine at a dose of 1.6mg/kg. An alternative to this is acepromazine at a dose of 10mg/kg intramuscularly. The blood will then be collected using a Vacutainer set where one needle is inserted into the blood vessel while the other will be placed into a serum separator tube. A maximum of 3mls of blood will be collected for the pre-test. Once the pre-test returns favourable positive results the primary immunization injection will be given to the rabbit. The antigen will be given at a concentration of 400-500µg/ml. Prior to delivery of the immunization injection, the inoculation sites will be prepared by removal of fur after which medicated soap, an alcohol rinse as well as aseptic solution will be used to clean the site. An equal volume of antigen and immunologic adjuvant (aluminium hydroxide) will be mixed and administered using two syringes and a three way stopcock. The antigen/adjuvant cocktail will be administered intradermally on 6 sites on the rump using a 22-26 G (gauge) needle. A maximum of 0.05ml will be injected at each site and the rabbit will be monitored for 10 minutes before it is returned to its cage after which the animal will be checked at 30 minutes intervals as it recovers from sedation.

Daily observation of the rabbit will be implemented and any intervening therapeutic requirements undertaken by the designated veterinarian and other animal care staff. The fur around the injection sites will be cut and the areas cleaned with antiseptic according to necessity and if analgesia is required 0.05mg/kg of buprenorphine will be administered to ensure that the animal is comfortable. Monitoring and treatment records will be maintained for the animal used for this research.

A secondary immunization will be given to the rabbit after 3 weeks. This will be done after the animal is tranquilized using the aforementioned ketamine/xylazine (or acepromazine) cocktail. The procedure and monitoring to be followed for this immunization will be the same as for the first immunization. 3 weeks after the secondary immunization, the first blood collection will be conducted. The rabbit will be sedated prior to the blood collection after which it will be placed in a restraining box. A maximum of 10% of the rabbit's blood will be collected at an interval of once every two week.

Once completed, the antibody production protocol is expected to contribute to the integration of a *Pseudomonas aeruginosa* biosensor that will aid in the reduction of diagnostic waiting for patients afflicted with infections resulting from *P. aeruginosa* bacteria. The study will also contribute to the body of knowledge regarding new efficient ways of diagnosing infectious disease using portable diagnostic devices.

*This protocol is adapted from "*Methods and Procedures of Antibody Production (Rabbits, Rats and Mice)*, 2010-2013, University of Massachusetts Animal Care."

APPENDIX III: IMMUNIZATION PROTOCOL

RABBIT IMMUNIZATION PROTOCOL

Primary Rabbit Immunization, Health Status Assessment and Blood Collection

The 4 rabbits that were selected for the antibody generation process were first subjected to an initial blood collection before immunization with the live *P. aeruginosa* antigens. Once the animals were determined to be disease free, they were each injected with the same dose of antigen. Rabbit 1 was injected intravenously through the medial ear vein while rabbit 2 was injected subcutaneously in two sites on its back. Rabbit 3 was injected intramuscularly in two sites through the left hind leg. The rabbits were restrained with a clean towel and then anaesthetized with halothane/oxygen mixture dosed initially at 5% Halothane for induction and reduced to 2.5% for maintenance. Table 1 below illustrates the primary immunization of the rabbits while Figure 4.10 shows the blood collection;

Rabbit	Injection Volume (ml)	Dose of Antigen	Dose of Halothane	Pre-Immunization Bleed (ml)
1 (IV)	0.75	3.75×10^6 CFU	5% (2.5% maintenance)	10
2 (SC)	0.75	3.75×10^6 CFU	5% (2.5% maintenance)	10
3 (IM)	0.75	3.75×10^6 CFU	5% (2.5% maintenance)	10
4 (Control)	N/A	N/A	5% (2.5% maintenance)	10

Table 1: Primary rabbit Immunization and blood collection

Figure 1: Rabbit immunization and blood collection after anaesthesia with halothane

1st Secondary Rabbit Immunization

14 days after the primary immunization, the secondary immunization of the rabbits was carried out. Rabbit1, 2 and 3 were restrained with a clean towel and sequentially immunized via the appropriate route. Two 0.5 McFarland Scale standards were used for antigen preparation as was the case for the primary immunization. After the immunization, the rabbits were monitored for 30 minutes. Table 2 below shows doses and volume of antigen used for each rabbit;

Rabbit	Injection Volume	Dose of Antigen
1 (IV)	0.75 ml	3.75 X 10^6 CFU
2 (SC)	0.75 ml	3.75 X 10^6 CFU
3 (IM)	0.75 ml	3.75 X 10^6 CFU

Table 2: Secondary immunization of rabbits 1, 2 and 3

2nd Secondary Booster Immunization

The second antigen booster immunization was done 28 days after the primary immunization. The rabbits (1, 2 and 3) were monitored for about one hour after the immunization. No adverse post immunization reactions were noted during the monitoring period.

Test Bleed

35 days after the primary immunization, the test bleed was done. Rabbit 1, 2, 3 and 4 were all bled during this phase of antibody production. The rabbits were first restrained using a sterile towel and then sedated with halothane/oxygen mixture dosed initially at 5% for induction and reduced to 2.5% for maintenance after the rabbits were fully anaesthetized. The ears of the rabbits were shaved and then sterilized with a swab moistened with methylated spirit after which the marginal ear veins and central ear arteries were used for blood collection. Blood collection was done with sterile needles and syringes while the rabbit's ears were held horizontally to maximize blood collected from each rabbit. After blood collection from each rabbit, gentle pressure was applied to the site used for bleeding for about 1 minute to stop the bleeding. Once the bleeding was controlled each rabbit was placed back into its respective cage. The rabbits were continually monitored as before to ensure that they remained in relatively good condition. Table 3 shows the relative amounts of blood collected from each rabbit during the test bleed;

Rabbit	Route	Amount (ml)
1	Central ear artery	10
2	Medial ear vein	8
3	Medial ear vein	10
4	Central ear artery	15

Table 3: Test bleed data for rabbit 1-4

3rd Secondary Booster Immunization

The third antigen booster immunization was given 42 days after the primary immunization. Rabbits 1, 2 and 3 were all immunized via the appropriate route of administration and the appropriate dose as earlier determined in Table 1 above. Each rabbit was monitored for one hour after the immunization in order to ensure that no adverse reactions occurred after the injections. After the monitoring period was completed, the rabbits were then placed back into their respective cages. Further monitoring was conducted daily to ensure that the rabbits were not in any form of distress.

Terminal Bleed and Blood Collection

The terminal bleed for rabbit 1, 2 and 3 were done 49 days after the primary immunization. The rabbits were each anaesthetized with xylazine and ketamine whose doses were calculated based on the weight of each rabbit. Once anaesthetized, the rabbits were each shaved and sterilized in order to prepare them for surgery. Each rabbit had its neck tissue surgically opened to enable access to the carotid artery. Having gained access to the carotid, the artery was then cut and the rabbit bled into a 50 ml Vacutainer® bottle. The rabbits were bled one after the other and the veterinary surgeon thereafter confirmed each of them dead after about 20 minutes. Once the death of each rabbit was confirmed, the carcasses were placed into bioharzard bags and frozen in a morgue refrigerator to wait for disposal by incineration. The blood that was collected was centrifuged and various amounts of serum collected as shown in Table 4 below. The serum was then stored in Vacutainer® bottles at – 20° C until needed.

Rabbit	Blood (ml)	Serum Collected (ml)
1	56	20
2	50	17
3	50	18

Table 4: Terminal rabbit bleed and blood collection

APPENDIX IV: ANTIBODY PURIFICATION

Polyclonal Antibody Purification Protocol

1. **Extraction of Polyclonal antibodies from Serum**
   - Centrifuge serum sample at 10,000 rpm for 15 minutes then filter to remove solids and lipids in the sample.
   - Secondary filtration with a filter with pore size between 0.22µm - 1 µm can be carried out to prepare samples for column chromatography. The corresponding pore sizes relate to chromatographic media as follows;

Nominal pore size of filter	Particle size of chromatographic medium
1µm	90 µm and greater
0.45 µm	34µm
0.22 µm	3, 10, 15 µm or when extra clean samples or sterile filtration is required

Table 1 (*Antibody Purification Handbook*, Amersham Biosciences, Edition AC 18-1037-46, p-16).

2. **Removal of Impurities**

   Lipoproteins: precipitate using dextran sulphate in the presence of calcium ions (Ca^{+}). Remove precipitate by centrifugation. The following procedure is used to achieve the removal of lipoproteins from the serum; 0.04 ml of 10% dextran sulphate solution and 1 ml of 1M $CaCl_2$ are added per ml of sample and mixed for 15 minutes after which the mixture is centrifuged at 10,000 RPM for 10 minutes. The resulting precipitate is discarded and the sample is exchanged into a suitable buffer to enable purification in a desalting column.

3. **Precipitation of Antibodies from Serum**

   The following table provides a summary of the agents that can be use for precipitating antibodies from serum;

Precipitation agent	Comment
Ammonium sulphate	Stabilizes proteins. Helps reduce lipid content. Antibody concentration should be > 1mg/ml. Sample can be concentrated into a pellet. Most samples retain native form. Excellent if Hydrophobic Interaction Chromatography (HIC) is next purification step.
Caprylic acid	The sample remains in supernatant and is not concentrated. Antibody concentration should be > 1mg/ml.
Polyethylene glycol	Stabilizes proteins. Mainly used for polyclonal antibodies and monoclonal IgM. IgMs precipitate more readily than IgG's. PEG-600 behaves as a M_r 50,000 – 100, 000 globular protein in gel filtration and is easily separated from IgM, but difficult to remove from smaller molecules.
Ethacridine	Sample remains in supernatant and is not concentrated. Used mainly for commercial preparation. Precipitates lipids, DNA, viral particles and endotoxins. A toxic compound.

Table 2; Precipitating Agents (*Antibody Purification Handbook,* Amersham Biosciences, Edition AC 18-1037-46, p-19).

- Precipitation is only effective for proteins with concentrations higher than 1mg/ml while the use of 35-40% saturated solutions has the ability to reduce sample contamination with transferring and albumin.

Reagents Required for Precipitation

(a) A saturated solution of ammonium sulphate solution prepared by adding 100g ammonium sulphate to 100 ml of distilled water and stirring until complete dissolution.

(b) The buffer for the first purification step is 1 M Tris-HCl or PBS at pH 8.0.

The following is the procedure used for precipitation of polyclonal antibodies;

i. A 0.45 µm filter can be used to filter the sample or alternatively the sample can be centrifuged (10,000RPM) at +4 °C.
ii. A 1 M Tris-HCl or PBS (pH 8.0) is then added to the sample in the ratio 1:10 to regulate the pH. 1 part Tris-HCl is added to 10 parts of sample by volume.
iii. The sample is then stirred gently and the saturated ammonium sulphate is added in a drop wise fashion. The solution usually turns milky at 20% saturation but should be made up to 50% saturation and continually stirred for an hour.
iv. The milky solution is centrifuged for 20 minutes at 10,000 RPM.
v. Once centrifugation is completed, the supernatant is then removed and the resulting pellet washed twice by placed it in an equal volume of ammonium sulphate solution having the same concentration to prevent the protein pellet redissolving or causing more precipitation. The pellet is then centrifuged once more.
vi. The protein pellet is then dissolved in a small amount of 1 M Tris-HCl.
vii. Sephadex G-25 is used to remove ammonium sulphate in the desalting column. This is done via clarification/ buffer exchange using the Sephadex G-25.

*NOTE: Precipitation of a target protein or the contaminants can be achieved by varying the % saturation of ammonium sulphate/sample solution.

4. Further Purification of Antibodies

Multi-step purification of polyclonal antibodies from serum may often be required. This may involve the combination of two or more techniques. In cases were only one rapid purification step is needed, affinity chromatography can be used as it is able to give a high level of purity and amount required for research needs. [1]

For the purposes of this research, two techniques that will be used together for antibody purification will be ammonium sulphate precipitation and a polishing step where gel filtration in an agarose column will be applied.

The characteristics of IgG and IgM are listed in the table below;

Molecular Weight	M_r 150,000 – 160,000 (IgG) M_r 900,000 (IgM)
Isoelectric Point (pI)	4-9, >6.0 for most, usually more basic than other serum proteins
Hydrophobicity	IgG is more hydrophobic compared to other proteins and precipitates more easily in ammonium sulphate
Solubility	IgG is very soluble in aqueous buffers. Lowest solubility near pI or in very low salt concentration
Temperature Stability	Relatively stable at room temperature
pH Stability	Stable over wide range of pH, but ustable in very acidic buffers
Carbohydrate Content	2-3% for IgG, 12% for IgM

Table 3: Adapted from *Antibody Purification Handbook,* Amersham Biosciences, Edition AC 18-1037-46, p-55.

APPENDIX V: FTIR SPECTRUM OF POLYANILINE

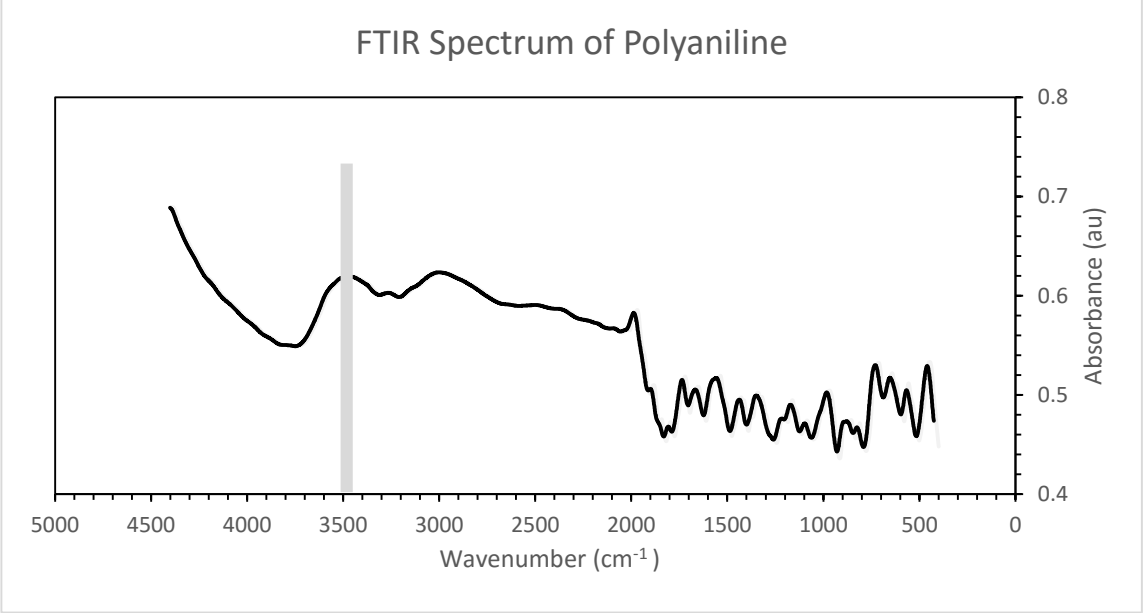

Figure 7.1: FTIR spectrum of polyaniline showing the N-H peak at 3500 cm $^{-1}$